UNIVERSITY OF ALBERTA

Laboratory Investigations on Upward Gas-Liquid Transport From Low-Pressure Reservoirs During Slug-To-Annular Flow Pattern Transitions

By

Edinson Hernando Vargas

A thesis
submitted to the Faculty of Graduate Studies and Research
in partial fulfillment of the requirements for the degree of

Master of Science
in
Petroleum Engineering

Department of Civil and Environmental Engineering

Edmonton, Alberta
Fall , 2006

Library and Archives Canada

Published Heritage Branch

395 Wellington Street
Ottawa ON K1A 0N4
Canada

Bibliothèque et Archives Canada

Direction du Patrimoine de l'édition

395, rue Wellington
Ottawa ON K1A 0N4
Canada

Your file Votre référence
ISBN: 978-0-494-22394-9
Our file Notre référence
ISBN: 978-0-494-22394-9

NOTICE:
The author has granted a non-exclusive license allowing Library and Archives Canada to reproduce, publish, archive, preserve, conserve, communicate to the public by telecommunication or on the Internet, loan, distribute and sell theses worldwide, for commercial or non-commercial purposes, in microform, paper, electronic and/or any other formats.

The author retains copyright ownership and moral rights in this thesis. Neither the thesis nor substantial extracts from it may be printed or otherwise reproduced without the author's permission.

AVIS:
L'auteur a accordé une licence non exclusive permettant à la Bibliothèque et Archives Canada de reproduire, publier, archiver, sauvegarder, conserver, transmettre au public par télécommunication ou par l'Internet, prêter, distribuer et vendre des thèses partout dans le monde, à des fins commerciales ou autres, sur support microforme, papier, électronique et/ou autres formats.

L'auteur conserve la propriété du droit d'auteur et des droits moraux qui protège cette thèse. Ni la thèse ni des extraits substantiels de celle-ci ne doivent être imprimés ou autrement reproduits sans son autorisation.

In compliance with the Canadian Privacy Act some supporting forms may have been removed from this thesis.

While these forms may be included in the document page count, their removal does not represent any loss of content from the thesis.

Conformément à la loi canadienne sur la protection de la vie privée, quelques formulaires secondaires ont été enlevés de cette thèse.

Bien que ces formulaires aient inclus dans la pagination, il n'y aura aucun contenu manquant.

Canada

ABSTRACT

Laboratory experiments conducted in the past to observe advantages and limitations regarding possible utilization of small diameter tubes (SDT) operating under slug or pseudo-slug flow patterns to remove liquids from low-pressure reservoirs have been extended to pipe diameters up to 3/4".

By increasing the gas injection rate, it was possible to observe the effect of transition from slug to annular flow pattern on the liquid production rate under a broad range of reservoir pressure conditions.

Experimental results have been compared with existing mechanistic models for evaluating the flow patterns, transitions and pressure drop. A new tool for assessing the level of pressure oscillations as an indication of flow-pattern transition related instabilities was developed, calibrated and used.

Effects of pipe diameter, reservoir pressure and interfacial tension on liquid transportation were observed and quantified. In addition, local turbulence promoters have been inserted and their effect on production enhancement has been evaluated.

AKNOWLEDGEMENTS

I gratefully acknowledge the guidance and support from Dr. Peter Toma and Dr. Ergun Kuru.

I am thankful to Mr. Sean Watt for his invaluable technical advice and help to relocate and modify experimental set up.

I am also grateful to Dr. Tayfun Babadagli and Dr. Marek Reformat, members of the thesis committee, for the pertinent technical input and corrections.

I would like to extend my gratefulness to COLFUTURO, institution from Colombia, for their economic support.

Finally, I would like to thank my loving daughter, wife, parents and brothers for their patience and unconditional support during my studies.

DEDICATION

To my loved wife Ledy and my daughter Nathaly who are my greatest motivation. To my parents Jose and Irma for making this possible. To my brothers Edgar, Oscar and Joselín.

TABLE OF CONTENTS

ABSTRACT

CHAPTER 1 1

INTRODUCTION 1
1.1 Overview 1
1.2 Statement of the problem 2
1.2.1 Liquid Accumulation at the wellhead level (load-up) 2
1.3 Methods for liquid unloading 3

1.4 Objective and scope of the research 4
1.4 Structure of the Thesis 6
CHAPTER 2 7

LITERATURE REVIEW 7

2.1 Slug Flow Pattern 7
2.1.1 Slug flow modeling 8
2.2 Slug to Annular Flow Pattern Transition in Vertical Tubes 12
2.2.1 Slug - Churn Pattern Boundary Modeling 12
2.2.2 Transition to Developed Annular Flow (STA) 16
2.3 Modeling of Slug-to-Churn Transition Stage 20
2.3.1 Estimation of the Drag Force 21
2.3.2 Friction and Gravity Forces Calculation 24
2.4 Annular two-phase flow pattern 25
2.4.1 Ansari's Model 25
CHAPTER 3 30

LABORATORY EQUIPMENT AND EXPERIMENTAL PROGRAM 30
3.1 Experimental set up 30
3.1.1 Turbulent Promoters 32
3.2 Pressure Transducer Calibration 34
3.3 Data acquisition system (DAS) 36
3.4 Measurement of injected air flowrate 39
3.4 Experimental Procedure 41
3.4.1 Liquid preparation and physical properties 41
3.4.2 Experimental procedure 42
CHAPTER 4 44

EXPERIMENTAL RESULTS AND ANALYSIS 44

4.1 Experiments with 20 mm ID tube using tap water 45
4.1.1 Visual observations (20 mm ID and tap water) 47
4.1.2 Bottom Hole Pressure (BHP) Oscillations (D=20 mm) 50
4.2 12 mm tube 53
4.2.1 Visual observations (12 mm tube) 55
4.2.2 Bottomhole pressure (BHP) (12 mm ID) 57
4.3 Experiments with the 8 mm ID tube. 59
4.3.1 Oscillations of bottomhole pressure (BHP) with 8 mm ID 60
4.4 The effect of tube diameter 62
4.4.1 Comparative observations regarding the oscillations of bottomhole pressure 65
4.5 Water-methanol (W-M) mixture (ID=20 mm) 66
4.5.1 The bottomhole pressure oscillations (ID=20 mm) and W-M 69
4.6 Water-methanol (W-M) mixture and D=12 mm 71
4.6.1 Oscillations of bottomhole pressure (D=12 mm, W-M mixture) 72
4.7 RMS for 20 mm and 12 mm tubes with W-M 72
4.8 Effect of local turbulent promoters (LTP) 73
4.8.1 LTP experiments (D=20 mm) 74
4.8.2 LTP for SDT 83
4.8 Experiments with 8 mm tube using LTP 88
CHAPTER 5 90

5.1 Slug-churn transition stage 90

5.2 Churn-to-annular transition stage - comparison of experimental results with numerical models 93

5.3 Production characteristic – comparison of experimental and modeled data for 20 mm tubes 94
5.4 Putra's laboratory data and model for pressure drop during STC transition 97
5.5 Comparison of experimental data with Ansari's model [10] for annular flow 98
5.6 Comparison of the experimental results and Putra's model for churn flow 100
5.7 Comparison of calculated (Ansari model [11]) and experimental pressure drop in the annular flow pattern zone 104
5.8 Potential field applications of SDT 105
5.8.1 Hypothetical field Situations 106
CHAPTER 6 113

CONCLUSIONS AND RECOMENDATIONS 113

6.1 Conclusions 113
6.2 Recommendations 114
APPENDIX A 119

EXPERIMENTAL RESULTS FOR THE WATER/AIR GAS LIFT SYSTEM 119

A.1 20 mm tube's experimental data 119
A.1.1 35 % Submergence Level 119
A.1.2 16.66 % Submergence Level 119
A.1.3 12.5 % Submergence Level 120
A.1.4 8.33 % Submergence Level 120
A.1.5 4.16 % Submergence Level 120
A.1.6 RMS of FBHP for 20 mm tube. 121
A.2 12 mm tube's experimental data 121
A.2.1 16.66 % Submergence Level 121
A.2.2 12.5 % Submergence Level 122
A.2.3 8.33 % Submergence Level 122
A.2.4 4.16 % Submergence Level 123
A.2.5 RMS of FBHP for 12 mm tube. 124
A.3 8 mm tube's experimental data 125
A.3.1 16.66 % submergence level 125
A.3.2 4.16 % submergence level 125
A.3.3 RMS of FBHP for 8 mm tube. 126
APPENDIX B 127

EXPERIMENTAL RESULTS FOR THE 127

WATER-METHANOL/AIR GAS LIFT SYSTEM 127

B.1 20 mm tube's experimental data 127
B.1.1 16.66 % Submergence level 127
B.1.2 12.5 % Submergence level 127
B.1.3 8.33 % Submergence level 128
B.1.5 RMS of FBHP for 20 mm tube. 129

B.2 12 mm tube's experimental data 129
B.2.1 16.66 % Submergence level 129
B.3 8 mm tube's experimental data 130
B.3.1 16.66 % Submergence level 130
APPENDIX C 131

EXPERIMENTAL RESULTS FOR THE WATER/AIR GAS LIFT SYSTEM ULIZING

LTPs IN THE 20 mm TUBE. 131

C.1 Data for one 19 mm ID LTP located at the middle of the tube 131
C.1.1 16.66 % submergence level 131
C.1.2 4.16 % submergence level 131
C.1.3 RMS of FBHP data. 132
C.2 Data for one 19 mm ID LTP located at the bottom of the tube 132
C.2.1 16.66 % submergence level 132
C.2.2 4.16 % submergence level 133

C.2.3 RMS of FBHP data 133
C.3 Data for two 19 mm ID LTPs located at the bottom and top of the tube 134
C.3.1 16.66 % submergence level 134
C.3.2 4.16 % Submergence level 134
C.3.3 RMS of FBHP data 135
C.4 Data for one 17 mm ID LTP located at the middle of the tube 136
C.4.1 16.66 % submergence level 136
C.4.2 4.16 % Submergence level 136
C.4.3 RMS of FBHP data 137
C.5 Data for one 17 mm ID LTP located at the bottom of the tube 138
C.5.1 16.66 % submergence level 138
C.5.2 4.16 % submergence level 138
C.5.3 RMS of FBHP data 139

C.6 Data for two 17 mm ID LTPs located at bottom and top of the tube 139
C.6.1 16.66 % submergence level 139
C.6.2 4.16 % Submergence level 140
C.6.3 RMS of FBHP 140
APPENDIX D 141

EXPERIMENTAL RESULTS FOR THE WATER/AIR 141

GAS LIFT SYSTEM UTILIZING LTPs IN THE 12 mm ID TUBE. 141

D.1 Data for the 11 mm ID LTP located at the middle of the tube. 141
D.1.2 12.5 % submergence level 142
D.1.3 8.33 % submergence level 142
D.1.4 4.16 % submergence level 143
D.1.5 RMS of FBHP data 144
D.2 Data for the 9 mm ID LTP located at the middle of the tube. 145
D.2.1 16.66 % Submergence level 145
D.2.2 12.5 % Submergence level 145
D.2.3 8.33 % Submergence level 146
D.2.4 4.16 % Submergence level 146
D.2.5 RMS of FBHP data 147
APPENDIX E 148

EXPERIMENTAL RESULTS FOR THE WATER/AIR GAS LIFT 148

SYSTEM UTILIZING A 7 mm ID LTP IN 8 mm ID TUBE. 148

E.1 RMS of FBHP 148

LIST OF TABLES

Table 3.1. LTP sizes for the tubes utilized. 33
Table 3.2. Specifications of the correlated flowmeter (0 to 26 SLPM of air) 40
Table 3.3. Specifications of the direct-reading flowmeter (30 to 300 LPM of air) 40
Table 3.4. Air range of operation for the direct-reading flowmeter 41
Table 3.5. Submergence level used for the 8, 12 and 20 mm risers 42
Table 3.6. Air flow rate used for 4, 8, 12, and 20 mm ID riser 43

Table 4.1. Physical properties of water, methanol and water-methanol 60:40 mixture [2] 66

Table 5.1. Data within churn flow pattern [12] 97
Table 5.2 Input data [35] used for validation of Ansari's model in the annular flow pattern zone 99
Table 5.3. Data for field case (20 mm tube) 107
Table 5.4. Data for field case (12 mm tube) 107

Table A.1.1. Data for 20 mm Tube. 35 % Submergence level (water-air) 119
Table A.1.2. Data for 20 mm Tube. 16.66 % Submergence level (water-air) 119
Table A.1.3. Data for 20 mm Tube. 12.5 % Submergence level (water-air) 120
Table A.1.4. Data for 20 mm Tube. 8.33 % Submergence level (water-air) 120
Table A.1.5. Data for 20 mm Tube. 4.16 % Submergence level (water-air) 120
Table A.1.6. RMS of FBHP for 20 mm tube (Water-Air). 121

Table A.2.1. Data for 12 mm tube. 16.66 % Submergence level (water-Air) 121
Table A.2.2. Data for 12 mm tube. 12.5 % Submergence level (water-Air) 122
Table A.2.3. Data for 12 mm tube. 8.33 % Submergence level (water-Air) 122
Table A.2.4. Data for 12 mm tube. 4.16 % Submergence level (water-Air) 123
Table A.2.5. RMS of FBHP for 12 mm tube. 124

Table A.3.1. Data for 8mm tube. 16.66 % submergence level 125
Table A.3.2. Data for 8mm tube. 4.16 % submergence level 125
Table A.3.3. RMS of FBHP for 8 mm tube. 126

Table B.1.1. Data for 20 mm ID tube (water-methanol). 16.66 % Submergence 127
Table B.1.2. Data for 20 mm ID tube (water-methanol). 12.5 % Submergence 127
Table B.1.3. Data for 20 mm ID tube (water-methanol). 8.33 % Submergence 128
Table B.1.4. Data for 20 mm ID tube (water-methanol). 4.16 % Submergence 128
Table B.1.5. RMS of FBHP for 20 mm ID tube (water-methanol) 129

Table B.2.1. Data for 12 mm ID tube (water-methanol). 16.66 % Submergence 129

Table B.3.1. Data for 8 mm ID tube (water-methanol). 16.66 % Submergence..... 130

Table C.1.1. Data for 20 mm ID tube (water) using one 19 mm ID LTP (middle). 16.66 % Submergence level..... 131
Table C.1.2. Data for 20 mm ID tube (water) using one 19 mm ID LTP (middle). 4.16 % Submergence level..... 131
Table C.1.3. RMS of FBHP for 20 mm ID tube (water) using one 19 mm ID LTP (middle)..... 132

Table C.2.1. Data for 20 mm ID tube (water) using one 19 mm ID LTP (bottom). 16.66 % Submergence level..... 132
Table C.2.2. Data for 20 mm ID tube (water) using one 19 mm ID LTP (bottom). 4.16 % Submergence level..... 133
Table C.2.3. RMS of FBHP for for 20 mm ID tube (water) using one 19 mm ID LTP (bottom)..... 133

Table C.3.1. Data for 20 mm ID tube (water) using two 19 mm ID LTPs (bottom & top). 16.66 % Submergence level..... 134
Table C.3.2. Data for 20 mm ID tube (water) using two 19 mm ID LTPs (bottom & top). 4.16 % Submergence level..... 134
Table C.3.3. RMS of FBHP for 20 mm ID tube (water) using one 19 mm ID LTP (bottom & top)..... 135

Table C.4.1. Data for 20 mm ID tube (water) using one 17 mm ID LTP (middle). 16.66 % Submergence level..... 136
Table C.4.2. Data for 20 mm ID tube (water) using one 17 mm ID LTP (middle). 4.166 % Submergence level..... 136
Table C.4.3. RMS of FBHP for 20 mm ID tube (water) using one 17 mm ID LTP (middle)..... 137

Table C.5.1. Data for 20 mm ID tube (water) using one 17 mm ID LTP (bottom). 16.66 % Submergence level..... 138
Table C.5.2. Data for 20 mm ID tube (water) using one 17 mm ID LTP (bottom). 4.166 % Submergence level..... 138
Table C.5.3. RMS of FBHP for 20 mm ID tube (water) using one 17 mm ID LTP (bottom)..... 139

Table C.6.1. Data for 20 mm ID tube (water) using one 17 mm ID LTP (bottom & top). 16.66 % Submergence level..... 139
Table C.6.2. Data for 20 mm ID tube (water) using one 17 mm ID LTP (bottom & top). 4.16 % Submergence level..... 140
Table C.6.3. RMS of FBHP for 20 mm ID tube (water) using one 17 mm ID LTP (bottom & top)..... 140

Table D.1.1. Data for 12 mm ID tube (water) using one 11 mm ID LTP (middle). 16.66 % Submergence level 141
Table D.1.2. Data for 12 mm ID tube (water) using one 11 mm ID LTP (middle). 12.5 % Submergence level 142
Table D.1.3. Data for 12 mm ID tube (water) using one 11 mm ID LTP (middle). 8.33 % Submergence level 142
Table D.1.4. Data for 12 mm ID tube (water) using one 11 mm ID LTP (middle). 4.16 % Submergence level 143
Table D.1.5. RMS of FBHP for 12 mm ID tube (water) using one 11 mm ID LTP (middle) 144

Table D.2.1. Data for 12 mm ID tube (water) using one 9 mm ID LTP (middle). 16.66 % Submergence level 145
Table D.2.2. Data for 12 mm ID tube (water) using one 9 mm ID LTP (middle). 12.5 % Submergence level 145
Table D.2.3. Data for 12 mm ID tube (water) using one 9 mm ID LTP (middle). 8.33 % Submergence level 146
Table D.2.4. Data for 12 mm ID tube (water) using one 9 mm ID LTP (middle). 4.16 % Submergence level 146
Table D.2.5. RMS of FBHP for 12 mm ID tube (water) using one 9 mm ID LTP (middle) 147

Table E.1. RMS of FBHP for 8 mm ID tube (water) using one 8 mm ID LTP (middle). 148

LIST OF FIGURES

Figure. 2.1. Upward vertical slug flow 8
Figure. 2.2. The slug, churn and annular flow regimes in vertical upwards annular gas-liquid flows [14]..... 13
Figure. 2.3. Transition from slug flow to churn flow [13]..... 14
Figure 2.4. Liquid entrained fraction as a function of the total liquid mass flux: p = 2 bara (approximately 200 kPa) [25] 19
Figure. 2.5. Entrainment and experimental pressure gradient in the churn–annular region: p = 2 bara (200 kPa), m_L = 47 kg m^2 s^{-1} [23]..... 20
Figure 2.6. Annular flow pattern..... 26

Figure. 3.1 Experimental set up 32
Figure. 3.2. The Local Turbulent Promoter (LTP) 33
Figure 3.3. View of the LTP during gas-liquid upward lifting 33
Figure 3.4 Pressure transducers for FBHP and air line..... 34
Figure 3.5. Omega® DPI 610 pressure calibrator 35
Figure 3.6. Calibration curve for the 50 psi diaphragm. 35
Figure 3.7. Calibration curve for the 5 psi diaphragm. 35
Figure 3.8. The Instrunet equipment..... 36
Figure 3.9. Graphical data acquisition. 37
Figure 3.10. Example of the "Instrunet" software setup..... 38
Figure 3.11. Direct-reading (left) and correlated (right) flowmeters..... 39

Figure 4.1. Water flow rate as a function of air flow rate for 20 mm ID tube (tap water) 46
Figure 4.2. Superficial liquid velocity as a function of superficial air velocity for the 20 mm ID tube (tap water)..... 47
Figure 4.3. Photographic evidence of CTA (4.16% submergence, ID=20 mm) (a) Ugs = 10.61 m/s. and Uls = 0.035 m/s (b). Ugs = 17.45 m/s and Uls = 0.105 m/s (c) Ugs = 22.9 m/s and Uls = 0.119 m/s 48
Figure 4.4. Photographic evidence of CTA (a) Ugs = 8.01 m/s. and Uls = 0.0356 m/s (b). Ugs = 17.45 m/s and Uls = 0.120 m/s (c) Ugs = 22.9 m/s and Uls = 0.127 m/s 48
Figure 4.5. Photographic evidence of CTA (a) Ugs = 6.63 m/s. and Uls = 0.0343 m/s (b). Ugs = 17.45 m/s and Uls = 0.148 m/s (c) Ugs = 22.9 m/s and Uls = 0.149 m/s..... 49
Figure 4.6. Photographic evidence of CTA (16.66 % submergence 20 mm ID) (a) Ugs = 7.58 m/s. and Uls = 0.071 m/s. (b) Ugs = 10.77 m/s and Uls = 0.136 m/s (c). Ugs = 17.45 m/s and Uls = 0.185 m/s (d) Ugs = 22.9 m/s and Uls = 0.189 m/s..... 49
Figure 4.7. RMS of oscillating BHP for 20 mm ID tube. (a) 4.16 % submergence. (b) 8.33 % submergence. (c) 12.5 % submergence. (d) 16.66 % submergence. 51
Figure 4.8. Comparison of RMS and water production curves for the 20 mm tube. (a) 16.66 % submergence level. (b) 4.16 % submergence level. 53
Figure 4.9. Superficial liquid velocity versus superficial air velocity for (12 mm ID and tap water). 54

Figure 4.10. Photographic evidence of water-air upward transportation (4.16% submergence 12 mm ID) (a) Ugs = 10.89 m/s. and Uls = 0.0061 m/s (b). Ugs = 16.25 m/s and Uls = 0.0172 m/s (c) Ugs = 23.9 m/s and Uls = 0.019 m/s 56
Figure 4.11. Photographic evidence of water-air upward transportation (16.66% submergence 12 mm ID) (a) Ugs = 10.89 m/s. and Uls = 0.062 m/s (b). Ugs = 16.25 m/s and Uls = 0.057 m/s (c) Ugs = 23.9 m/s and Uls = 0.0475 m/s 56
Figure 4.12. RMS of oscillating bottomhole pressure (12 mm ID) (a) 4.16 % submergence. (b) 8.33 % submergence. (c) 12.5 % submergence. (d) 16.66 % submergence. 58
Figure 4.13. Comparison of RMS and superficial water velocity versus superficial gas injected velocity (12 mm tube). (a) 16.66 % submergence level. (b) 8.33 % submergence level. 59
Figure 4.14. Superficial liquid velocity versus superficial air velocity (8 mm ID) 60
Figure 4.15. RMS of Flowing Bottom Flow Pressure for the 8 mm ID tube. (a) 4.16 % submergence. (b) 16.66 % submergence. 61
Figure 4.16. Comparison of RMS and water production curves for the 8 mm tube and 16.66 submergence level. 62
Figure 4.17. Superficial water velocity versus superficial air velocity for 20 mm, 12 mm, 8 mm and 4 mm tubes. (a) S=4.16 % (b) S=8.33 %(c) S=12.5 % (d) S=16.66 % ... 64
Figure 4.18. Comparison of RMS with 8, 12 and 20 mm tubes (a) S=4.16 % 65
Figure 4.19. Superficial liquid velocity as a function of superficial air velocity for the 20 mm ID tube using the water-methanol mixture. (a) S=16.66 %. (b) S=12.5 % (c) S= 8.33 % (b) S=4.16 % 68
Figure 4.20. Comparison of RMS versus superficial gas velocities for water only and W-M mixture measured with 20 mm ID (a) S=4.16 % (b) S=8.33 % (c) S=12.5 % (d) S=16.66 % 70
Figure 4.21. Superficial liquid (W-M) velocity versus superficial air velocity (12 mm ID S=16.66 %) 71
Figure 4.22. RMS of Flowing Bottom Flow Pressure for the 12 mm ID tube. (a) 4.16 % submergence. (b) 8.33 16.66 % submergence (water-methanol mixture and tap water) 72
Figure 4.23. RMS recorded for 12 and 20 mm tubes. (a) S=4.16 % (b) S=16.66 % 73
Figure 4.24. Comparison of superficial liquid velocity as a function of superficial air velocity for the 20 mm ID (the base line and three different LTP placements for S=4.16 %. (a) 19 mm LTP (b) 17 mm LTP 75
Figure 4.25. Superficial liquid velocity as a function of superficial air velocity for the 20 mm ID tube using three different placements of LTP's for S=16.66 %. (a) 19 mm LTP (b) 17 mm LTP 76
Figure 4.26. RMS versus gas superficial velocity for base-line and for two LTP designs positioned at ½ depth (20 mm tube, S=4.16 %) 77
Figure 4.27. RMS versus flowrate of gas for base-line and 19 mm LTP's positioned at ½, top and bottom (20 mm tube, S=4.16 %) 78
Figure 4.28. RMS versus gas superficial velocity for base-line and three 17 mm LTP's positions (20 mm tube, S=4.16 %) 78
Figure 4.29. RMS versus gas superficial velocity for base-line and for two LTP designs positioned at ½ depth (20 mm tube, S=8.33 %) 78

Figure 4.30. RMS versus gas superficial velocity for base-line and two 19mm LTP positions (20 mm tube, S=8.33 %) 79
Figure 4.31. RMS versus gas superficial velocity for base-line and two 17 mm LTP positions (20 mm tube, S=8.33 %) 79
Figure 4.32. RMS versus gas superficial velocity for base-line and two LTP designs positioned at ½ depth (20 mm tube, S=12.5 %)..... 80
Figure 4.33 RMS versus gas superficial velocity for base-line and two LTP designs positioned at ½ depth (20 mm tube, S=12.5 %)..... 80
Figure 4.34 RMS versus gas superficial velocity for base-line and 17 mm LTP's positioned at bottom and ½ depth (20 mm tube, S=12.5 %) 81
Figure 4.35 RMS versus gas injected for base-line and two LTP designs positioned at ½ depth (20 mm tube, S=16.6 %) 81
Figure 4.36 RMS versus gas injected for base-line and 19 mm LTP designs positioned at ½ depth, bottom and top (20 mm tube, S=16.6 %) 82
Figure 4.37 RMS versus gas injected for base-line and 17 mm LTP designs positioned at ½ depth, bottom and top (20 mm tube, S=16.6 %) 82
Figure 4.38 Superficial liquid velocity versus superficial air velocity for the 12 mm ID tube for 4.16 % submergence using two different LTP positioned at 1/2 of tube depth . 83
Figure 4.39 Superficial liquid velocity versus superficial air velocity for the 12 mm ID tube for 8.33 % submergence using two different LTP positioned at ½ depths..... 84
Figure 4.40 Superficial liquid velocity as a function of superficial air velocity for the 12 mm ID tube for 12.5 % submergence using two different LTP at the middle of the tube 84
Figure 4.41 Superficial liquid velocity as a function of superficial air velocity for the 12 mm ID tube for 16.66 % submergence using two different LTP at the middle of the tube 85
Figure 4.42. Snapshots comparing the base-line and LTP gas-liquid upward flow in 12 mm tube and S=4.16 % (a) Ugs = 10.89 m/s with 11 mm LTP. (b) Ugs = 10.9 m/s without LTP. (c) Ugs = 23.9 m/s with 11 mm LTP. (b) Ugs = 23.9 m/s base-line 86
Figure 4.43. Snapshots comparing the base-line and LTP gas-liquid upward flow in 12 mm tube and S=16.16 % (a) Ugs = 10.89 m/s with 11 mm LTP. (b) Ugs = 10.9 m/s without LTP. (c) Ugs = 23.9 m/s with 11 mm LTP. (b) Ugs = 23.9 m/s base-line 86
Figure 4.44 RMS versus superficial gas velocity observed for the base-line and two sizes of LTP located at ½ of depth (12 mm tube and S= 4.16 %) 87
Figure 4.45 RMS versus superficial gas velocity observed for the base-line and two sizes of LTP located at ½ of depth (12 mm tube and S= 8.33 %) 87
Figure 4.46 RMS versus superficial gas velocity observed for the base-line and two sizes of LTP located at ½ of depth (12 mm tube and S= 12.5 %) 88
Figure 4.47 RMS versus superficial gas velocity observed for the base-line and two sizes of LTP located at ½ of depth (12 mm tube and S= 16.6 %) 88
Figure 4.48. RMS of FBHP for 8 mm tube using 7 mm ID LTP for 4.16 % submergence level..... 89
Figure 4.49. RMS of FBHP for 8 mm tube using 7 mm ID LTP for 16.66 % submergence level..... 89

Figure 5.1 Calculated slug-churn transition boundary and the production characteristic determined in this study (D=20 mm S=16.66 %) 90

Figure. 5.2 Calculated slug-churn transition boundary and laboratory measured gas lift characteristic (D=12mm, S=16.6%) 91
Figure 5.3 Calculated slug-churn transition boundary and measured production characteristic for the 8 mm tube (air-water). 92
Figure 5.4 Calculated slug-churn transition boundary and measured characteristics for the 4 mm tube (air-water). 93
Figure 5.5 Calculated churn-annular transition boundary and visual observations. 94
Figure 5.6 Superficial velocity of liquid (water) versus air superficial velocity – laboratory (D=20 mm S=16.6%) versus modeled data (Ansari [10]) 94
Figure 5.7 The SDP [2,4] model developed for small diameter pipes (under pseudo-slug flow pattern) and present data obtained in laboratory (D=20 mm, S=16.6% or 50.8 cm H_2O) 95
Figure 5.8 Maximum transportation depth versus gas injected calculated with the SDP model [2,4] and present experiments (D=20mm, S=35% or 106.7 cm H_2O) 96
Figure 5.9 Calculated (Ansari [10] and Hasan [7]) and measured production characteristic (D=20 mm, S=35%) 96
Figure 5.10 Pressure drop versus gas injection experimental results and modeled data (Putra's [12] model) for churn flow pattern 98
Figure 5.11. Comparison between field data and Ansari model 99
Figure 5.12 Experimental results (D=20 mm, S=16.6%) and calculated data using Putra's model [12] 100
Figure 5.13 Experimental results (D=20 mm, S=12.5%) and calculated data using Putra's model [12] 101
Figure 5.14 Experimental results (D=20 mm, S=8.33%) and calculated data using Putra's model [12] 101
Figure 5.15 Experimental results (D=20 mm, S=4.16%) and calculated data using Putra's model [12] 102
Figure 5.16 Experimental results (D=12 mm, S=16.16%) and calculated data using Putra's model [12] 102
Figure 5.17 Experimental results (D=12 mm, S=8.33%) and calculated data using Putra's model [12] 103
Figure 5.18 Experimental results within churn flow and Putra's model prediction (8 mm tube and S=16.66 %) 103
Figure 5.19 Calculated and experimemental BHP versus superficial gas velocity (D=20 mm, S=16.6% , U(ls)= 0.18 m/s) 104
Figure 5.20 Calculated and experimental BHP versus superficial gas velocity data (D=20 mm, S=16.6% , U(ls)= 0.1 m/s) 104
Figure 5.21 Calculated and experimental BHP versus superficial gas velocity data (D=12 mm, S=16.6% , U(ls)= 0.042 m/s) 105
Figure 5.22 Calculated and experimental BHP versus superficial gas velocity data for various tube diameters (D=12 mm, S=16.6% , U(ls)= 0.042 m/s) 105
Figure 5.23 Suggested completion schematic for liquid unloading using small diameter tubes 108
Figure 5.24 Pressure versus depth for 20 mm and 12 mm ID tube removing 0.119 m^3/day of water 109

Figure 5.25 Superficial gas velocity versus depth calculations for 20 mm and 12 mm ID tube removing 0.119 m^3/day of water 109
Figure 5.26 Pressure versus depth calculations for 20 mm and 12 mm ID tube for the same liquid superficial velocities [U(ls)=0.0044 m/s] 110
Figure 5.27 Superficial gas velocity versus depth calculated for 20 mm and 12 mm ID tube for the same liquid superficial velocities [U(ls)=0.0044 m/s]. 110
Figure 5.28 Pressure versus depth caloculated for 20 mm and 12 mm ID (2.714 m^3/day of water removed) 111
Figure 5.29 Superficial gas velocity calculated for 20 mm and 12 mm ID tube (2.714 m^3/day of water removed) 111
Figure 5.30 Effect of the surface pressure in the prediction of pressure versus depth profile (20 mm tube – 2.714 m^3/day of water) 112
Figure 5.31. Effect of the surface pressure in the prediction of gas superficial velocity versus depth (20 mm tube – 2.714 m^3/day of water) 112

NOMENCLATURE

Symbol	
A	Cross section area of the pipe, (m^2)
FBHP	Flowing Bottom Hole Pressure, (psi)
C_o	Distribution coefficient. Usually Co=1.2
D	Internal tube diameter, (m)
d	Bubble diameter, (m, mm)
dP	Differential pressure
$\left\|\frac{dp}{dz}\right\|$	Absolute differential pressure with respect to the length (Pa/m)
f	Friction factor
f_M	Moody friction factor (Blasius Equation)
g	Acceleration of gravity, (m/s^2)
H	Holdup (Ansari's model)
"H"	Harmathy Bubble.
h	Length of Liquid column measured from the gas injection point, (m)
ID	Internal tube diameter, (m)
k	Constant (0.68 for drops, 1.14 for bubbles)
L	Tubing Length, (m).
LTP	Local Turbulent Promoter
P	Pressure (Pa)
Q	Flow rate, (m^3/s)
RMS	Root Mean Square
Re	Reynolds Number (dimensionless)
SDP	Small Diameter Pipe model
s	Submergence.
t	Time, (s)
T-D	Taylor-Dumitrescu Bubble

U	Velocity, (m/s)

Subscripts

g	Gas
L	Liquid

Superscripts

s	Superficial

Greek Symbols

$\bar{\alpha}$	Average void fraction
α	Void fraction
β	Ratio between the liquid slug length and the slug unit length (Ansari and Hasan's model)
δ_L	Film thickness, (m)
Δ	Difference (i.e. Difference of density, pressure, etc.)
ρ	Density (m^3/s)
μ	Viscosity (MPa.s)
σ	Surface tension, (N/m, Dyna/cm)

CHAPTER 1
INTRODUCTION

1.1 Overview

Marginal gas wells generally undergo liquid loading problems, which can cause the premature abandonment of a well/field before being fully exploited under present (price of gas and available new technologies) commercial conditions. This liquid accumulation besides of exerting additional backpressure on the well also can reduce the effective gas permeability around the perforations. A liquid inflow (brine) of only 0.119 m^3/day (1 bbl/day) that is not removed can create a back pressure of 280 kPa/day in a 6 in ID casing. Once the hydrostatic pressure due to the column of liquid that is being accumulated equals the reservoir pressure the gas well stops producing.

The liquid loading is also a common condition for Coal Bed Methane (CBM) wells, even at early stages of production, due to the low reservoir pressure of CBM reservoirs. The minimum reservoir pressure (or-net-liquid column height above the gas injector defined as submergence level) required for any conventional artificial-lift methods limits the possibilities to successfully unload a large number of gas wells with negative effect on ultimate gas recovery limit [1].

The present work is an extension of the investigation initiated at University of Alberta/Petroleum Department during 2002-2005 [2] particularly aiming at assessing the effectiveness of 4, 8 and 12 mm ID tubes to transport liquid under low submergence conditions.

This study encompass tube diameters up to 20 mm; a new compressed air sources have been installed to observe the liquid transportation when the flowrate of the injected gas is progressively increased to superficial velocities usually required for annular flow patterns. This created the possibility to closely investigate the stages of transition from bubble to slug and, then to annular flow patterns for a broad ranges of tube diameters and

reservoir pressures (submergence). The transition from slug to annular flow pattern being of considerable practical significance was given special consideration in this study.

1.2 Statement of the problem

1.2.1 Liquid Accumulation at the wellhead level (load-up)

In maturing gas fields, as a consequence of decreasing the pressure of gas reservoirs, the liquid (usually water produced by a nearby aquifer or commingled with gas or condensate formed in the upper zones of the well/tubing) starts accumulating in the bottomhole zone of the gas well. The detection of this problem is not always obvious [3]. A gas well may be partially load-up with liquids and still continues to produce gas before the gas production is totally interrupted. There are some signs that may indicate the existence of this problem such as abrupt decline in gas production and increment of liquid production.

It is unanimously accepted [3] that a minimum reservoir pressure is required for transporting the gas and water to the wellhead. Effective transportation of liquid from deeper wells and under lower pressure reservoirs requires a better understanding of mechanism of upward gas-liquid transportation and finding suitable artificial gas-liquid lifting technologies.

Assessment of the particular flow pattern is a prerequisite of better understanding and scaling the experimental data to field conditions. From practical point of view, effective and economic upward well transportation of gas and water is achieved as a slug or as an annular flow pattern. Usually the slug flow is preferred for transportation of relatively large amount of liquid during gas lift operations and annular flow is the preferred strategy for gas well unloading. However, due to important pressure-temperature decrease encountered during upward transportation of gas and liquid from deep wells, transition from slug to annular flow occurs with possible negative consequences on stability and transport effectiveness, particularly important for low pressure reservoir conditions.

Use and limitation of small diameter tubes for transporting a relatively small amount of liquid, but under low or extremely low reservoir pressure was presented and discussed [4]. A pseudo-slug flow pattern regime was observed, investigated and numerically modeled.

To observe and quantify transitions from slug to annular flow, this work considerably expands the physical conditions previously used for SDT. The effect of diameter to liquid transport effectiveness and changing the slug-to-annular flow pattern boundary position is observed and discussed.

Laboratory experiments are designed and performed to observe the effect of tube diameter, reservoir pressure, surface tension and of local turbulence promoters on gas-liquid upward transportation effectiveness. For scaling laboratory measurement to field conditions, existing mechanistic models are used and compared with experimental results.

1.3 Methods for liquid unloading

Both natural and artificial lifting is used for liquid unloading [3]. Cost-benefit applied to the particular conditions of a given well [5] is used to compare and select a certain unloading strategy. Depth of the well, reservoir pressure, amount of liquid to remove, gas production, and the nature of fluids are among key design conditions. The liquid produced and accumulated at the bottomhole level can be disposed (pumped) in an underneath formation or produced. For continuous production of liquid and gas, a well developed, "healthy" annular flow regime is the preferred solution. This requires maintaining the local (function of depth-pressure) gas velocity at a value exceeding the local critical calculated value. The "Turner" model is a well accepted method for calculating this critical (minimum required) gas velocity. To achieve this condition for the entire depth of the well/tubing the size of the tubing is sometimes changed or the well head pressure is altered. Foaming the gas, swabbing or siphon using compressed gas are also used for shallow wells situations.

The utilization of small diameter tubes (SDT) [4] combined with gas lift may be an economical alternative to remove relatively small volumes of liquids from low-pressure, shallow gas reservoirs. Fig. 5.23 suggests an unloading method using SDT, where liquid is separately produced through SDT and the gas is released in the annulus (casing-tubing) space. The application of this method could be continuous or intermittent depending on the necessity of liquid removal. A small compressor would be necessary for the gas lift system and the surface pressure for the SDT may be as low as possible. The use of SDT and conventional (1" or larger) tubes for unloading liquids depends on the prevailing mechanism controlling the gas-liquid transport. Annular flow pattern is the preferred way for conventional tubes, pseudo-slugs (alternating long bubbles and liquid plugs and a liquid film fallback) is considered when gas and liquid is transported upward with SDT. The conditions encountered during transition from slug (or pseudo-slug) flow pattern and developed annular flow are insufficiently described in the literature yet considered essential for controlling the liquid unloading operations.

1.4 Objective and scope of the research

The main objective of this research is to assess experimentally and analytically the effectiveness of removing liquids from very low-pressure reservoirs, particularly with SDT. The variables used in this experimental study include: diameter tube, surface tension, local turbulent promoters (LTP) and reservoir pressure. Each experiment is performed at almost constant reservoir pressure (indicated as submergence) and conducted during a progressive increase of gas flowrate. The liquid transport effectiveness is assessed as liquid produced versus injected gas rate.
Of particular interest is observing the conditions (flow-pressure) encountered during transition from slug (pseudo-slug) to annular during progressive increase of gas injected.

Surface tension was lowered from 0.072 N/m (tap water) to 0.047 N/m (water-methanol 60-40 %). The effect of local turbulence promoters (LTP) on liquid production was separately investigated. A turbulence promoter designed as a local diameter reduction (up

to 47 % cross-sectional area reduction) was manufactured of plastic sheet and inserted at pre-determined levels.

Reservoir pressure (submergence) was simulated in the laboratory by maintaining a certain level of water above the gas injector (positioned at the bottomhole level).

The level of fluctuations of the bottom hole pressure was quantified using the root mean square (RMS) procedure applied to a high-response pressure-related voltage signal.

Slug or pseudo slug as well as annular flow patterns have been observed frequently during the laboratory experiments; observing and assessing the transition from slug to annular (including the slug-to-churn transition stage) was given a special attention.

The boundary between flow patterns have been numerically calculated using existing models and compared with laboratory data. In order to accomplish the objectives mentioned the following has been completed:

1) Approximately 1320 experimental runs (including repetitions) have been performed and data processed using a consistent detailed procedure.
2) Literature review of mechanistic models frequently used for gas-liquid flow description.
3) Upgrade the existing flow loop to accommodate up to 20mm ID tubes and installation of a data acquisition system for continuous recording of the flowing bottomhole pressure (FBHP) average and momentary values (describing the pressure oscillation level).
4) Fabrication and installation of local turbulent promoters (LTP).
5) Record the FBHP for the whole range of air injected for each submergence level and performing RMS calculations.
6) Use the numerical models for the slug flow pattern developed by (Hasan[7] and Ansari[10]) and slug-to annular transition model developed by (Putra[12]) as well

as the annular flow pattern model suggested by (Ansari[10]) for comparing present and other (literature) experimental data.

7) Discuss the results and suggests the mechanistic models that better describes the laboratory experiments in view of potential field applications.
8) Compare and discuss existing slug-to-annular transition models
9) Perform video-recording of several experiments in order to analyze the flow patterns and obtain descriptive pictures from it.

1.4 Structure of the Thesis

Chapter 1 presents a general outline of the problem of unloading gas wells with very small reservoir pressures. It includes, overview, technologies for liquid unloading, statement of the problem, objectives and scope of the research.

Chapter 2 is a literature review of mechanistic models describing slug flow, churn flow and annular flow and transitions.

Chapter 3 explains the experimental program. It includes the details of the experimental set up, calibration procedure for pressure transducer and flowmeters, and test procedures for water-air, water –methanol-air and water-LTP-air tests.

Chapter 4 discusses the experimental results and major observations.

Chapter 5 presents and discuss numerical results of frequently used models described in chapter 2 as well as models employed in the former research[2] simulating present experiments.

Chapter 6 includes conclusions and recommendations.

CHAPTER 2

LITERATURE REVIEW

An overview of frequently used mechanistic models and their suitability for describing the present experiments is presented. Models that predict and explain the transition boundaries between the slug to annular two-phase flow patterns mainly encountered during this laboratory study are also reviewed.

The two-phase flow patterns frequently observed during this laboratory work are: slug, (churn as a transition stage from slug-to annular) and annular flow. In the field, they can occur simultaneously, at different level-pressure conditions, along the tube since the superficial gas velocity varies significantly with depth-pressure conditions. The aspect of the slug flow pattern observed in small diameter tubes is somewhat different with the slug flow pattern observed in conventional tubes [2]; however, mechanistic models used to explain and calculate transitions in conventional tubes are used throughout this investigation.

2.1 Slug Flow Pattern.

A typical representation of slug flow pattern is shown in fig. 2.1. It can be observed that most of the gas is contained in the Taylor-Dumitrescu (T-D) bubble and in the "Harmathy's" bubbles (usually – with conventional diameter tubes) found in the liquid slug. During the upward movement of the T-D bubbles a thin liquid falling back film continuously reduces the amount of liquid transported as slug between the T-D bubble train. This film mixes in the tail of the T-D bubble with the preceding liquid slug [6] prior to cascading to the lower slug zone. Most of the liquid transported upward is found in the slug sub-pattern (containing "H" bubbles). The thickness of back flowing liquid film is neglected by the majority of calculating models, however in small diameter tubes diminishing the amount of liquid during upward transport due to counter-current flow of the film is significant and considerably limits the depth of transportation [2]. Specific for SDP is the disappearance of "H" bubbles found in the slug zone (due to coalescence into

the T-D bubble); this lead to an altered slug flow pattern identified as "pseudo-slug". However, it was directly measured [2] and demonstrated that the terminal, ascending velocity of T-D bubbles demonstrated and measure (by D. Dumitrescu, 1943 and G. Taylor 1953) can be similarly calculated for SDT.

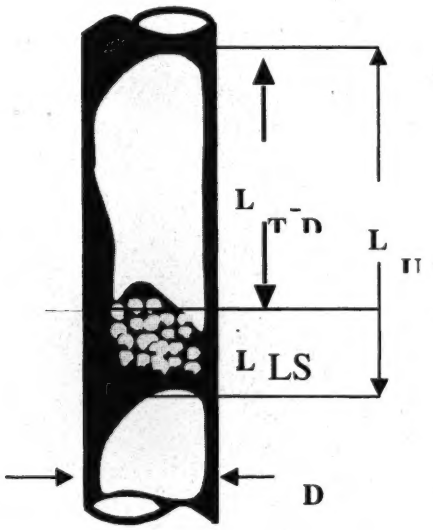

Figure. 2.1. Upward vertical slug flow

2.1.1 Slug flow modeling

2.1.1.1 Hasan's model [7]

The entire slug unit is divided in three main parts (fig. 2.1):
a) T-D bubble,
b) Liquid slug containing Harmathy bubbles.
c) fall-back liquid film.
To estimate the averaged void fraction, α an empirical correlation is used [8]:

$$\alpha = \frac{L_{T-D}}{L_U}\alpha_{T-D} + 0.25U_g^s \quad \text{for} \quad U_g^s \le 0.4\, m/s \qquad 2.1$$

$$\alpha = \frac{L_{T-D}}{L_U}\alpha_{T-D} + 0.1 \qquad \text{for} \quad U_g^s > 0.4\, m/s \qquad 2.2$$

In order to calculate the void fraction at each section of the slug unit and the local gas velocity U_g a drift-flux model [9] is applied. In the T-D bubble region the void fraction is calculated using equation 2.3.

$$\alpha_{T-D} = \frac{U_g^s}{U_{gT-D}} = \frac{U_g^s}{C_o U_m + U_{T-D\infty}} \qquad 2.3$$

In the liquid slug region the void fraction, α_{LS}, is calculated with the equation 2.4,

$$\alpha_{LS} = \frac{U_g^s}{U_{gLS}} = \frac{U_g^s}{C_o U_m + U_{t\infty}} \qquad 2.4$$

Where terminal velocities for the Harmathy and T-D bubbles are calculated by equations 2.5 and 2.6 respectively.

$$U_{t\infty} = 1.53\left[\frac{\Delta\rho g\sigma}{\rho_l^2}\right]^{0.25} \qquad 2.5$$

$$U_{T-D\infty} = 0.35\left(\frac{gD\Delta\rho}{\rho_l}\right)^{1/2} \qquad 2.6$$

The static and frictional pressure losses in the pipe are calculated as follows:

$$\left(\frac{dP}{dL}\right)_{friction} = \frac{f_M \rho_m U_m^2}{2D}(L_{T-D})\beta \quad , (\text{Pa}) \qquad 2.7$$

$$\left(\frac{dP}{dL}\right)_{static} = \rho_m g(L_{T-D}) \quad \text{, (Pa)} \qquad 2.8$$

β is the ratio between the liquid slug length, L_{LS}, and the slug unit length, L_U .

$$\beta = \frac{L_{LS}}{L_U} \qquad 2.9$$

2.1.1.2 Ansari's Model [7]

This model uses the mass balance of gas and liquid within the slug unit combined with empirical correlations. The slug flow is described in more detail than in Hasan's model and considers the liquid film velocity, which can be an important factor in the efficiency of liquid transporting. The liquid hold up is calculated independently for the TD bubble and liquid slug. The overall mass balance is expressed using eight unknowns quantities ($\beta, H_{LTD}, \alpha_{LS}, U_{gTD}, U_{LTD}, U_{GLS}, U_{LLS}, and\ U_{TD}$) and same number of equations. The following are the steps recommended by Ansari's model for solution:

1. The T-D bubble velocity ($U_{T\text{-}D}$) and liquid slug void fraction (α_{LS})are calculated as:

$$U_{TD} = 1.2U_m + 0.35\left[\frac{gD(\rho_L - \rho_G)}{\rho_L}\right]^{0.5} \qquad 2.10$$

$$\alpha_{LS} = \frac{U_g^S}{0.425 + 2.65U_m} \qquad 2.11$$

2. The liquid hold up (H_{LTB}) in the T-D bubble is obtained by solving 2.12

$$\left(9.916\sqrt{gD}\right)\left(1-\sqrt{1-H_{LTB}}\right)^{0.5} H_{LTD} - U_{TD}\left(1-H_{LTD}\right) + \overline{A} = 0 \qquad 2.12$$

$$\overline{A} = \alpha_{LS} U_{LTD} + \left(1-\alpha_{LS}\right)\left[U_m - \alpha_{LS}\left\{1.53\left[\frac{\sigma_L g\left(\rho_L - \rho_G\right)}{\rho_L^2}\right]^{0.25}\left(1-\alpha_{LS}\right)^{0.5}\right\}\right] \qquad 2.13$$

3. The liquid fall back velocity U_{LTD} is determined by 2.14[11].

$$U_{LTD} = \sqrt{196.7\ g\ \delta_L} \qquad 2.14$$

δ_L is the geometrical average film thickness along the T-D bubble and is calculated by 2.15:

$$\delta_L = \frac{D}{2}\left(1-\sqrt{\alpha_{TD}}\right) \qquad 2.15$$

4. The liquid velocity in the liquid slug (U_{LLS}) is obtained by equation 2.16

$$\left(U_{TDCC} - U_{LLS}\right) H_{LLS} = \left[U_{TD} - \left(-U_{LTD}\right)\right] H_{LTD} \qquad 2.16$$

5. The liquid slug void fraction, α_{LS}, is calculated by the following equation

$$U_{gLS} = 1.2U_m + 1.53\left[\frac{g\sigma_L\left(\rho_L - \rho_G\right)}{\rho_L^2}\right]^{0.25}\left(1-\alpha_{LS}\right)^{0.5} \qquad 2.17$$

6. α_{TB} is obtained by equation 2.18

$$\left(U_{TD} - U_{gLS}\right)\left(1-H_{LLS}\right) = \left(U_{TD} - U_{gTD}\right)\left(1-H_{LTD}\right) \qquad 2.18$$

7. Equation 2.19 is solve for β

$$U_{LS} = (1-\beta)U_{LLS}H_{LLS} - \beta U_{LTD}H_{LTD} \qquad 2.19$$

8. Static and frictional pressure losses are calculated as a function of β

$$\left(\frac{dP}{dL}\right)_{friction} = \frac{f_{LS}\rho_{LS}.U_m^2}{2D}.(1-\beta) \quad , (\text{Pa/m}) \qquad 2.20$$

$$\left(\frac{dP}{dL}\right)_{static} = ((1-\beta).\rho_{LS} + \beta\rho_g).g \quad , (\text{Pa/m}) \qquad 2.21$$

2.2 Slug to Annular Flow Pattern Transition in Vertical Tubes

The first stage of this transition is commonly called churn pattern and, due to difficulties encountered when direct laboratory observations are used to assess the transitions, is one of the most controversial flow patterns. The gas velocity range at which slug-to-annular transition occurs appears to be greater than the range of superficial gas velocity during the bubble-to-slug transition and is not well defined as yet.

2.2.1 Slug - Churn Pattern Boundary Modeling

The transition region is highly disturbed and large waves flow up the channel mix together with regions of falling liquid films [13]. The occurrence of backward flow is what makes the transition flow better differentiate from annular flow as shown in figure 2.3. Yet there is a continuous gas core for both cases [14]. The transition is more irregular when is closer to the slug flow than when is closer to annular flow. This boundary has also been considered as unstable slug [15].

Van Hout [16] defines three regions in the liquid slug as in fig. 2.3. These are the wake region, developed region and the intermediate region. The wake region is populated of

bubbles where turbulence is high and the void fraction is relatively large [13]. The developed region is more like bubbly flow and the void fraction is similar to that. Between the two regions mentioned there is an intermediate one, which is fed by bubbles coming from the center of the wake region and then split around. When more gas is injected into the system the wake region becomes larger and more turbulent while the developed region becomes smaller [13]. When this region almost disappears the turbulence in the wake region starts affecting the Taylor- Dumitrescu bubble coming behind as shown by a dashed line in fig. 2.3. At this point the liquid slug turns out to be too gassy making it quite sensitive to be broken by a little increment of gas injection and subsequently the Taylor- Dumitrescu bubble is distorted.

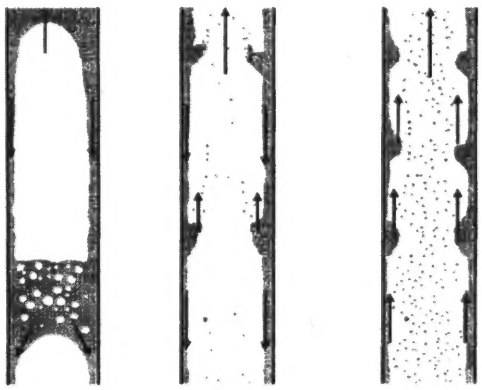

Figure. 2.2. The slug, churn and annular flow regimes in vertical upwards annular gas-liquid flows [14].

Van Hout [16] concluded from his experiments that when the liquid slug length is as low as 15 percent of the entire slug the flow is very close to boundary between slug and transition flow. Other workers as Brauner and Barnea [17] suggested the boundary to take place when the void fraction in the liquid has reached its maximum cubic packing considering the bubbles perfect spheres. This maximum packing possible occupies 52 percent of the total volume. Later on experiments conducted by Barnea and Shemer in 1989 suggests these values to be among 0.52 and 0.60.

Chen and Brill [13] consider these values to be α_s <= 0.52 (void fraction in the liquid slug) and β_s <= 0.15 which is the ratio between liquid slug length and the entire length of the slug.

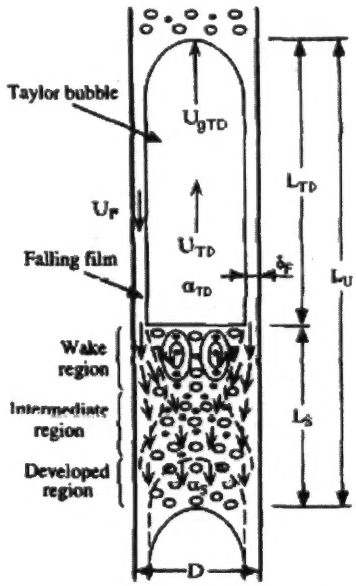

Figure. 2.3. Transition from slug flow to churn flow [13]

To mathematically determine the superficial gas velocity for which takes place the transition for a given superficial liquid velocity they assume that the slug unit is incompressible and that the two-phase flow along the slug unit is the same at any cross section. As the two- phase flow approaches the slug-churn transition the slippage between the bubbles and liquid in the liquid slug becomes negligible. A volumetric balance at the Taylor-Dumitrescu Bubble yields:

$$U_l^s + U_g^s = \alpha_{TD} U_{TD} - (1 - \alpha_{TD}) U_F \qquad 2.22$$

Where U_l^s and U_g^s are the superficial liquid and gas velocities respectively, α_{TD} is the void fraction in the Taylor- Dumitrescu bubble section and U_{TD} is the gas velocity within

the Taylor-Dumitrescu Bubble. U_F is the liquid film velocity around the Taylor - Dumitrescu bubble .

If the slug flow is fully developed U_F can be calculated as a free falling film and in this case the thickness of the film, δ_F, is constant and can be determined using a geometric relation in terms of diameter of the tube, D, and the void fraction, α_{TD}, at the Taylor Dumitrescu bubble section assuming that there is no entrained gas in the film as follows:

$$\delta_F = \frac{\left(1-\alpha_{TD}^{0.5}\right)D}{2} \qquad 2.23$$

Utilizing the expression equation by Wallis [17]:

$$\delta_F\left[\frac{(\rho_L-\rho_G)g}{\rho_L v_L^2}\right]^{\frac{1}{3}} = kR_{eF}^{\ m} \qquad 2.24$$

U_F can be estimated since Reynolds number of the film, R_{eF}, is a function of it. Brill and Chen [13] introduced the turbulent coefficients k and m recommended by Fernandes [19] (k=0.0682, m=0.67). After solving equation 2.24 for U_F and substituting the constants for turbulent flow it yields:

$$U_F = 9.916\left[\frac{gD\left(\rho_l-\rho_g\right)\left(1-\alpha_{TD}^{0.5}\right)}{\rho_L}\right]^{0.5} \qquad 2.25$$

To calculate the transport velocity Nicklin's [9] drift velocity equation is used:

$$U_{g_{T-D}} = 1.2\left(U_l^s + U_g^s\right) + 0.35\left[\frac{gD\left(\rho_L-\rho_g\right)}{\rho_L}\right]^{\frac{1}{2}} \qquad 2.26$$

When doing a mass balance of the gas over the whole slug unit it can be written as:

$$U_g^s = \alpha_s \beta_s \left(U_l^s + U_g^s\right) + U_{TD}\alpha_{TD}\left(1-\beta_s\right) \qquad 2.27$$

If a moving reference system is considered to be in the Taylor - Dumitrescu bubble with a velocity, $U_{gT\text{-}D}$, and doing a gas balance relative to this system yields:

$$\alpha_{TD} = \frac{\alpha_s U_{gT-D} - \alpha_s \left(U_l^s + U_g^s\right)}{U_{gT-D} - U_{TD}} \qquad 2.28$$

Solving for U_{TD} after combining 2.27 and 2.29 it is obtained:

$$U_{TD} = \frac{\alpha_s L_s U_{gT-D}\left(U_l^s + U_g^s\right) - U_g^s U_{gT-D}}{-U_g^s + \alpha_s \beta_s \left(U_l^s + U_g^s\right) - \alpha_s \left(1-L_s\right)\left(U_T - U_l^s - U_g^s\right)} \qquad 2.29$$

With equations 2.2, 2.25, 2.26, 2.28 and 2.29 can be estimated the superficial gas velocity for a known value of superficial liquid velocity.

Equation 2.30 presents a correlation proposed by Tengesdal for the slug to churn flow boundary which was developed to fit experimental data [20]. For this correlation the overall void fraction in the slug unit is considered to be 0.78 which is the transition value of the void fraction from slug to churn for this case.

$$u_g^s = 12.19\left(1.2u_l^s + 0.345\sqrt{gD\frac{\rho_L - \rho_g}{\rho_L}}\right) \qquad 2.30$$

2.2.2 Transition to Developed Annular Flow (STA)

The most accepted "deliquification" criteria recommended for assessing the "minimum gas velocity" required for producing the liquid resulted during gas production , the "Turner" (or "T-H-D" model [21]) calculates the critical gas velocity required for obtaining a "developed annular" flow pattern.

Two flow conditions are required for calculating this transition:

a. The upward gas velocity should exceed the velocity required to support the larges droplet (formed through atomization of liquid film-gas core interface),

b. The largest droplet formed through atomization of wavy interface is the result of the ratio of dynamic and surface tension forces (defined as Weber number) – The balance of drag and gravity forces acting on a spherical liquid drop [22] is Indicated in eq. 2.31:

$$C_d \frac{\pi d^2 \rho_g U_g^{s\,2}}{2} = \frac{\pi d^3}{6} g(\rho_l - \rho_g) \qquad 2.31$$

The gas superficial velocity for which the transition from churn to annular pattern occurs (eq. 2.32), U_g^s , [21] depends on the density of the liquid droplets, ρ_l, the acceleration of gravity, g, the diameter of larger droplets, d, and a drag coefficient, C_d ($C_d \approx 0.4$ for high-Reynolds number situations, typical for transition to annular flow):

$$U_g^s = \sqrt{\frac{4gd(\rho_l - \rho_g)}{3C_d \rho_g}} \qquad 2.32$$

A droplet of diameter, d, a will be transported upward by the gas exceeding the velocity indicated by equation 2.32[17]. Atomization of the wavy interface (between the upward liquid film and the core of gas-droplets) is controlled by the equilibrium between dynamic and surface tension forces (Weber number eq. 2.33):

$$We = \frac{U_g^{s\,2} \rho_g d}{\sigma} \qquad 2.33$$

Turner [24] indicated that the transition to developed annular flow requires A minimum, critical Weber number of 30, where the droplet diameter d is the largest obtained in the spectrum of droplet size resulted from atomization of liquid film [23]. After combining equations 2.32 and 2.33 the transition velocity is obtained:

$$U_g^s = 3.01 \frac{g^{0.25}\sigma^{0.25}(\rho_l - \rho_g)^{0.25}}{\rho_g^{0.5}} \qquad [21] \qquad 2.34$$

Reversal of the flowing direction of liquid film (from downwards as specific to slug flow to upwards as in annular flow pattern) offers a good criteria for defining the occurrence of the onset of transition from churn to developed annular flow pattern. The flow reversal of liquid film is observed through a minimum of liquid entrainment of liquid in the core.

J.R. Barbosa Jr. and G.F. Hewitt [25], by measuring the amount of droplets entrained from the upward liquid film in the gas core, determined that the minimum of liquid entrained in the gas core occurs at $U_g^{s*} \approx 1$ (equation 2.35) regardless of the amount of liquid injected (fig. 2.4 and 2.5). The minimum value observed in the "U"-shaped curve describing the dimensionless liquid transported versus superficial gas velocity corresponds to the onset of developed annular flow. As the amount of liquid transported in the upward flowing of liquid film is relatively negligible when compared to the liquid transported as droplets, fig. 2.4 and 2.5 suggest that the during this transition, the total amount of liquid transported exhibit a minimum value.

The transition velocity for the onset of developed annular flow pattern by the flow reversal approach [26] is determined as follows:

$$U_g^s = \frac{1}{U_g^{s^*}} \sqrt{\frac{gD(\rho_L - \rho_g)}{\rho_g}} \qquad 2.35$$

Where $U_g^{s^*} \approx 1$ (dimensionless) at the point of the transition from churn to annular flow [27].

The entrainment fraction of droplets tends to lower when increasing the dimensionless gas superficial velocities until the entire film is flowing upward (fig. 2.4). The minimum

value of liquid entrained fraction increases with the total amount of liquid injected, but its position with respect to superficial gas velocity is almost the same (fig.2.4).

J.R. Barbosa Jr. and G.F. Hewitt [25] state that this behavior is probably due to two competing mechanisms of droplets entrainment (of different magnitudes depending on the gas velocitiy). Azzopardi [28] identified these two mechanisms of droplet entrainment as: a. at relatively low gas velocities, open-ended bubbles are formed and then burst due to the action of the gas undercutting large (rolling) waves; b. at much higher gas velocities, the crest of the wave is moved upward by the gas breaking into drops [25]. Experiments conducted by James [29] found that large droplets created by the first mechanism tend to have a tendency of being re-deposited while droplets created by the second mechanism tend to have a much higher residence time in the gas-droplet core.

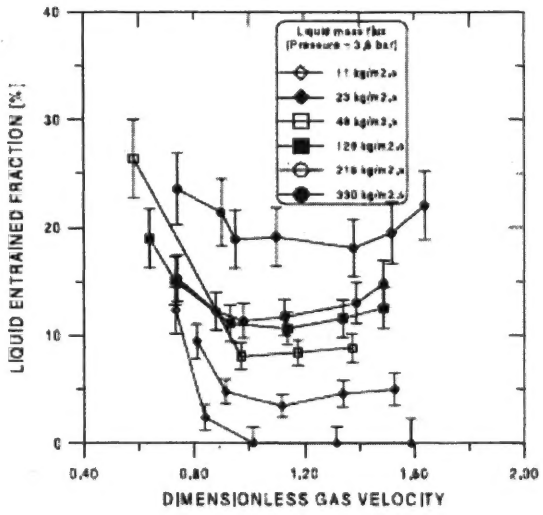

Figure 2.4. Liquid entrained fraction as a function of the total liquid mass flux: p = 2 bara (approximately 200 kPa) [25]

Fig. 2.5 compares the fraction of liquid entrained and the pressure gradient measured against dimensionless gas velocity and suggests that a minimum values for the two curves occurs at the same (dimensionless) gas velocity.

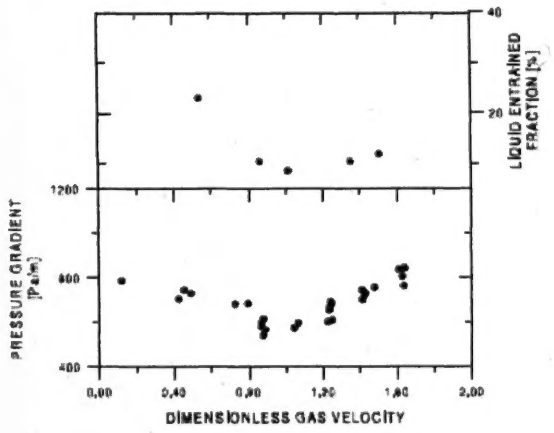

Figure. 2.5. Entrainment and experimental pressure gradient in the churn–annular region: p = 2 bara (200 kPa), m_L = 47 kg m^2 s^{-1} [23]

2.3 Modeling of Slug-to-Churn Transition Stage

Isshi and Mishima [30] (slug-to-churn transition stage) model was further adapted and simplified for isothermal flow conditions by Putra [12]. The two-fluid model [12] describes the mass and momentum balances for each phase as well as the inter-phase interactions. The interaction between the phases is flow pattern dependant.
The momentum balance is represented by the following expression:

$$\frac{\partial(\rho_k \alpha_k u_k)}{\partial t} + \frac{\partial(\rho_k \alpha_k u_i^2)}{\partial x} = -(M_{ik} + \tau_i) \qquad 2.36$$

Mass balance:

$$\frac{\partial(\rho_k \alpha_k)}{\partial t} + \frac{\partial(\rho_k \alpha_k u_i)}{\partial x} = 0 \qquad 2.37$$

The subscript k represents the phase; M_{ik} groups the interfacial drag forces on phase k and τ_i is the interfacial shear stress.

The acceleration term in the momentum balance can be neglected since it is small compared to the other factors contributing to the pressure gradient in the churn flow pattern. The terms that are time dependant can be cancelled out as well since a steady-state flow is considered.

Rewriting the momentum equation for each phase under the assumptions made it yields:

Gas phase:

$$F_{ig} + F_{wg} + F_{gg} + \alpha \frac{\partial P}{\partial x} = 0 \qquad 2.38$$

Liquid phase:

$$F_{il} + F_{wl} + F_{gl} + (1-\alpha)\frac{\partial P}{\partial x} = 0 \qquad 2.39$$

The interface drag forces (per unit of volume) F_{ig} and F_{il} have the same magnitude and opposite directions. F_{wg} is the friction force (per unit of volume) between the gas and the wall and can be considered zero since it is the liquid phase which is most in contact with the wall[31]. F_{wl} is the friction force (per unit of volume) between the liquid phase and the wall of the tube. F_{wg} and F_{gl} are the static forces (per unit of volume) due to the acceleration of gravity.

After combining equations 2.38 and 2.39 is obtained:

$$-(1-\alpha)F_{gg} - F_{ig} + \alpha F_{wl} + \alpha F_{gl} = 0 \qquad 2.40$$

2.3.1 Estimation of the Drag Force

The most critical term in the equation 2.40 is F_{ig} which is highly dependent on type of interaction between the two phases.

Generally, a drag force that acts on a particle can be written as follows:

$$F_d = \frac{1}{2}\rho_c C_d U_r |U_r| A_d \qquad 2.41$$

Where ρ_c is the density of the continuous phase, C_d is the drag coefficient (dependent on the interaction nature between continuous and dispersed phases), U_r is the relative velocity between the dispersed and the continuous phase and A_d is the projected area of a typical particle of the dispersed phase.

Ishiii and Mishima [30] came out with the following equation to account for drag force transferred from the liquid to the gas phase.

$$F_{ig} = \frac{1}{8}\rho_l a_i C_d \left(\frac{r_{sm}}{r_D}\right)(U_g - U_l)|U_g - U_l| \qquad 2.42$$

$\frac{r_{sm}}{r_D}$ is the ratio of Sauter mean radius to maximum radius of a particle r and is equal to 1 for a spherical shape. Putra [12] uses a value of 0.05 for liquid superficial velocities leas than 0.2 m/s and 0.1 for bigger liquid superficial velocities. This is in order to represent the shape of the particles of the dispersed phase (liquid) in the churn flow.

Kocamustafaogullari and Ishi [32] defined the interfacial area per volume of the mixture, a_i, either for slug o churn-turbulent flow as:

$$a_i = \frac{4.5}{D}\left(\frac{\alpha - \alpha_s}{1-\alpha_s}\right) + \frac{3\alpha_{gs}}{r_{sm}}\left(\frac{1-\alpha}{1-\alpha_s}\right) \qquad 2.43$$

α_s is the void fraction in the liquid slug, α is the average void fraction in the slug unit, r_{sm} is Sauter mean radius and D the diameter of the tube. The Taylor bubble is

represented by the first term of equation and the bubbles in the slug by the second term. In order to make the equation more specific for churn flow a roughness parameter equal to 1.1 is introduced [12].

The void fraction in the liquid slug can be calculated using the correlation suggested by kurul and Podowski [33] as follows:

$$\alpha_s = \begin{Bmatrix} \alpha & (0 \le \alpha < 0.25) \\ 0.3929 - 0.5714\alpha & (0.25 \le \alpha < 0.6) \\ 0.05 & (0.6 \le \alpha < 1) \end{Bmatrix} \quad 2.44$$

Kocamustafaogullari and Huandg [34] give the Sauter mean radius by:

$$r_{sm} = 0.53\left(\frac{\sigma}{\rho_l^{\frac{1}{3}}}\right)^{\frac{1}{3}}\left\{\frac{\alpha(1-\alpha)D^2}{U_m\left(\frac{dp}{dz}\right)_{two-phase}}\right\}^{\frac{2}{9}} \quad 2.45$$

Where $\left(\frac{dp}{dz}\right)_{two-phase}$ can be calculated utilizing the Martinelli-Nelson pressure drop correlation as follows;

$$\left(\frac{dp}{dz}\right)_{two-phase} = \phi_g^2\left(\frac{dp}{dz}\right)_g^s \quad 2.46$$

And,

$$\phi_g^2 = \frac{1}{\alpha_{Martinelli}^{5/2}} \quad 2.47$$

Where $\alpha_{Martinelli}$ can be correlated by [12]:

$$\alpha_{Martinelli} = \left(1 + X^{0.8}\right)^{-.0378} \quad 2.48$$

And,

$$X = \frac{\left(\frac{\partial p}{\partial z}\right)_l^s}{\left(\frac{\partial p}{\partial z}\right)_g^s}^{0.5}$$

2.49

Utilizing the Ishii's correlation [30] for the drag coefficient it yields:

$$C_d = \frac{8}{3}\left(1-\left(\frac{\alpha-\alpha_s}{1-\alpha_s}\right)\right)^2 \qquad 2.50$$

2.3.2 Friction and Gravity Forces Calculation

As stated the friction forces against the wall of the tube are mainly due to the interaction liquid-wall and can be calculated as follows:

$$F_{wl} = \left(\frac{\partial P}{\partial x}\right)_f = f\frac{\rho_l u_l^2}{2D} \qquad 2.51$$

Where,

$$f = \begin{cases} \dfrac{64}{R_e} & \text{if } R_e \le 2100 \\ \dfrac{0.184}{R_e^{0.2}} & \text{if } R_e > 2100 \end{cases} \qquad 2.52$$

And,

$$R_e = \frac{DU_l}{\upsilon_l} \qquad 2.53$$

The gravity forces are generated by the weight of the column of water and column of gas and it can be calculated as follows:

Gas phase:

$$F_{gg} = \alpha \rho_g g \qquad 2.54$$

Liquid Phase:

$$F_{gl} = (1-\alpha)\rho_l g \qquad 2.55$$

The void fraction is the only unknown and can be obtained by iterating with void fraction values and simultaneously solving equations 2.40 to 2.55 until equation 2.40 is satisfied.

2.4 Annular two-phase flow pattern

In this flow, which is developed at high superficial gas velocities, there is a liquid film and a gas core as illustrated in fig. 2.7. There could be presence of gas bubbles in the film as well as liquid droplets in the gas core. As mentioned the interface between the gas and the liquid film tends to be very wavy where, atomization and deposition of liquid droplets occur.

2.4.1 Ansari's Model

This approach is very similar to Alves's model [35] where some ideal assumptions are made in order to simplify the model as follows:

a. Isothermal conditions and fully developed annular flow
b. Film thickness,δ, is considered constant
c. Homogeneous flow in the gas core (none slip velocity between droplets and gas).
d. Incompressible fluids.

e. Negligible acceleration forces which means that the effective velocity of the two-phase transportation does not change significantly with time.

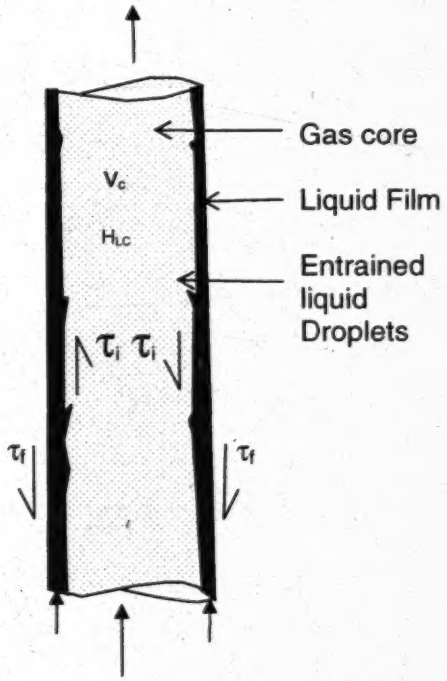

Figure 2.6. Annular flow pattern.

Taking as a reference figure 2.7 and with the above assumptions the linear momentum balance on gas core and the liquid film is given by equations 2.56 and 2.57.

$$A_c\left(\frac{dp}{dL}\right)_c - \tau_i S_i - \rho_c A_c g \sin\theta = 0 \qquad 2.56$$

$$A_F\left(\frac{dp}{dL}\right)_F + \tau_i S_i - \tau_F S_F - \rho_L A_F g \sin\theta = 0 \qquad 2.57$$

ρ_c is the density of the core and is calculated as homogeneous flow as follows:

$$\rho_c = \rho_L(1-\alpha_c) + \rho_g \alpha_c \qquad 2.58$$

Hence the liquid fraction, $(1-\alpha_c)$, in the core can be obtained by equation 2.59:

$$(1-\alpha_c) = \frac{F_E U_l^s}{U_l^s + F_E U_g^s} \qquad 2.59$$

Where F_E the fraction of liquid entrained in the core and is correlated by Wallis' equation [18].

$$F_E = 1 - e^{[-0.125(U_{crit}-1.5)]} \qquad 2.60$$

$$\text{Where } U_{crit} = 10000 \frac{U_g^s \mu_g}{\sigma_L} \left(\frac{\rho_g}{\rho_L}\right)^{1/2} \qquad 2.61$$

The film shear stress in equation 2.57 is calculated as follows for Moody friction factor:

$$\tau_F = (f_M)_F \rho_L \frac{U_F^{\ 2}}{8} \qquad 2.62$$

The Reynolds number for the film is:

$$\mathrm{Re}_F = \frac{\rho_L U_F^{\ 2} d_{HF}}{\mu_L} \qquad 2.63$$

Where the film velocity is given by:

$$U_F = \frac{q_L(1-F_E)}{A_F} = \frac{U_l^s(1-F_E)}{4\bar{\delta}(1-\bar{\delta})} \qquad 2.64$$

The hydraulic diameter of the film:

$$d_{HF} = 4\bar{\delta}(1-\bar{\delta})D \qquad 2.65$$

Substituting 2.90 in 2.79 yields:

$$\tau_F = \frac{f_F}{8}(1-F_E)^2 \rho_L \left[\frac{U_L^s}{4\delta(1-\bar{\delta})}\right]^2 \qquad 2.66$$

Expressing the film shear stress in terms of the superficial liquid pressure drop $\left(\frac{dp}{dl}\right)_{SL}$ yields:

$$\tau_F = \frac{D(1-F_E)^2}{4\left[4\bar{\delta}(1-\bar{\delta})\right]^2} \frac{f_F}{f_{SL}} \left(\frac{dp}{dl}\right)_{SL} \qquad 2.67$$

Where $\left(\frac{dp}{dl}\right)_{SL} = \frac{f_{SL}\rho_L U_L^{s\,2}}{2D}$ 2.68

Superficial liquid Reynolds number is expressed by:

$$\mathrm{Re}_{SL} = \frac{\rho_L U_L^s D}{\mu_L} \quad 2.69$$

The shear stress between at the interface in equations 2.56 and 2.57 is calculated as follows:

$$\tau_i = f_i \rho_c \frac{U_c^{\,2}}{8} \quad 2.70$$

Where the core velocity is obtained by:

$$U_c = \frac{U_{sc}}{\left(1-2\bar{\delta}\right)^2} \quad 2.71$$

The friction factor at the film-core interface is a function of the friction factor (expressed with superficial velocity of gas), f_{sc}, and a factor Z calculated using Wallis's expression [17] for high liquid entrainment and Whalley- Hewitt's expression [36] for low liquid entrainment fraction (see F_E eq.2.60):

$$f_i = f_{sc} Z \quad 2.72$$

$$Z = 1 + 300\bar{\delta} \qquad for \qquad F_E > 0.9 \quad 2.73$$

$$Z = 1 + 24\left(\frac{\rho_L}{\rho_g}\right)^{1/3} \bar{\delta} \qquad for \qquad F_E < 0.9 \quad 2.74$$

Substituting equation 2.70 in 2.71 and expressing in terms of superficial core pressure drop is obtained:

$$\tau_i = \frac{D}{4}\frac{Z}{\left(1-2\bar{\delta}\right)^4}\left(\frac{dp}{dL}\right)_{sc} \quad 2.75$$

The superficial core Reynolds number is given by:

$$\mathrm{Re}_{SC} = \frac{\rho_c U_c^{s\,2} D}{\mu_c} \quad 2.76$$

Where $U_c^s = F_E U_L^s + U_g^s$ 2.77

The average viscosity of the gas-droplets (assumed homogeneous flow) core is given by:

$$\mu_c = \mu_g \alpha_c + \mu_L (1 - \alpha_c) \qquad 2.78$$

Solving 2.73 for effective core pressure drop, $\left(\frac{dp}{dL}\right)_c$, after having substituted τ_i, the interface wetted perimeter, S_i, the cross-sectional core area, A_c, in 2.73 is otained:

$$\left(\frac{dp}{dL}\right)_c = \left(\frac{Z}{(1-2\bar{\delta})^5}\right)\left(\frac{dp}{dL}\right)_{sc} + \rho_c g \sin\theta \qquad 2.79$$

Similarly solving 2.74 for $\left(\frac{dp}{dL}\right)_f$, after having substituted τ_i, τ_F, S_i, cross-sectional film area A_F, and the wall wetted perimeter S_F is obtained:

$$\left(\frac{dp}{dL}\right)_f = \frac{f_f}{f_{sL}}\left(\frac{(1-F_E)^2}{64\delta(1-\bar{\delta})^3}\right)\left(\frac{dp}{dL}\right)_{sL} - \left(\frac{Z}{4\delta(1-\bar{\delta})(1-2\bar{\delta})^3}\right)\left(\frac{dp}{dL}\right)_{sc} + \rho_L g \sin\theta \qquad 2.80$$

Assuming that there is equilibrium in the flow the pressure drop occurring at the core is equal to the pressure drop at the film. Therefore equations 2.79 and 2.80 can be equated and solved for the film thickness,δ, since it is the only variable. Then the total pressure drop can be calculated with either equation 2.79 or 2.80.

CHAPTER 3
LABORATORY EQUIPMENT AND EXPERIMENTAL PROGRAM

3.1 Experimental set up

The flow loop at University of Alberta, previously used for assessing the gas lift effectiveness with small diameter tubes [2] was upgraded for tubes up to 20 mm ID and for high-speed pressure recording and used for the experiments in this study. The following modifications have been made to the flow loop:

- In addition to the existing 4,8,12, mm ID tubes (previously used [2]), the system was upgraded to accommodate 20 mm ID PVC tube
- An additional line was installed to measure the flowing bottomhole (FBHP) and static pressures (fig. 3.1, section # 7, and fig. 3.4).
- The air source was upgraded in order to increase air pressure from 60 to 100 psig.

The apparatus is composed of five main sections (fig. 3.1):

Section #1 is a vertical storage tank A 6 inches (15.24 cm) OD x 10 feet long (304.8 cm) clear PVC pipe is used. A pre-determined water level is selected for each experiment to provide the desired "reservoir pressure" or submergence.

Section #2 is a 2 inches (50.8 cm) OD clear PVC pipe, which connects the storage tank to the air injection section,

Section #3 is the 2" PVC pipe gas-liquid injection/mixing device..
Compressed air is injected through a nozzle, #6, coaxially located inside the riser. This design allows the air to flow freely inside the riser and avoid air-water blockage at the entrance.

Section #4,contains the observation tubular element and is designed to accommodate various diameters of tubes. Clear PVC tubes of 20 mm,12 mm, 8.0 mm and 4 mm ID were used for the present work.

Section #5 is the gas-liquid separator located at the top of the apparatus. It is built from 2" ID clear PVC. The air separated from the liquid is piped to a vent. The water is collected in the annulus section formed by the riser and the receiving tube in the separator, (fig. 3.1 #15). The test could be run in a closed or open loop depending on whether the liquid production is required for the experiment or not. Once the water overflows the chamber #5 it has two possible paths, to return the storage tank #1, or to be collected in the liquid collector #12 and weighted..

The liquid collector #12 receives the water from the production line. The receiving cup rests on an electronic scale, #10programmed to display the flow rate in Kg/min. The scale had a precision of ±0.2 g.

The air flow rate is measured in section # 9; (see section 3.4 for details equipment details). The injected air pressure is measured (Fig. 3.3, #8,) using a "Validyne"® pressure transducer with a 75 psi diaphragm. For the FBHP and static pressure a 5 psi diaphragm was used.

Seven parameters were monitored: (1) Air flow rate, (2) liquid flow rate, (3) atmospheric pressure, (4) temperature, (5) injected air pressure, (6) reservoir pressure and (7) bottom pressure of the observation tubing. In addition, the air-liquid surface tension was separately measured using a Du-Nouy ring tensiometer and a precision scale.

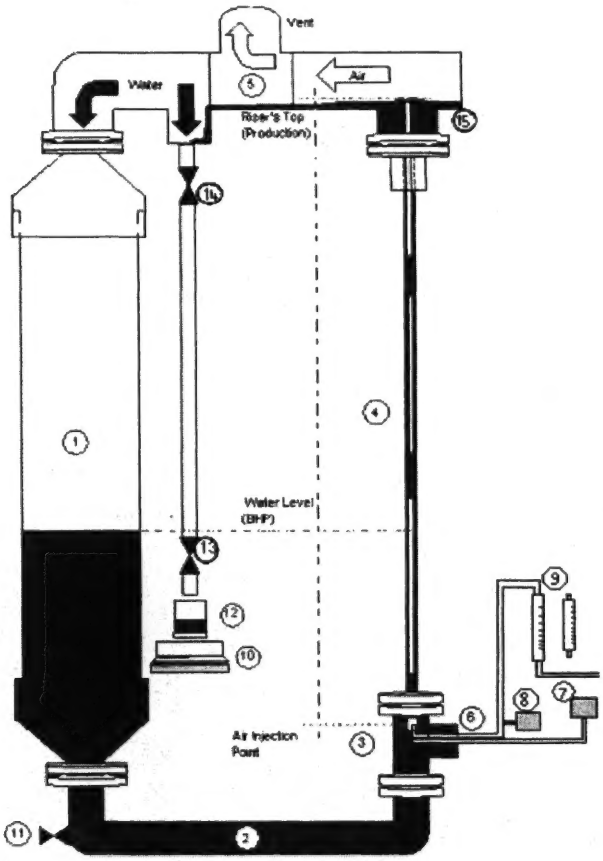

Figure. 3.1 Experimental set up

3.1.1 Turbulent Promoters

The local turbulent promoters (LTP) were built from a thin (less than 1 mm) plastic sheet. Fig. 3.2 is a sketch of LTP. The LTPis inserted at the desired level in the PVC observation tube (riser) (fig. 3.3). Two different LTP sizes were used for the 12, and 20 mm ID tubes and one size for the 8 mm tube as shown in table 3.1

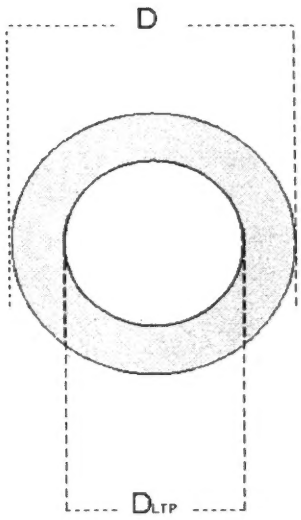

Figure 3.2. The Local Turbulent Promoter (LTP)

Table 3.1. LTP sizes for the tubes utilized.

ID LTP (mm)	ID Tube (mm)	Area Reduction %
19	20	9.75
17	20	27.75
11	12	15.97
9	12	43.75
7	8	23.44

Figure 3.3. View of the LTP during gas-liquid upward lifting

3.2 Pressure Transducer Calibration

The two Validyne® pressure transducers (Fig. 3.4) used for bottom hole pressure measurements and air pressure are equipped with high sensitive stainless steel membranes rated in accordance to the range of pressure to be measured.

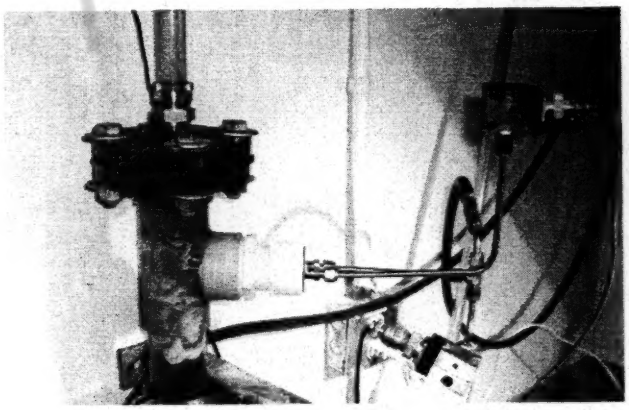

Figure 3.4 Pressure transducers for FBHP and air line

The calibration of pressure transducers was performed with an Omega® DPI 610 (Fig. 3.5).A precision of ±0.025 psi is obtained.

The signal conditioning box has an output of 0 to 5 Volts. The calibration process consists of a consecutive adjustment of "zero" and "span" calibration screws in such a way that the maximum and minimum pressure values will be equivalent to 0 and 5 volts, respectively. The calibration curves are linear and are shown in figs 3.6 and 3.7

Figure 3.5. Omega® DPI 610 pressure calibrator

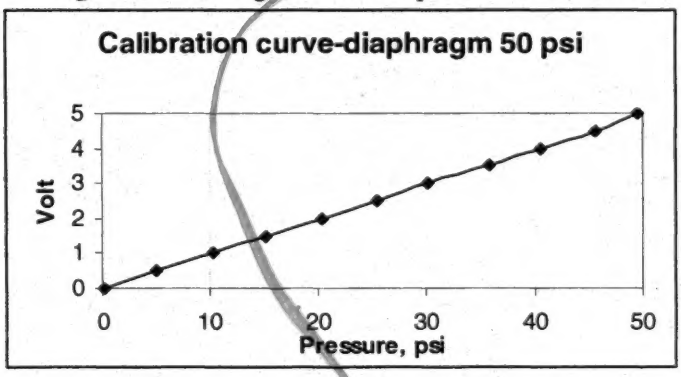

Figure 3.6. Calibration curve for the 50 psi diaphragm.

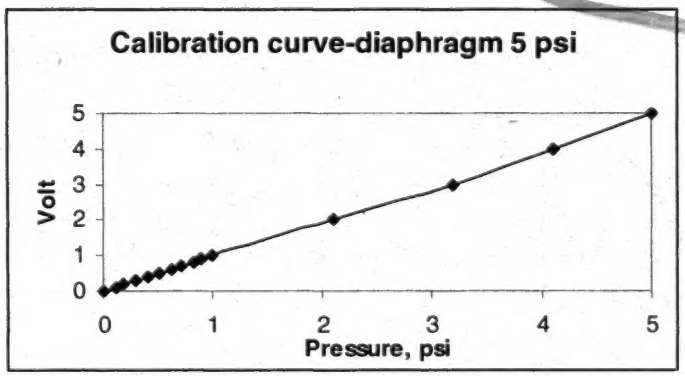

Figure 3.7. Calibration curve for the 5 psi diaphragm.

3.3 Data acquisition system (DAS)

The pressure data was gathered by using the "Instrunet" data acquisition system consisting of the data acquisition box and the controller card (fig. 3.8). The DAS box includes 16 analog inputs, 8 analog outputs, and 8 digital input and out put lines. The controller is an independent computer in itself that utilizes a 32-bit microprocessor and an onboard RAM to control all aspects of data acquisition process.

The Instrunet World Software manages monitors and operates the "Instrunet" network. Additionally, it digitizes long continuous waveforms, spools them to disk, views incoming waveforms in real-time and then allows post acquisition viewing much like a memory oscilloscope.

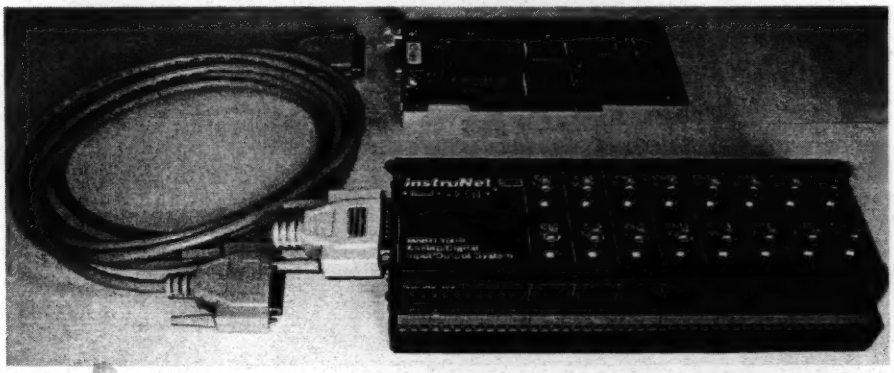

Figure 3.8. The Instrunet equipment

Data is recorded in one long continuous stream (fig. 3.9); or they are digitized in short segments where each segment begins after a specified triggered event (oscilloscope mode). Any one of the analog or digital input channels can be used as a trigger signal. Recorded data are stored into a temporary RAM memory or onto a permanent file on disk. The dialog box is programmed to indicate the sample rate and number of points digitized; the network page is used to select which channels are digitized. After setting up the system; the Network Save, "Start" or "Stop" or "Record" keys are activated to

save, start, stop and save DATA on the RAM memory or to transfer them to disk (post-acquisition). The "Open" key loads waves from disk for viewing.

A spreadsheet format of the system is illustrated in fig. 3.10 and , used to set and view channel parameters such as sensor type, integration time, analog filter options, and digital filter options. Each channel has its own row in the spreadsheet, with the various options in the columns.

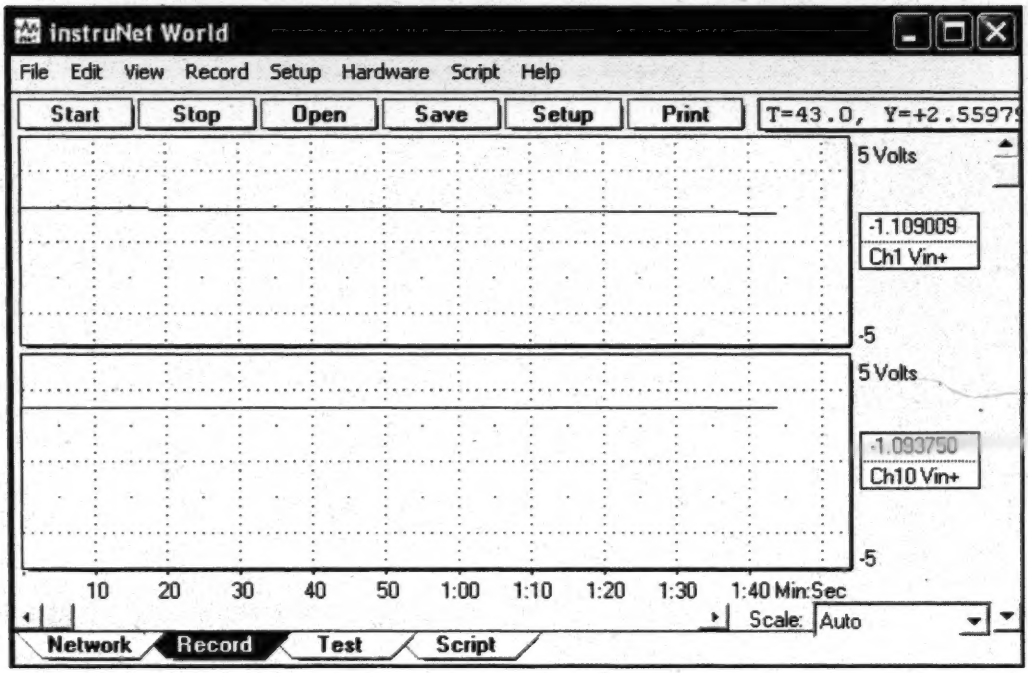

Figure 3.9. Graphical data acquisition.

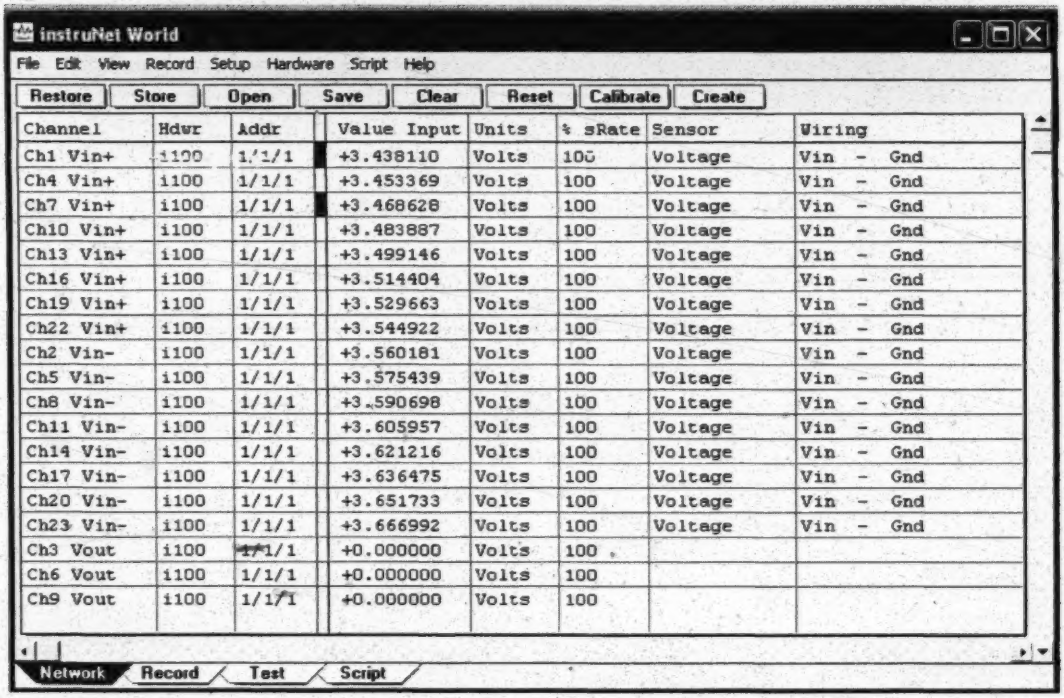
instruNet World
File Edit View Record Setup Hardware Script Help
Restore Store Open Save Clear Reset Calibrate Create
Network Record Test Script

Channel	Hdwr	Addr	Value Input	Units	% sRate	Sensor	Wiring
Ch1 Vin+	i100	1/1/1	+3.438110	Volts	100	Voltage	Vin - Gnd
Ch4 Vin+	i100	1/1/1	+3.453369	Volts	100	Voltage	Vin - Gnd
Ch7 Vin+	i100	1/1/1	+3.468628	Volts	100	Voltage	Vin - Gnd
Ch10 Vin+	i100	1/1/1	+3.483887	Volts	100	Voltage	Vin - Gnd
Ch13 Vin+	i100	1/1/1	+3.499146	Volts	100	Voltage	Vin - Gnd
Ch16 Vin+	i100	1/1/1	+3.514404	Volts	100	Voltage	Vin - Gnd
Ch19 Vin+	i100	1/1/1	+3.529663	Volts	100	Voltage	Vin - Gnd
Ch22 Vin+	i100	1/1/1	+3.544922	Volts	100	Voltage	Vin - Gnd
Ch2 Vin-	i100	1/1/1	+3.560181	Volts	100	Voltage	Vin - Gnd
Ch5 Vin-	i100	1/1/1	+3.575439	Volts	100	Voltage	Vin - Gnd
Ch8 Vin-	i100	1/1/1	+3.590698	Volts	100	Voltage	Vin - Gnd
Ch11 Vin-	i100	1/1/1	+3.605957	Volts	100	Voltage	Vin - Gnd
Ch14 Vin-	i100	1/1/1	+3.621216	Volts	100	Voltage	Vin - Gnd
Ch17 Vin-	i100	1/1/1	+3.636475	Volts	100	Voltage	Vin - Gnd
Ch20 Vin-	i100	1/1/1	+3.651733	Volts	100	Voltage	Vin - Gnd
Ch23 Vin-	i100	1/1/1	+3.666992	Volts	100	Voltage	Vin - Gnd
Ch3 Vout	i100	1/1/1	+0.000000	Volts	100		
Ch6 Vout	i100	1/1/1	+0.000000	Volts	100		
Ch9 Vout	i100	1/1/1	+0.000000	Volts	100		

Figure 3.10. Example of the "Instrunet" software setup

The pressure data saved were processed in Excel where the root-mean-square (RMS) was computed in order to quantify the intensity of the bottom hole pressure oscillations. The sample rate was set to 1000 points per second (estimated to be at least 3 times of actual oscillations frequency). The root-mean-square (RMS) of X data representing the pressure/voltage variable values, is :

$$RMS = \sqrt{\frac{\sum_{i=1}^{n} X_i^2}{n}} \qquad 3.1$$

3.4 Measurement of injected air flowrate

Two different air-calibrated variable-area rotameters are illustrated in figure 3.11: for a flow rate range of 0 to 26 SLPM (right hand side) and for 30 to 432 SLPM (left hand side). The flowmeter for the lower range is a correlated rotameter. This means that it is designed to measure the flow rate of different gases and even water. In this case that it was used to measure air (a perfect gas correlation was use to convert the reading into standard l/m of air). The rotameter used for the higher range of flowrates is a direct-reading flowmeter, which means that the reading is in LPM at the specific conditions of pressure. The specifications for both flowmeters are shown in tables 3.2 and 3.3.

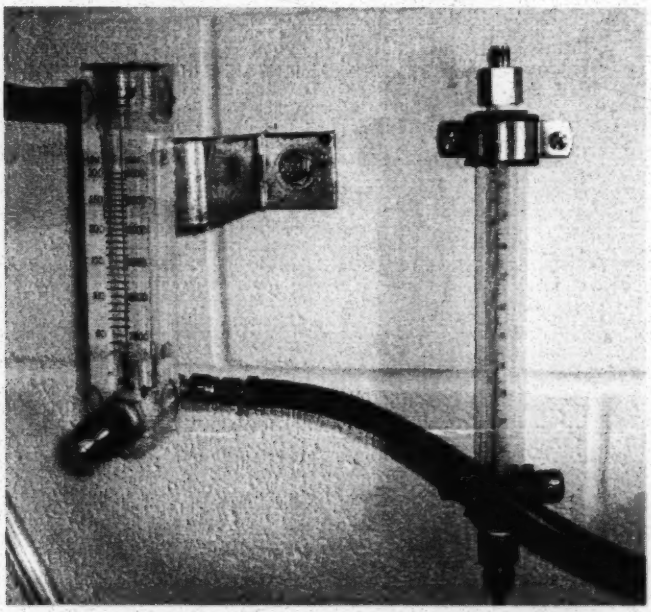

Figure 3.11. Direct-reading (left) and correlated (right) flowmeters

Table 3.2. Specifications of the correlated flowmeter (0 to 26 SLPM of air)

Media		liquid or gas
Flow rate	air	26,680 (mL/min)
	water	745 (mL/min)
Accuracy		±2% full-scale
Repeatability		±0.25%
Material	Housing	Aluminum
	Flow Tube	Borosilicate Glass
	fitting	Aluminum
	o-ring	Buna N
	float	316 Stainless Steel
Max operating temperature		250°F (121°C)
Max pressure		100 psi
Connections		1/4" NPT(F)

Table 3.3. Specifications of the direct-reading flowmeter (30 to 300 LPM of air)

Media		Gases
Flow rate (air)		30-280 LPM
Accuracy		±3% full-scale
Repeatability		±0.5% full-scale
Material	Housing	Acrylic
	fitting	Brass
	o-ring	Buna N
	float	316 SS
Max operating temperature		150°F (65°C)
Max pressure		100 psi
Connections		1/4" NPT(F)
Dimensions		1 3/8"W x 6 1/2"H x 2 1/8"D
Scale		Metric, 100-mm

When using the direct reading flowmeter for high flow rates, the air flow rates need to be adjusted for standard conditions at the nozzle exit. Assuming an isentropic expansion at exit of the nozzle the flow can be calculated as follows [39]:

$$Q_2 = Q_1\left(\frac{p_2}{p_1}\right)^{\frac{1}{k}} \qquad 4.2$$

Where k is the isentropic exponent that is equal to 1.402 in the case of air for temperatures smaller than 50 ° C. Table 3.3 shows these calculations for the air range of operation of the direct-reading flowmeter.

Table 3.4. Air range of operation for the direct-reading flowmeter

LPM	Pressure (psig)	SLPM
30	1.8	32.58
40	2.1	44.00
50	2.97	57.02
60	4.03	71.34
70	5.45	87.68
80	7.62	107.81
90	10.09	130.72
100	15.9	168.82
110	19.4	200.64
120	28.5	259.17
130	39.3	329.28
140	46.2	386.42
150	49.8	431.36

3.4 Experimental Procedure

3.4.1 Liquid preparation and physical properties

Tap water and water-methanol mixture were used for the tests. A mixture of 60 water - 40% methanol by volume was prepared to modify the interfacial tension (IFT). The IFT

value decreased from 72 dyne/cm (water) to 38 dyne/cm for the selected water-methanol mixture.

The liquid density was calculated by measuring the volume of liquid in a calibrated cup and the weight of the cup with fluid. The density of the fluid was recorded as the ratio between weight and volume at the measured liquid temperature.

The liquid viscosity was determined using the Brookfield Viscometer Model DV-II[2]. The measured viscosity for water was 1.003 cP, for pure methanol 0.540 cP, and for the 60/40% water-methanol mixture 1.710 cP.

The liquid properties were measured three times and an average value was used for calculations [2].

3.4.2 Experimental procedure

The experimental procedure is consisted of in six steps:

1. **Calibrations**: pressure transducers.
2. **Adjustment of submergence**: The storage tank was filled with the liquid up to a certain liquid level corresponding to the selected submergence value. Table 3.5 shows the values used for the 4, 8 mm, 12 mm and 20 mm risers.

Table 3.5. Submergence level used for the 8, 12 and 20 mm risers

Liquid level from the gas injection point, cm							
4.0 mm Riser		7.8 mm Riser		12.0 mm Riser		20.0 mm Riser	
Liquid level, cm	**Submergence %**	**Liquid level, cm**	**Submergence %**	**Liquid level, cm**	**Submergence %**	**Liquid level, cm**	**Submergence %**
50.8	16.66	50.8	16.66	50.8	16.66	106.7	35.00
38.1	12.50	38.1	12.50	38.1	12.50	50.8	16.66
25.4	8.33	25.4	8.33	25.4	8.33	38.1	12.50
12.7	4.16	12.7	4.16	12.7	4.16	25.4	8.33
						12.7	4.16

3. **Verification of proper operation of transducers**: The bottomhole pressure was measured under static conditions and compared with the theoretical static pressure value.
4. **Air flowrate adjustment**: During a single run the airflow was kept constant. The gas flow rate varied according to the diameter of the selected observation tube. Table 3.6 shows the airflow rate range used for the experiments.
5. **Recording of the liquid lifted:** The mass flow rate was calculated by dividing the mass of collected liquid by the collecting (run) time. The value was recorded in Kg/min.
6. **The above procedure** was repeated from steps 3 to 6 until all the gas flow rates were completed.

For the experiments with the local turbulent promoters (LTP) procedure 3 to 6 was followed. Some experiments were selected to be captured in images by using a special camera.

After finalizing all the experiments for one submergence value, steps 2 to 6 were repeated for the other submergence values. In order to observe repeatability, the complete sets of experiments were repeated three times for a single riser.

Table 3.6. Air flow rate used for 4, 8, 12, and 20 mm ID riser

Air flow rate range employed, SL/min			
4.0 mm Riser	**7.8 mm Riser**	**12.0 mm Riser**	**20.0 mm Riser**
0-2	0-100	0-200	0-432

CHAPTER 4

EXPERIMENTAL RESULTS AND ANALYSIS

The effectiveness of gas lifting is assessed by assessing the amount of liquid produced when a certain amount of gas is injected under a constant reservoir simulated pressure condition (submergence). Therefore, all experiments are mainly conducted under known, constant pressure and controlled gas injection flowrate. The amount of liquid produced and of gas injected is expressed in actual units (liters/min etc) or as superficial velocities. The use of superficial velocities offers the advantage of comparing the effectiveness of various diameters. For a pre-determined submergence and tube diameter a specific run characteristic is presented as the liquid production illustrated as a function of gas injected. The focus of previously completed experimental and numerical investigation [4] was assessing the effectiveness of 4mm, 8mm and 12 mm tube (SDT) to transport liquid under low submergence level. The two-phase flow pattern observed was mainly limited to the elongated bubble or pseudo slug flow pattern[2]. The negative effect of the downward liquid film flow was captured in a numerical model allowing to estimate the maximum depth allowed for an effective upward gas lifting and to transfer laboratory observations to field conditions.

The experimental investigations described in this work are considerably enlarging the envelope of previous work [2, 4], mainly through detailed observations made on the transition from slug to annular flow pattern. This is possible due to increasing the amount of gas injected and of the diameter of tubes up to 20 mm. The slug-to-annular transition was identified by direct observations of flow characteristics, by observing changes in the gas-liquid characteristic curve, and, through the record of pressure oscillation (RMS) employed for the first time in this context.

Therefore, the experimental results described in this study are observing the advantages and limitations of exploiting either the small-diameter tubes and pseudo-slug pattern conditions or, annular flow for various deliquification applications and the effect of

transition between slug and annular flow on liquid transported under low reservoir pressure conditions.

Local turbulence promoters and change of interfacial tension effects, mainly on altering the base-line gas lift characteristics add another dimension to this experimental study.

4.1 Experiments with 20 mm ID tube using tap water

Figs. 4.1 and 4.2 summarize the effect of submergence level on gas lifting efficiency for 20 mm tube (actual gas-liquid rates and superficial velocities are used in figs. 4.1 and 4.2 respectively). The following salient observations are made from comparing the graphics with direct observations on flow nature.

a. Gas lifting production characteristics

For submergence in excess of 16.6% (16.6 & 35%) the production characteristic exhibits two maxima of liquid produced; visual observations are suggesting that the first maxima (observed at gas flowrates under 40 liters/min) marks the onset of transition from slug to annular flow and the second maxima occurs after the developed annular flow pattern is established. For submergences lower than 16.6% the first maxima (indicating the onset of slug-to-annular transition) is not observed as liquid production is initiated only after annular flow gas injection conditions are met (or during the final stages of STA transition). In summary, three check points are generally (for submergences exceeding 16.6% and 20 mm ID) observed: 1. the onset of production (#1 fig. 4.1), 2.first maximum (corresponding to the end of slug flow pattern and beginning of STA transition) (#2 fig. 4.1), 3. minimum liquid produced during STA transition (#3 in fig. 4.1), 4. the second maximum observed during the developed annular flow (#5 fig. 4.1), 5. a decline of liquid produced with increasing the gas injected, observed after the second maximum liquid production (annular) is achieved. For 20 mm diameter, and submergences under 16.6% the first maximum (slug) is not observed and the onset of production occurs only after annular flow is observed. A similar behavior is observed when superficial velocities are used in lieu of actual flowrates (fig. 4.2)

b. Submergence (see table 3.5)

Figures 4.1 and 4.2 illustrate that for specific depth of the observation tube (3 m) an increase of submergence from 16.6 to 35% will increase the liquid flowrate by approximately 3 to 5 times. Further on, it is not possible to produce any liquid as a slug flow pattern for submergences under 16.6% and this is consistent withy all recommendations used for de-liquefactions where a developed annular flow is considered to be essential [3].

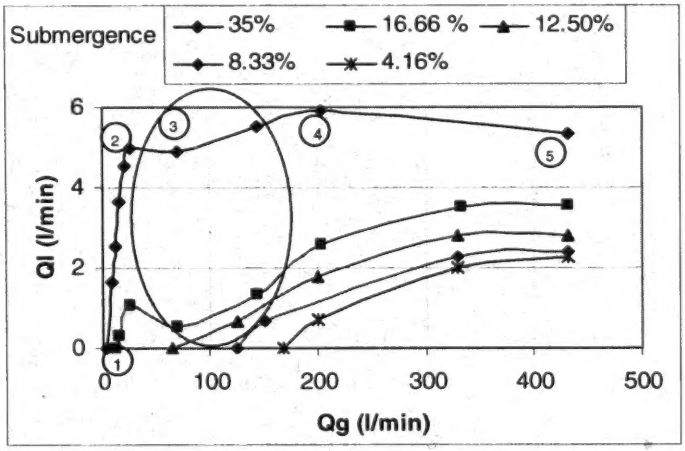

Figure 4.1. Water flow rate as a function of air flow rate for 20 mm ID tube (tap water)

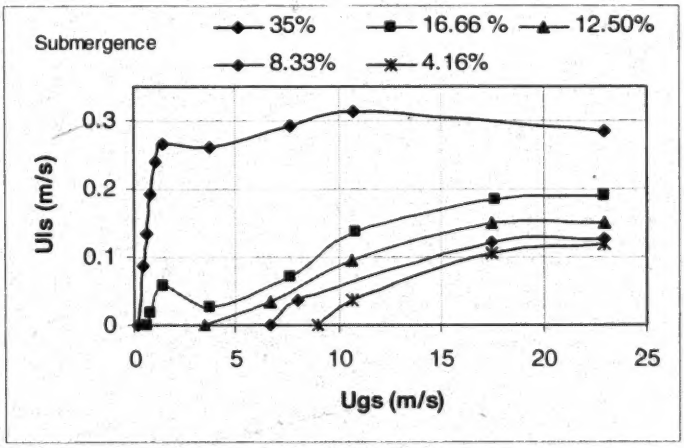

Figure 4.2. Superficial liquid velocity as a function of superficial air velocity for the 20 mm ID tube (tap water)

4.1.1 Visual observations (20 mm ID and tap water)

Figs 4.1 to 4.2 show pictures of the two-phase flow for gas velocities between 10 and 23 m/s at 4.16% submergence. Under these conditions slug or pseudo-slug pattern was not detected and visual observations suggest a transition from slug/churn to annular taking place.

A liquid film-core flow has been observed; however is difficult to notice if the film is flowing in the upward (annular) or the downward direction (typical for slug). It appears that for lower submergence experiments (figs 4.3 (a), 4.4 (a)) the waves tends to be bigger in amplitude compared to higher submergence levels under similar superficial air velocities (figs 4.5 (a), 4.6 (a)). Yet, once When the gas injected rate is further increased the size of the waves tends to decrease for all submergence levels (fig.s 4.2 (b) (c), 4.3 (b) (c), 4.4(b) (c), 4.5(b) (c) (d)). The amount and size of droplets formed seems to be dependent also on the submergence level and superficial air velocity as can be observed in pictures 4.2 to 4.5. Fig.s 4.2 (a), (b), (c), (4.16 % submergence) show no significant amount of droplets formed for any of the superficial air velocities used. For higher submergence levels, say 12.5 % (Fig. 4.4, Ugs = 6.63 m/s) and 16.66 % (Fig 4.5, Ugs =7.58) the amount of droplets formed are higher compared to lower submergence levels. For lower superficial air velocities the droplets tend to readily redeposit into the film due to their bigger size. Once the air injected is increased the droplets can be easily lifted and decrease significantly in size. For lower air rates the main mechanism of entrainment may be the breakdown of the wave by undercutting whereas for higher air flow rates the main mechanism may be when the crest of the wave is moved upward by the gas breaking it into [6] drops.

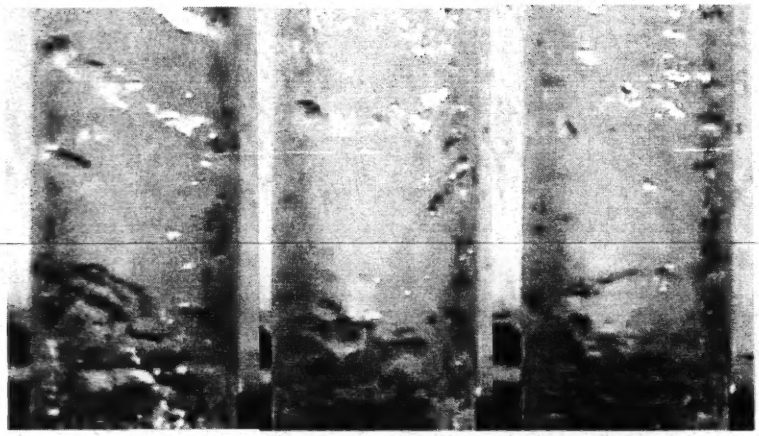

(a) (b) (c)

Figure 4.3. Photographic evidence of CTA (4.16% submergence, ID=20 mm) (a) Ugs = 10.61 m/s. and Uls = 0.035 m/s (b). Ugs = 17.45 m/s and Uls = 0.105 m/s (c) Ugs = 22.9 m/s and Uls = 0.119 m/s

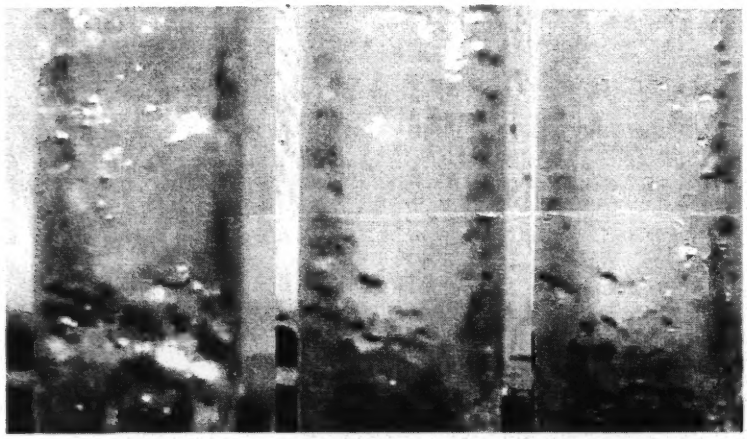

(a) (b) (c)

Figure 4.4. Photographic evidence of CTA (a) Ugs = 8.01 m/s. and Uls = 0.0356 m/s (b). Ugs = 17.45 m/s and Uls = 0.120 m/s (c) Ugs = 22.9 m/s and Uls = 0.127 m/s

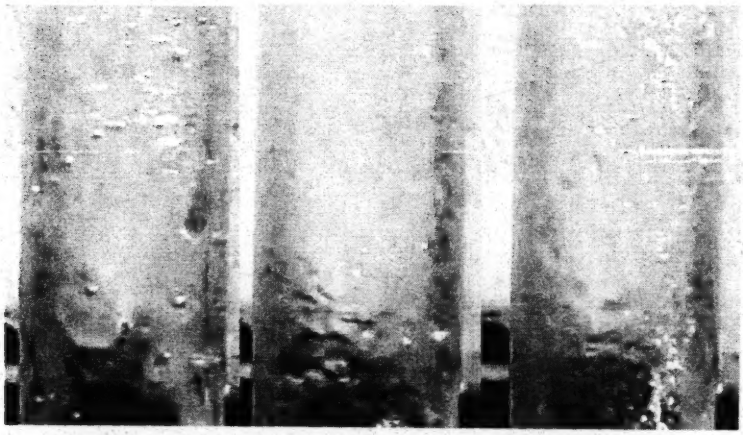

(a) (b) (c)

Figure 4.5. Photographic evidence of CTA (a) Ugs = 6.63 m/s. and Uls = 0.0343 m/s (b). Ugs = 17.45 m/s and Uls = 0.148 m/s (c) Ugs = 22.9 m/s and Uls = 0.149 m/s

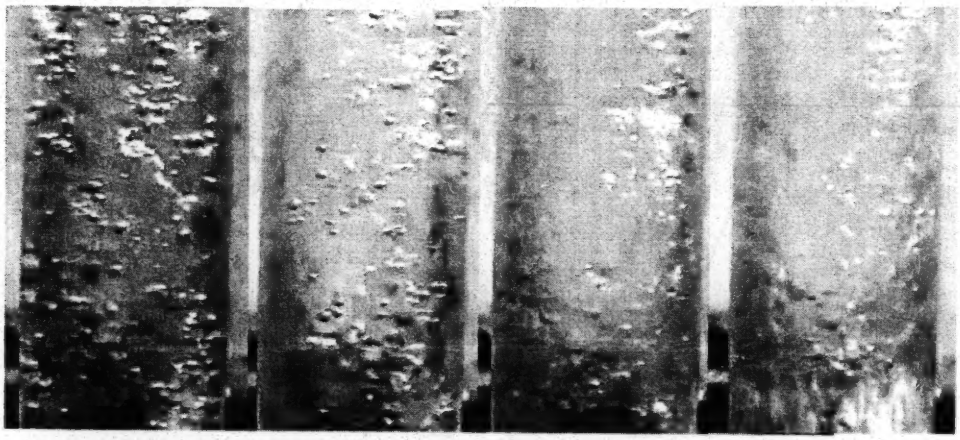

(a) (b) (c) (d)

Figure 4.6. Photographic evidence of CTA (16.66 % submergence 20 mm ID) (a) Ugs = 7.58 m/s. and Uls = 0.071 m/s. (b) Ugs = 10.77 m/s and Uls = 0.136 m/s (c). Ugs = 17.45 m/s and Uls = 0.185 m/s (d) Ugs = 22.9 m/s and Uls = 0.189 m/s

In fig.s 4.3 (b), 4.3 (c), 4.4 (b), 4.4 (c), 4.5 (b), 4.5 (c), 4.6 (c), 4.6(d) annular flow is fully developed. The entire film appears to move upwards. While in fig.s 4.3 (a), 4.4 (a), 4.5 (a), 4.6 (a) and 4.6 (b) a reverse of film direction appears to take place

4.1.2 Bottom Hole Pressure (BHP) Oscillations (D=20 mm)

Oscillations of FBHP are detected even after liquid and gas flowrates are stabilized. These pressure oscillations are related to void fraction variations along the riser and represents a valuable information on gas-liquid flow stability. Since the frequency of pressure oscillations can be up to 100 Hz an instrument designed for 1000 Hz was selected.

The root mean square RMS was calculated (eq.3.1) to assess the statistical magnitude of pressure oscillations. Figs 4.7 (a) to 4.7 (d) shows the RMS of the BHP versus superficial air velocity for submergence between 8.33-16.6%.

A maximum RMS is reached for a superficial air velocity of around 3 m/s regardless of submergence. This observation holds for submergences under 8.33% when no liquid production is recorded (see fig. 4.2) under U(gs)=5 m/s. However, a two phase upflow is visible up to a level under the top of the tube where net liquid production is recorded. This maximum RMS is an indication of the existence of an instable transitional flow, and is assimilated to the first stage of slug-to-annular flow pattern transition indicated in the literature as churn flow. In the case of 4.16% submergence the measured static pressure (no air flow) is 0.18 psi (5 in Column of water) and the maximum RMS recorded at flowing conditions is 0.271 psi. For 8.33 % the static pressure is 0.34 psi (10 in Column of water) and the maximum RMS recorded is 0.44 psi. For higher submergence levels this difference tends to decrease.

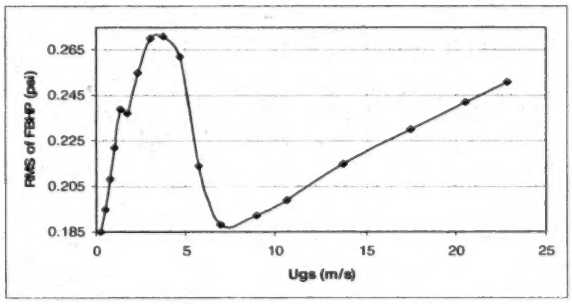

(a)

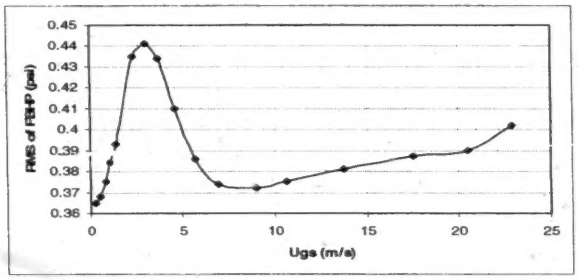

(b)

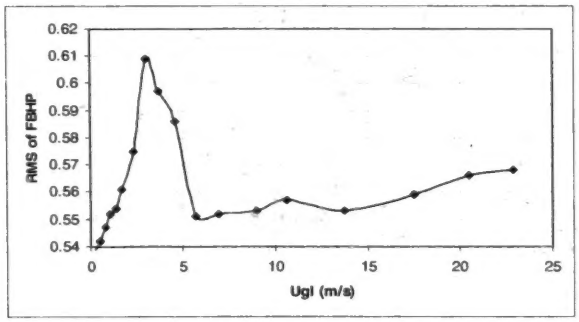

©

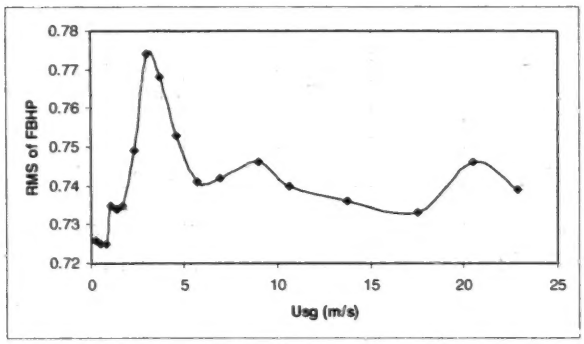

(d)

Figure 4.7. RMS of oscillating BHP for 20 mm ID tube. (a) 4.16 % submergence. (b) 8.33 % submergence. (c) 12.5 % submergence. (d) 16.66 % submergence.

With further increasing of injected air (after approximately 3 m/s when max, RMS is observed) a slow decline of the RMS value is observed for all submergences (figs. 4.7 a-d), until a minimum value is reached.

Therefore, the maximum detected RMS value doesn't depend on submergence but the minima observed after this maxima appears to be a function of submergence, or, implicitly of liquid transported.

Figures 4.8 (a) and 4.8 (b) compare both the amount of liquid transported and the RMS as functions of gas injected for two extreme submergences of 16.6 and 4.16%. A good coincidence between minima of water transportation (observed after the entrance into slug-to-churn transition) and maxima of RMS is observed for the 16.6% submergence (where net liquid production has been recorded). When combined with visual observations, the maxima of RMS indicating a high instability condition, is defined as an indication of churn gas-liquid activity or the first stage of slug-to-annular transition.

Fig. 4.8 (a) is for submergence level of 16.66 % and it can be observed form it that when the minimum water produced is reached the RMS reading is the highest. Conversely, the values of RMS for higher water produced are smaller. This indicates that the liquid holdup in the tube is bigger when less water is being produced contributing to rise the pressure losses. Fig. 4.8 (b) is for 4.16 submergence level. In this case no water is produced for superficial air velocity smaller than 8 m/s. The RMS values increases linearly with superficial air velocity as more water is produced. The water curve appears to be reaching its maximum point (fig. 4.8 (b)) at 22 m/s of superficial air velocity. After the water produced starts to decrease it is likely that the RMS curve will increase even faster. However, there was no more air available to attain higher superficial air velocities for the 20 mm tube.

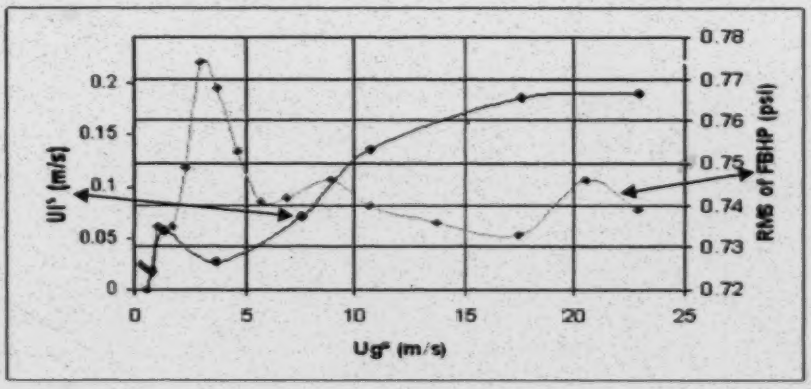

(a)

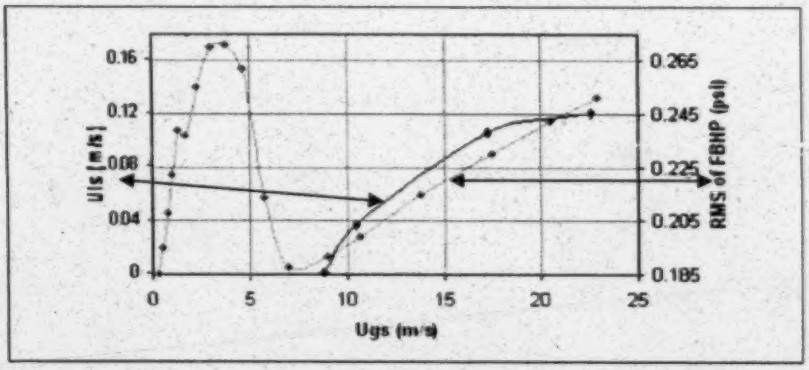

(b)

Figure 4.8. Comparison of RMS and water production curves for the 20 mm tube. (a) 16.66 % submergence level. (b) 4.16 % submergence level.

4.2 12 mm tube

Fig. 4.9 summarizes gas lifting characteristics [U(ls)=F(U(gs)] obtained for different submergence during this study and during a previously completed experimental study using a similar setup but with limited gas injection facilities [2]. A good reproducibility between present data and previously obtained data [2] is observed. However, this study reveals the behavior of air-water upward transport for a broader range of gas injection including the transition from slug-to-annular flow patterns.

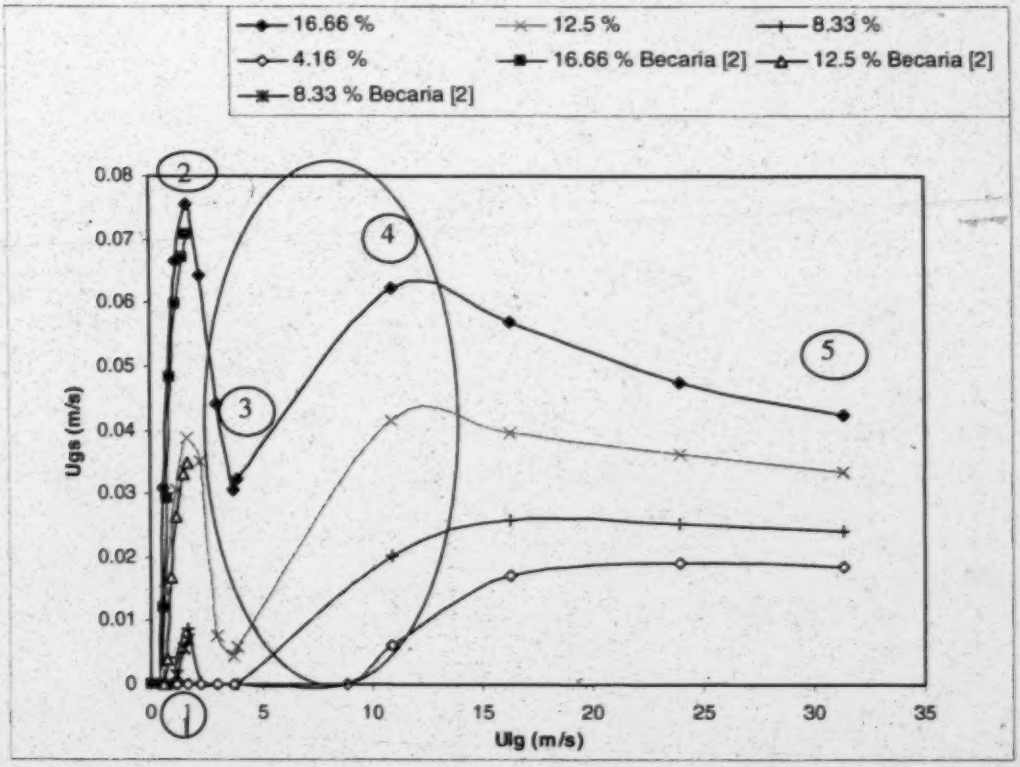

Figure 4.9. Superficial liquid velocity versus superficial air velocity for (12 mm ID and tap water).

The general shape of the gas lift production characteristics previously commented for 20 mm tube is also kept for 12 mm tubes at 16.6% submergence (figs. 41-4.2). However, the relative amount of net liquid transported as a pseudo-slug (#2 fig. 4.9) is by approximately 25% higher than the maximum liquid transported in the annular flow pattern (#4 fig.4.9). This situation is reversed (more liquid is transported as annular than as slug) for 20 mm tubes (fig. 4.2). In absolute values, a maximum superficial liquid velocity of approximately 0.189 m/s is achieved under annular flow pattern transportation with 20 mm tubes (16.66 % submergence), the maximum transported liquid under slug flow pattern being of approximately 3 times lower at same submergence in 12 mm tubes (In terms of water volume it is 8.5 times lower).

It is important to remark that the superficial air velocity for which the maximum amount of water is produced under "pseudo slug" flow appears to be independent on the submergence level. On the contrary, the superficial air velocity for which the maximum water produced is attained as annular flow depends on the submergence level.

The minimum production (specific to STA first transition stage indicated as a churn flow #3 fig. 4.9) is 50-400% under the maximum superficial liquid velocity recorded as slug or even annular flow pattern (fig. 4.9).

4.2.1 Visual observations (12 mm tube)

Figs 4.10 and 4.11 are snapshots taken during assumed annular flow (at 4.16 % and 16.66 % submergence). It is difficult to assess through direct observations the moment when annular flow is fully developed (end of transition). However, from inspecting the superficial velocity diagrams (fig. 4.9) the transition occurs between 11 and 14 m/s of superficial air velocity. Figs 4.10 (a) and 4.11 (b) show the two phase flow for a superficial air velocity of almost 11 m/s for the submergence 4.16 % and 16.66 % respectively. The main difference observed for these two levels of submergence is in the thickness of the film, which appears to be higher for lower submergence. In this case, the gas-droplets core (specific to annular flow) is completely developed.

If more air is injected the thickness of the film decreases and only upward, co-current gas-liquid film has been noticed (Figs 4.10 (b), 4.10(c), 4.11 (b), 4.11(c)).

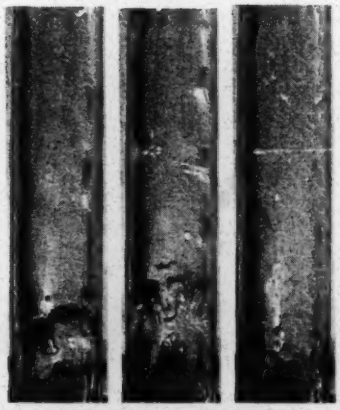

(a) (b) (c)

Figure 4.10. Photographic evidence of water-air upward transportation (4.16% submergence 12 mm ID) (a) Ugs = 10.89 m/s. and Uls = 0.0061 m/s (b). Ugs = 16.25 m/s and Uls = 0.0172 m/s (c) Ugs = 23.9 m/s and Uls = 0.019 m/s

Other important difference between the two submergence levels (4.16 % and 16.66 %) is formation of droplets. It can be observed that there is little formation of droplets for 4.16 % submergence level (fig. 4.10), whilst there are more droplets for 16.66 % submergence level (fig. 4.11). Certainly, due to the high speed of the gas core at the conditions for which the pictures were taken it is required a different method to quantify the droplet entrainment. Yet, it is enough to have a qualitative idea of the droplet creation.

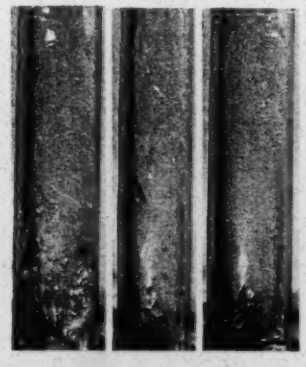

(a) (b) (c)

Figure 4.11. Photographic evidence of water-air upward transportation (16.66% submergence 12 mm ID) (a) Ugs = 10.89 m/s. and Uls = 0.062 m/s (b). Ugs = 16.25 m/s and Uls = 0.057 m/s (c) Ugs = 23.9 m/s and Uls = 0.0475 m/s

4.2.2 Bottomhole pressure (BHP) (12 mm ID)

The measured RMS of the BHP versus superficial gas velocity is illustrated in fig. 4.12 and indicate a similar shape as detected with 20 mm tubes (fig.4.8 a) with a maximum value indicating the occurrence of the slug-to-annular transition (churn)

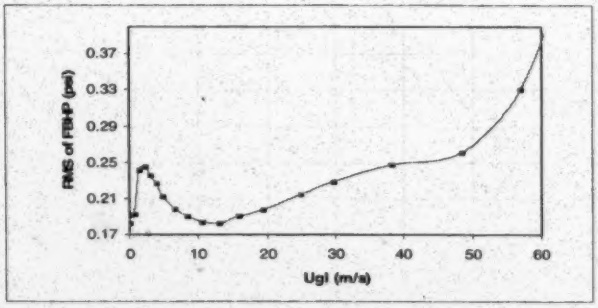

(a)

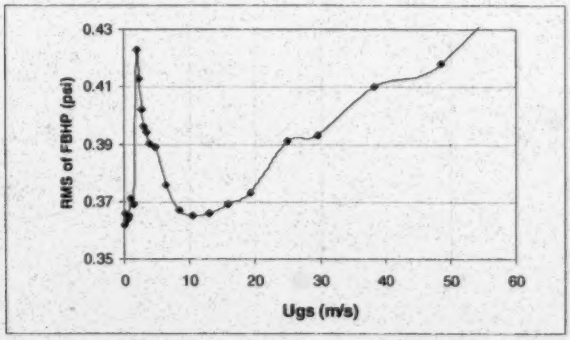

(b)

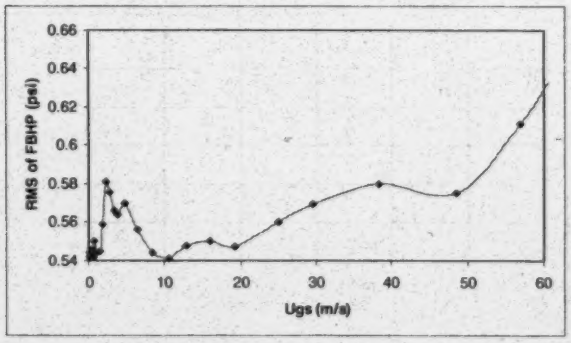

(c)

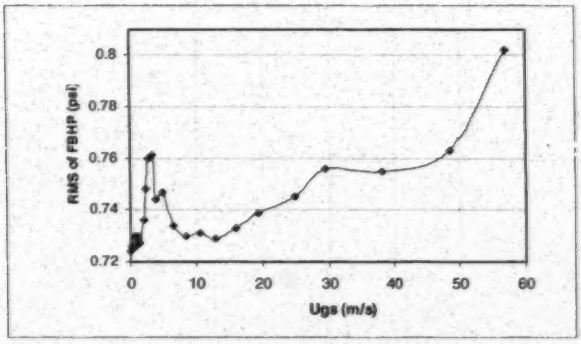

(d)

Figure 4.12. RMS of oscillating bottomhole pressure (12 mm ID) (a) 4.16 % submergence. (b) 8.33 % submergence. (c) 12.5 % submergence. (d) 16.66 % submergence.

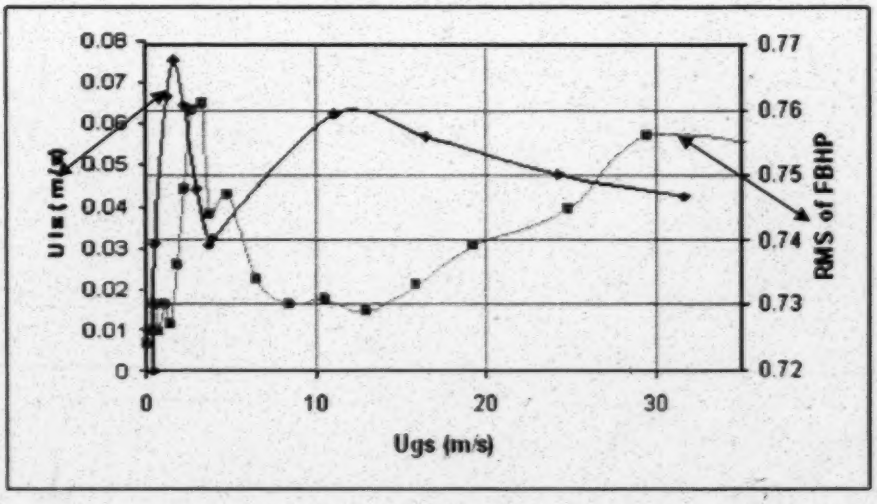

(a)

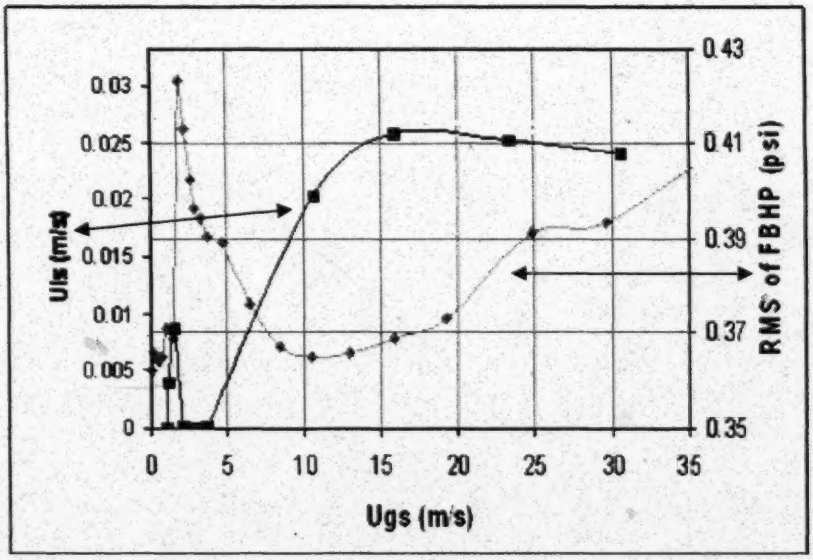

(b)

Figure 4.13. Comparison of RMS and superficial water velocity versus superficial gas injected velocity (12 mm tube). (a) 16.66 % submergence level. (b) 8.33 % submergence level.

The effectiveness of liquid transport is reflected in the RMS of flowing bottomhole pressure. As can be observed in figs. 4.13 (a) (16.66 % submergence) and 4.13 (b) (8.33 % submergence) the points where more water is produced correspond to relatively low RMS values. Conversely, the points of less water produced (within the churn flow) correspond to higher values of RMS. Once the water produced starts declining drastically (developed annular flow), so does the RMS value but increasing.

4.3 Experiments with the 8 mm ID tube.

Similarly to 12 mm tubes, for 8 mm the superficial velocity of liquid transported under pseudo-slug flow pattern exceed the maximum achieved under annular flow pattern (fig. 4.14).

The oval in fig. 4.14 marks the first stage of slug-to-annular transition (churn). The maxima of liquid transportation, observed for 20 and 12 mm tubes in the annular flow pattern region is hardly visible with 8 mm tubes (fig.4.14).

There is a point in which the liquid film is completely blown off and no water is produced. This occurs for superficial air velocities higher than 15 m/s (fig. 4.14).

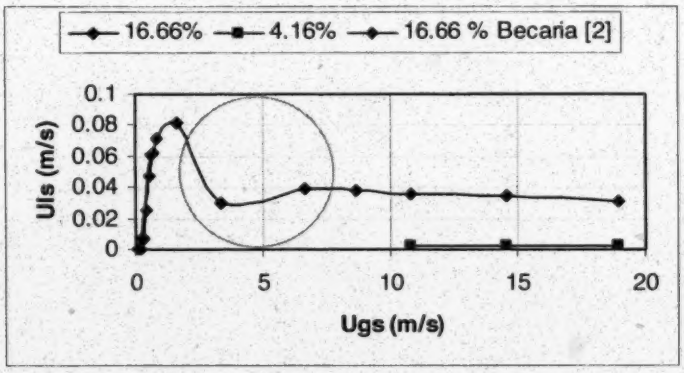

Figure 4.14. Superficial liquid velocity versus superficial air velocity (8 mm ID)

4.3.1 Oscillations of bottomhole pressure (BHP) with 8 mm ID

Turbulent structures and film reversing flow conditions induce a much lower level of oscillation. The maximum value of RMS recorded for 4.16 % submergence is 0.21 psi, which is much lower than that of the other two tubes under the same condition.

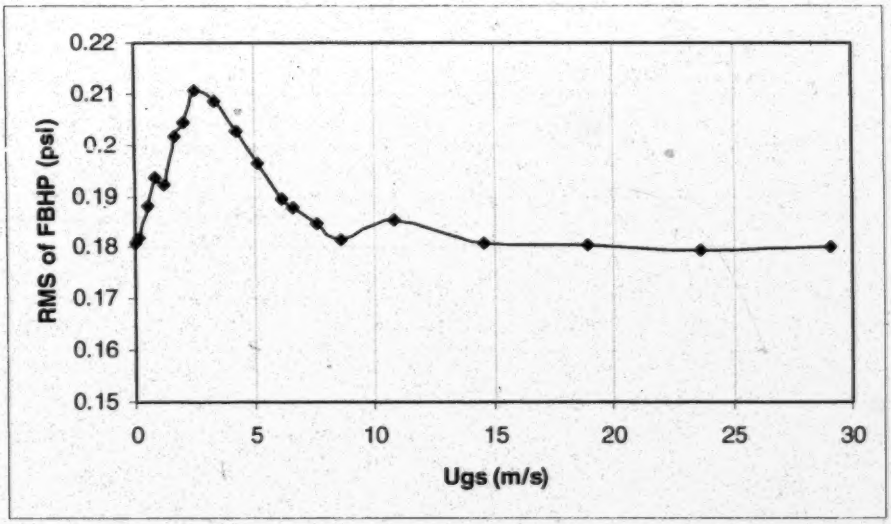

(a)

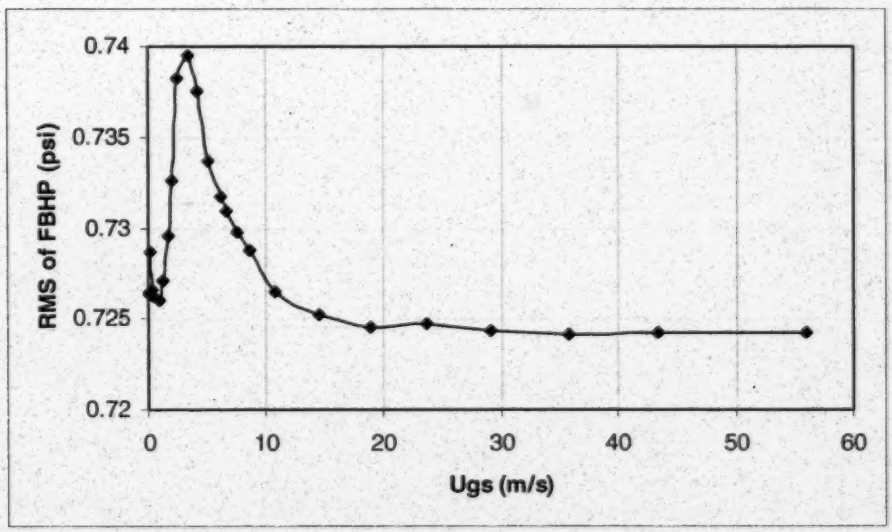

(b)

Figure 4.15. RMS of Flowing Bottom Flow Pressure for the 8 mm ID tube. (a) 4.16 % submergence. (b) 16.66 % submergence.

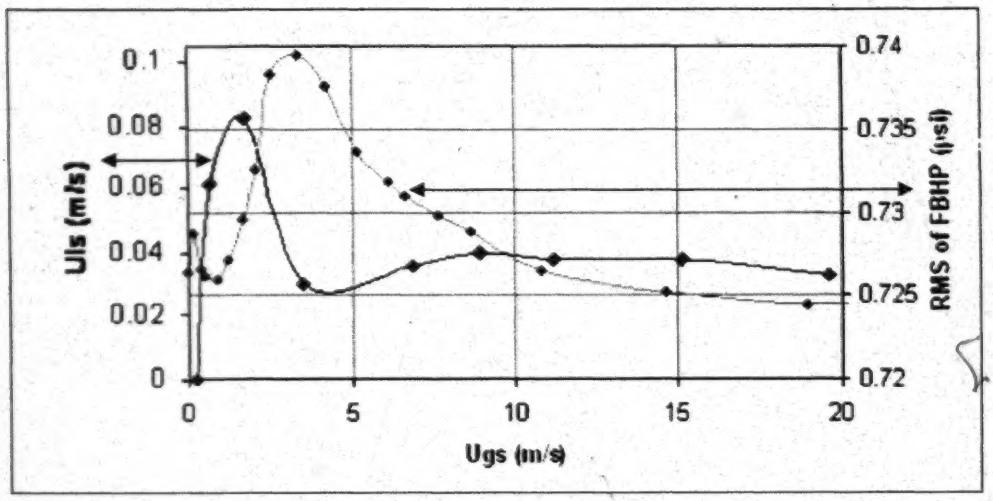

Figure 4.16. Comparison of RMS and water production curves for the 8 mm tube and 16.66 submergence level.

Fig. 4.16 compares the shape of the RMS and water production versus superficial gas velocity for 16.66 % submergence level. Again the maximum point of RMS recorded corresponds to the minimum in water production within the STA transition.

4.4 The effect of tube diameter

Each tube employed has a range of operation for which there is an advantage over the other ones. Fig. 4.17 (a) shows that for very low submergence level (4.16 %) the 20 mm tube has significant more capability to unload water than the other tubes. Certainly, it is required to inject a lot more air to accomplish this and with the energy itself of the reservoir is not enough to lift any liquid. The onset of production for the 20 mm tube and 12 mm tube is similar (8.7 m/s of superficial air velocity). In terms of barrels a day which is a more common way of quantifying the flow in a gas field, the maximum that could be transported with the 20 mm tube for 4.16 % submergence is about 20 barrel/day.

Regarding the 8.33 % submergence value (fig. 4.17 b), from an efficient point of view, the 4 mm tube performs better for the range 0.45 to 3 m/s of superficial air velocity. Yet,

in terms of volume the 12 mm tube has more capability to lift water in this range of superficial velocity. When using a superficial air velocity as low as 0.29 m/s the 4 mm tube is the only one that lifts some liquid. If a superficial air velocity higher than 6.6 m/s is utilized with a lift system as the one used, the 20 mm has significant more capability in lifting water than the other tubes. Similarly, this occurs with 12.5 % and 16.66 % submergence value in which the 20 mm tube is superior for high superficial air velocities. In the range of lower air velocity the 4 mm tube is more efficient for 12.5 % submergence value but for 16.66 % submergence value the 8 mm value is more efficient. However, the 12 mm and 20 mm tube lift more volume of water for the submergence levels 12.5 % and 16.66 % respectively.

The occurrence of the critical points in terms of superficial air velocity is very similar for all the tubes considering the 16.66 % submergence value (fig. 4.17 d).

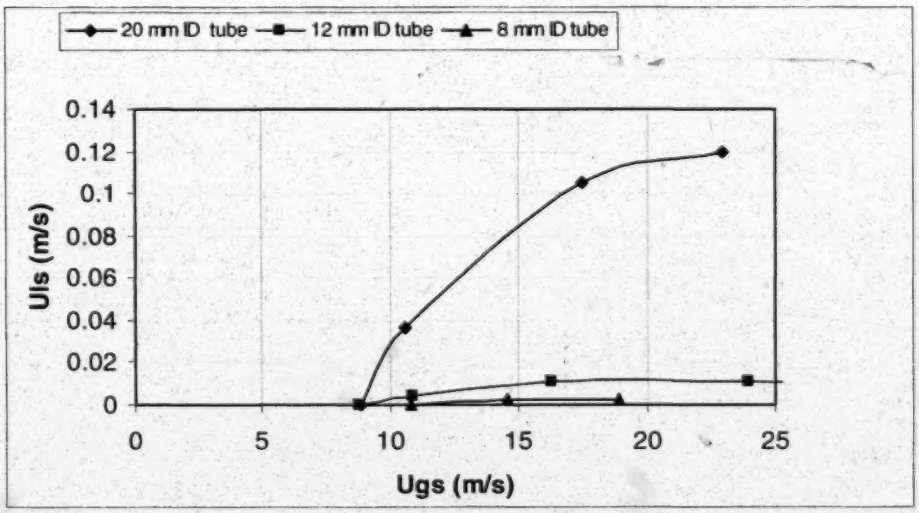

(a)

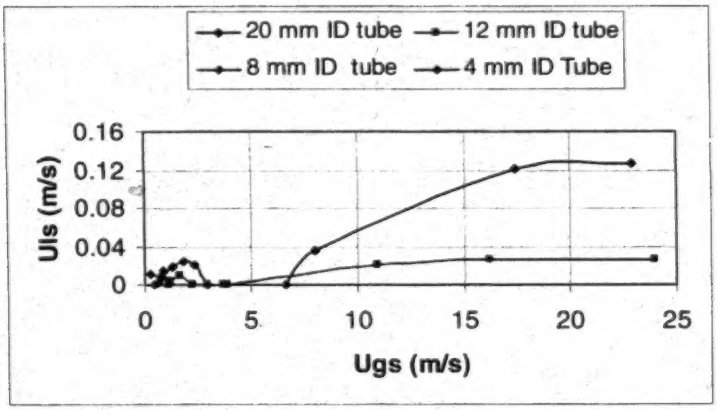

(b)

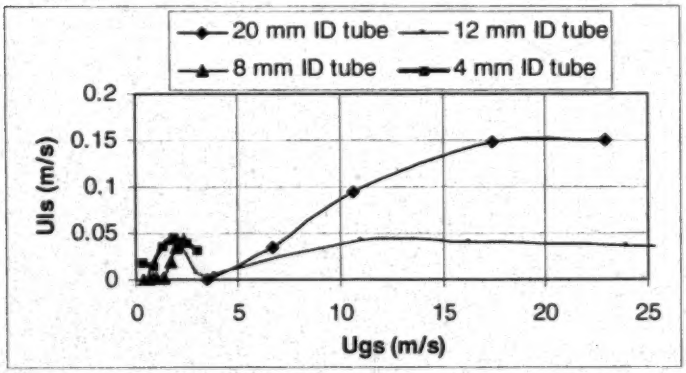

©

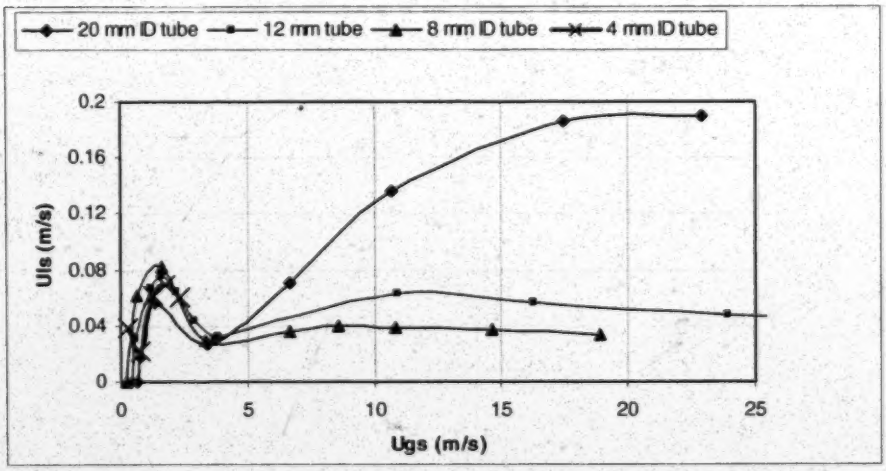

(d)

Figure 4.17. Superficial water velocity versus superficial air velocity for 20 mm, 12 mm, 8 mm and 4 mm tubes. (a) S=4.16 % (b) S=8.33 %(c) S=12.5 % (d) S=16.66 %

4.4.1 Comparative observations regarding the oscillations of bottomhole pressure

The RMS values tend to be lower for smaller diameter tubes either (regardless of submergence fig. 4.18 (a) and (b)). However for 0 to 1.5 m/s superficial air velocity the RMS values measured in 12 and 20 mm tubes and S=4.16% are similar (fig. 4.18 a). They are also similar for the air range of 0 to 2.7 m/s for 16.66 % submergence (fig. 4.18 b). The maximum value of RMS occurs at a similar superficial air velocity regardless of tube diameter (fig. 4.18 a, b).

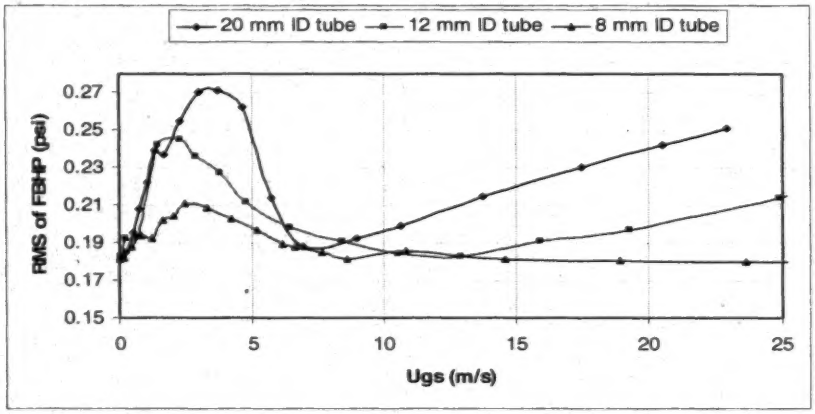

(a)

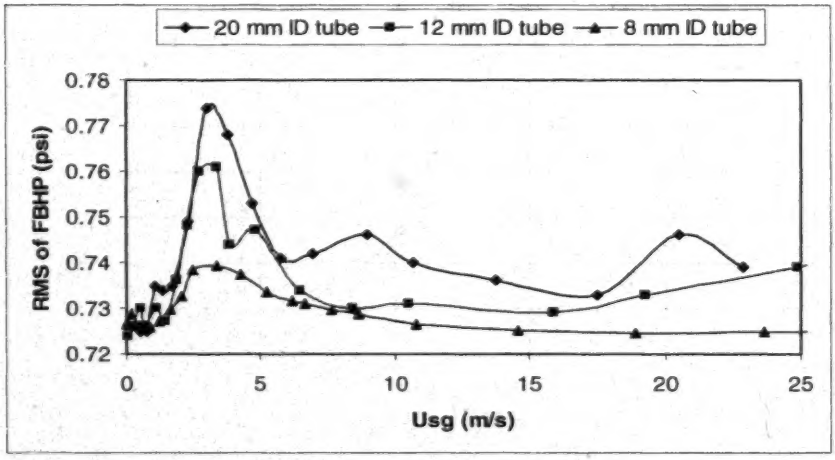

(b)

Figure 4.18. Comparison of RMS with 8, 12 and 20 mm tubes (a) S=4.16 % (b) S=16.66 %

4.5 Water-methanol (W-M) mixture (ID=20 mm)

To observe the effect of surface tension on gas lift liquid transport characteristics a 40-60% methanol-water mixture (properties in table 4.1) was used instead of tap water. The submergence levels used were the same as those used for the tap water. It is important to note that since the water-methanol mixture is 5.2 % lighter than the tap water, the hydrostatic pressure of a column of tap water is 5.2 % greater than that of the mixture. The surface tension undergoes a significant change from 72 Dynes/cm to 38 Dynes/cm. The viscosity increases approximately from 1 cp to 1.71 cp. Though the goal of using this mixture was to observe the effect in decreasing the surface tension, the viscosity and density affect the results as well.

Table 4.1. Physical properties of water, methanol and water-methanol 60:40 mixture [2]

Temperature	20 °C
Pressure	101.3 Kpa

PURE COMPOUNDS	**Molecular weight [g/mol]**	**Density @ SC, [g/cm3]**	**Viscosity cP**	**Surface Tension @ SC (25°C)**
Metanol	32	0.791	0.58	22.5
Water	18	0.998	0.99	72

METANOL-WATER MIXTURE				
MIX Methanol-Water %	**Molar Fraction**	**Visc. Mix @ 21°C cP**	**Surface tension @ 21°C Dyne/cm**	**Density @ 21°C g/cm^3**
40 – 60	0.27	1.71	38	0.947

Figs. 4.19 (a) to (b) compare the results for the water-methanol mixture and tap water. Particularly, for 16.66 % submergence level (fig. 4.19 a), the onset of production for the mixture is observed at a slightly smaller superficial air velocity than for water only (0.53 m/s for the mixture and 0.61 m/s for the tap water). There is a range of superficial air velocity in which the production of the water-methanol mixture exceeds the tap water (by 15 % at U(gs)=6.62 m/s). This effect (observed at 4.5 $<$U(gs)$<$8.5 m/s) appears to be

characteristic only for the first stage of STA transition or churn flow. The reduction of surface tension will reduce the maximum liquid unloading (obtained at $U_G^S \approx 20$ m/s by 12% (due mainly to reduction of droplet generation and film-core interface stabilization effect). It also will accelerate the STC transition with some positive effects on reducing the level of instabilities (generate by the flooding occurrence and intensity). Therefore, by reducing the surface tension (and this maybe the case when oil-steam is involved etc) the STC transition range is reduced, but, also, the effectiveness of deliquification measured through maximum achievable liquid superficial velocity) is also negatively lowered.

At lower submergence levels the onset of production is observed during a final stage of STA transition when the annular flow pattern is possible. Insignificant liquid transport differences only are noticed between W-M and water only.

The onset of production occurs at 3.4 m/s, 6.6 m/s, 8.75 m/s for 12.5 %, 8.33 % and 4.33 % submergence level respectively as can be seen in figs 4.19 b, c, and d. The production of tap water compared to the water-methanol mixture within the onset up to 10 m/s of superficial air velocity is very similar for these levels of submergence. After that the difference is bigger in favor of the tap water being 31 % for 4.16 % submergence level (fig. 4.19 d).

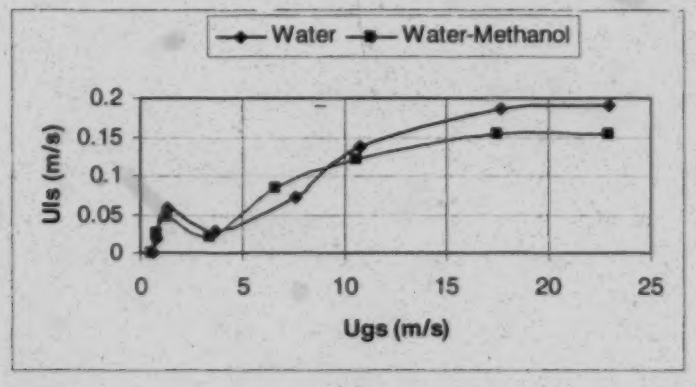

(a)

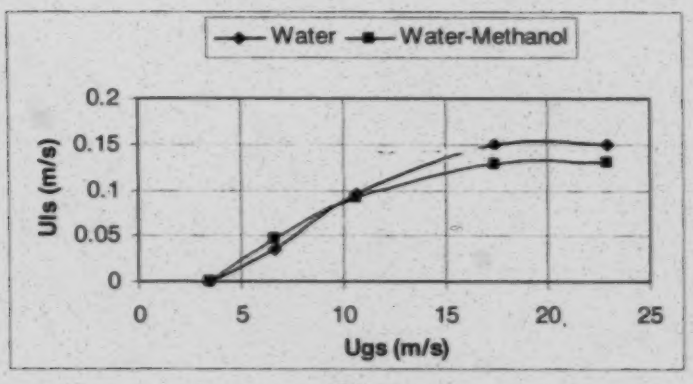

(b)

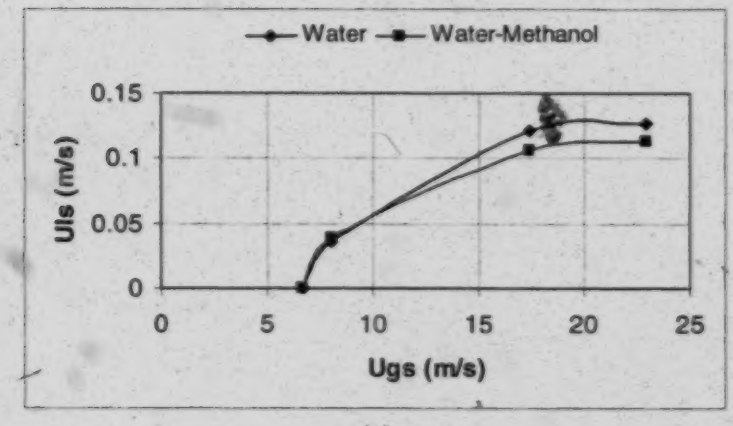

(c)

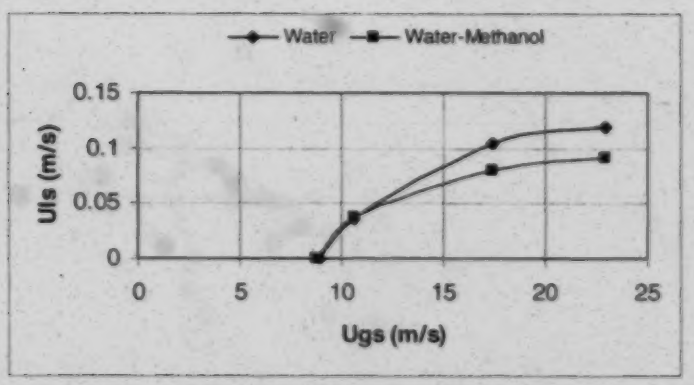

(d)

Figure 4.19. Superficial liquid velocity as a function of superficial air velocity for the 20 mm ID tube using the water-methanol mixture. (a) S=16.66 %. (b) S=12.5 % (c) S= 8.33 % (b) S=4.16 %

4.5.1 The bottomhole pressure oscillations (ID=20 mm) and W-M

The RMS of the water-methanol mixture tends to have a lower value than that of the tap water as can be seen in fig. 4.20. The RMS maximum point at STA transition occurs at very similar superficial air velocities and the shape of the curves is similar for each submergence level. Though, the difference between maximum point of the RMS in the transition and the minimum RMS for the mixture is less significant than for the tap water.

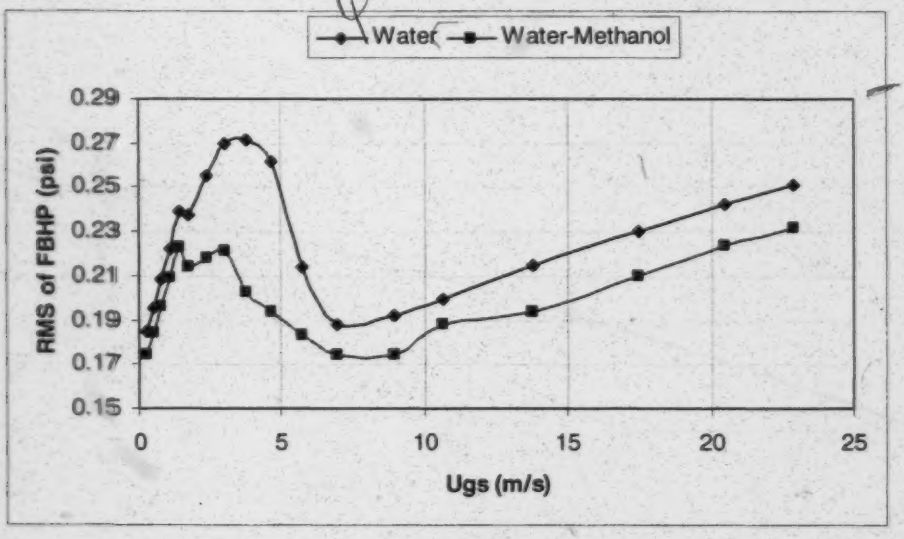

(a)

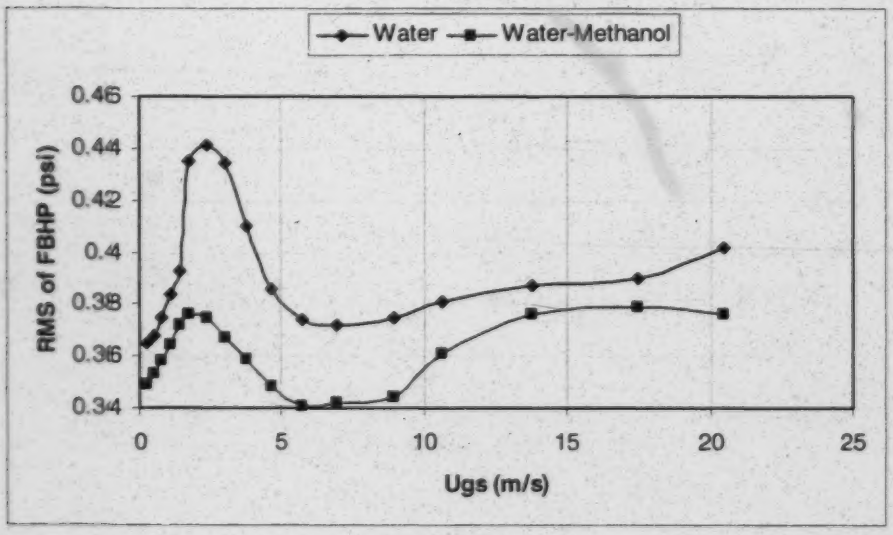

(b)

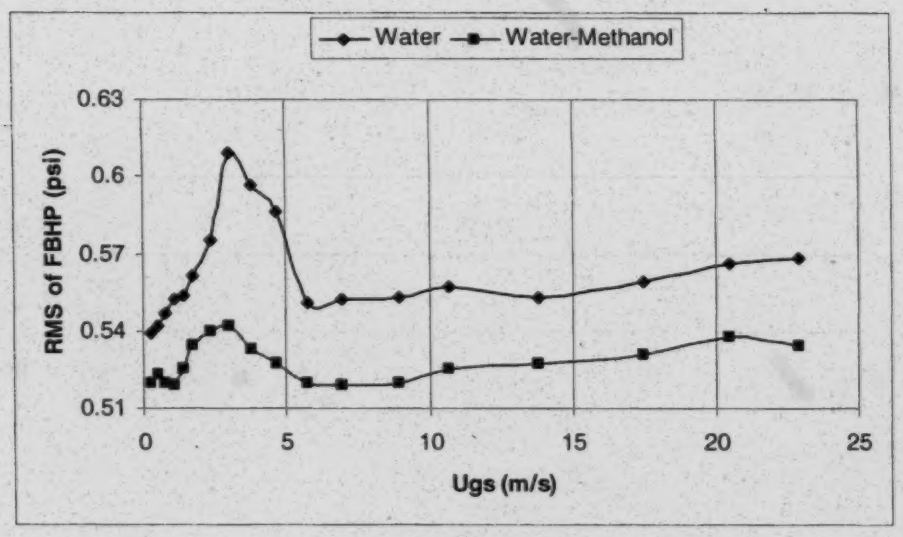

(c)

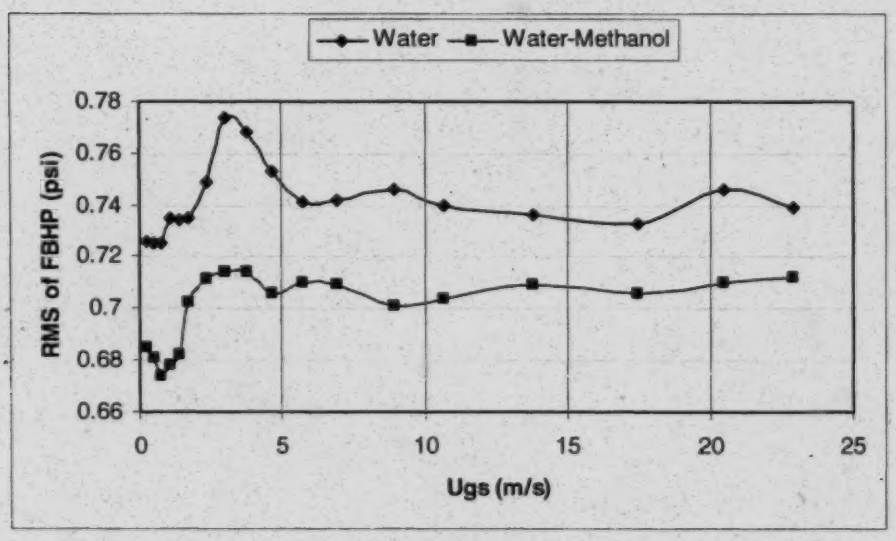

(d)

Figure 4.20. Comparison of RMS versus superficial gas velocities for water only and W-M mixture measured with 20 mm ID (a) S=4.16 % (b) S=8.33 % (c) S=12.5 % (d) S=16.66 %

4.6 Water-methanol (W-M) mixture and D=12 mm

As can be seen the shape of tap water and the W-M mixture curves are similar and maximum point of STA transition occurs at similar air superficial velocities. For the whole gas velocity range (including the slug, STA transition and developed annular) the liquid upward transport effectiveness of M-W is significantly inferior to water only. This observation is valid for SDT as experiments performed in 20 mm tubes indicate "mixed" results (fig 4.19). The lifting of the mixture compared to tap water in the 12 mm riser is more affected than in the 20 mm tube, especially in the "pseudo slug" and churn region. For instance, for 16.66 % submergence level the production of liquid decreases up to 36 % in the "pseudo slug" for the 12 mm tube whilst in the 20 mm tube it is decreased only by 18 %. And in the churn region there is some range for the 20 mm tube in which there is even more production with the mixture. Whereas the difference between tap water and mixture produced in the churn region for the 12 mm tube can be up to 37 %.

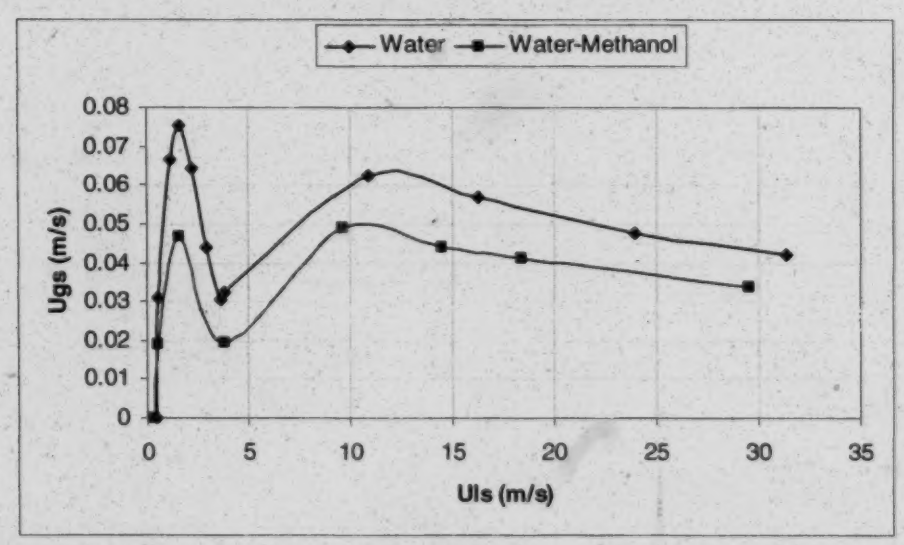

Figure 4.21. Superficial liquid (W-M) velocity versus superficial air velocity (12 mm ID S=16.66 %)

4.6.1 Oscillations of bottomhole pressure (D=12 mm, W-M mixture)

For the whole range of air superficial velocities, the measured RMS values for W-M mixture are lower than for water only (fig. 4.22). For 4.166 % submergence (fig. 4.22 a) the difference between tap water and W-M mixture are somehow smaller than differences observed for 16.66 % submergence (fig.4.22 b).

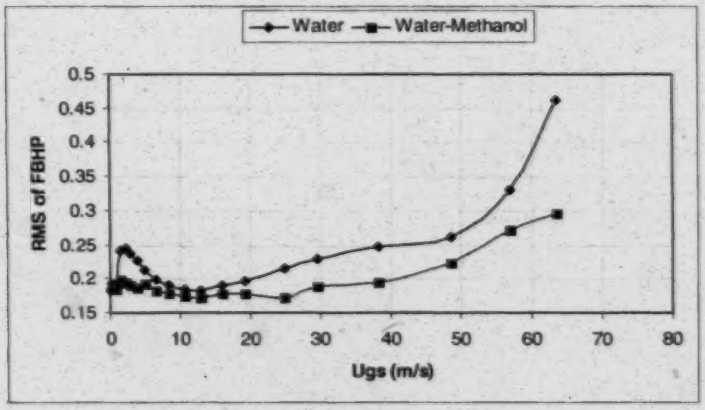

(a)

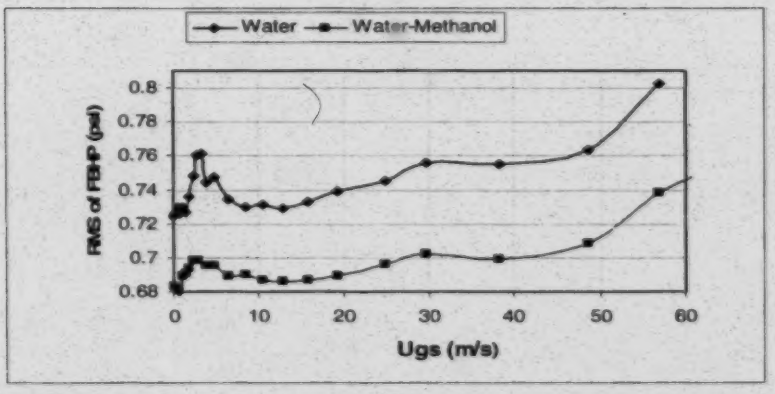

(b)

Figure 4.22. RMS of Flowing Bottom Flow Pressure for the 12 mm ID tube. (a) 4.16 % submergence. (b) 8.33 16.66 % submergence (water-methanol mixture and tap water)

4.7 RMS for 20 mm and 12 mm tubes with W-M

Similarly as the experiments with tap water the 12 mm tube tends to have smaller RMS values than that of the 20 mm tube which indicates lower degree of pressure oscillation.

However, for small superficial air velocities (0-1.5 m/s) the RMS values are comparable as observed in fig. 4.23 b. In this range the superficial liquid velocity is bigger or similar for the 12 mm tube than for the 20 mm tube, which can cause similar degree of pressure oscillation.

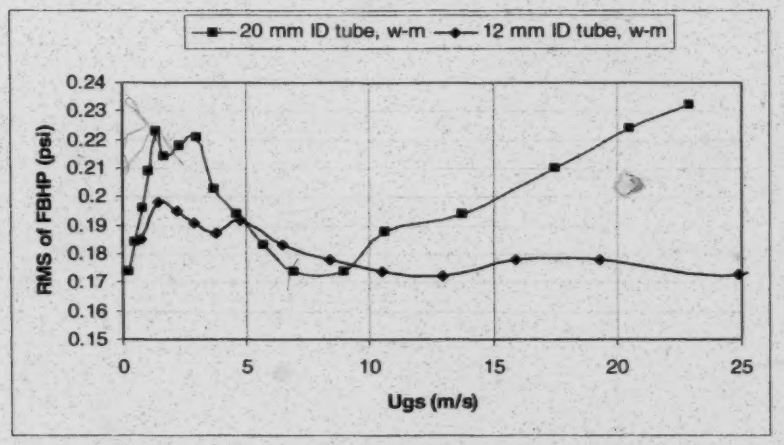

(a)

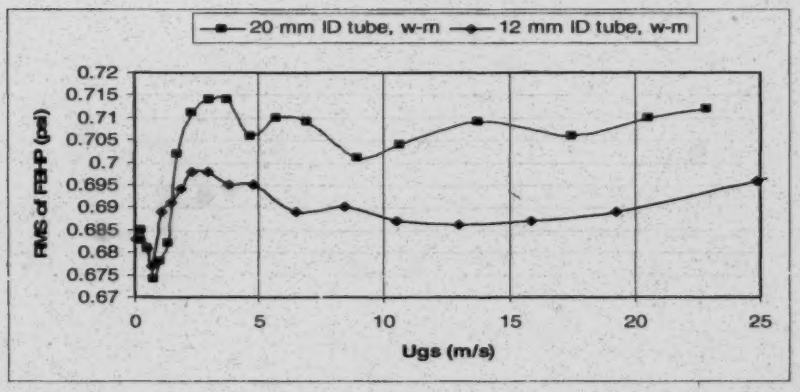

(b)

Figure 4.23. RMS recorded for 12 and 20 mm tubes. (a) S=4.16 % (b) S=16.66 %

4.8 Effect of local turbulent promoters (LTP)

In order to observe the LTP effect on overall liquid production efficiency and alterations of the base-line production characteristics due to a local reduction in diameter (Chapter

#3) a LPT device was inserted at pre-determined depth levels. The LTP is reducing the flow area from 20 to 17 mm. Experimental data indicates a negligible (if any) positive effect in increasing the liquid transported in 20 mm tubes. For the 20 mm tube two different LTP (19 mm and 17 mm ID) were employed as well as for the 12 mm tube (19 mm and 17 mm ID) and one LTP (7 mm ID) for the 8 mm tube. The location of LTP was varied only for the 20 mm tube which was at middle (1.5 m from exit), bottom (0.75 m from injection point) and top (0.75 m from exit). For 12 mm and 8 mm tube the LTP were located at middle only. Certainly this LTP creates an extra pressure drop for the two phase flow due to the turbulence that is generated. Nevertheless it also helps to encourage the atomization and entrainment of droplets in the air phase.

4.8.1 LTP experiments (D=20 mm)

The insertion of 19 mm ID LTP (area reduction of 9.75 %), indicated an insignificant effect for the case of 4.16 % submergence level regardless the LTP position (fig. 4.24 a). In the case of 16.66 % submergence value there is a reduction of up to 28 % in the transition from "pseudo slug" flow to churn flow when using two 19 mm LTP (top and bottom, fig. 4.25 a.). There is not a visible difference in the onset of production between the base line (BL – no LTP) case and 19 mm LTP Within the three different placement/configurations of 19 mm LTP the one that showed to have more effect in the liquid lifting was the two LTP (top and bottom).

The area reduction with 17 mm LTP is 27 % and amore visible effect of the base-line production characteristic than observed with 19 mm LTP is observed in figs 4.24 b and 4.25 b. Considering the 4.16 % submergence level (fig. 4.24 b) the decrease of water produced appears to augment with increasing of air injection. The onset of production for this submergence level is not affected by LTP. For the 16.16 % submergence level there is a reduction in liquid lifting for the whole air range of operation when using the 17 mm ID LTP (fig. 4.25 b).

In the annular region the difference between the water produced without LTP and with LTP tends to increase. This difference is not significant for the velocity ranges between

the point of local minimum production and annular flow. The least effect is indicated when LTP are positioned in the middle. The Two-LTP configuration appears to reduce even more the production. The LTP located at the bottom has an intermediate effect in the production.

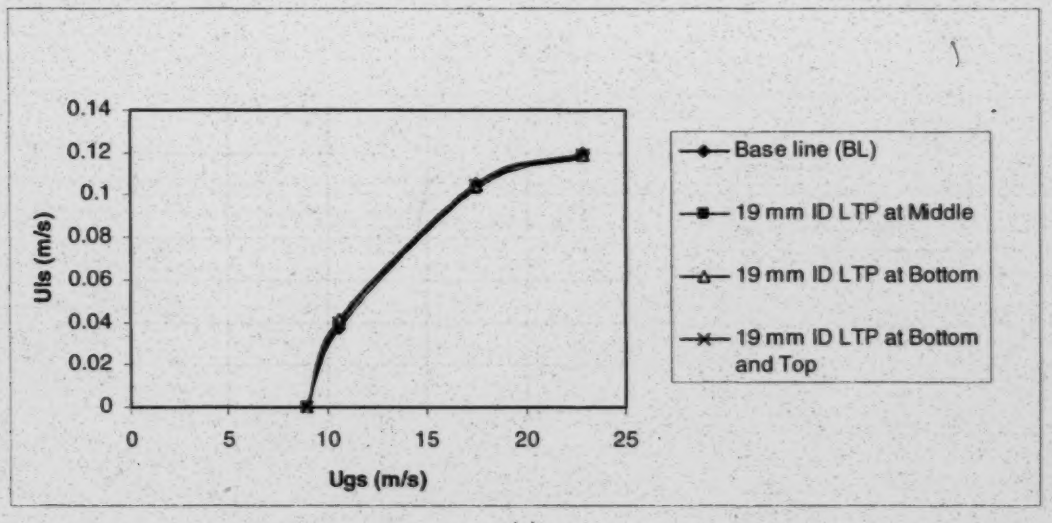

(a)

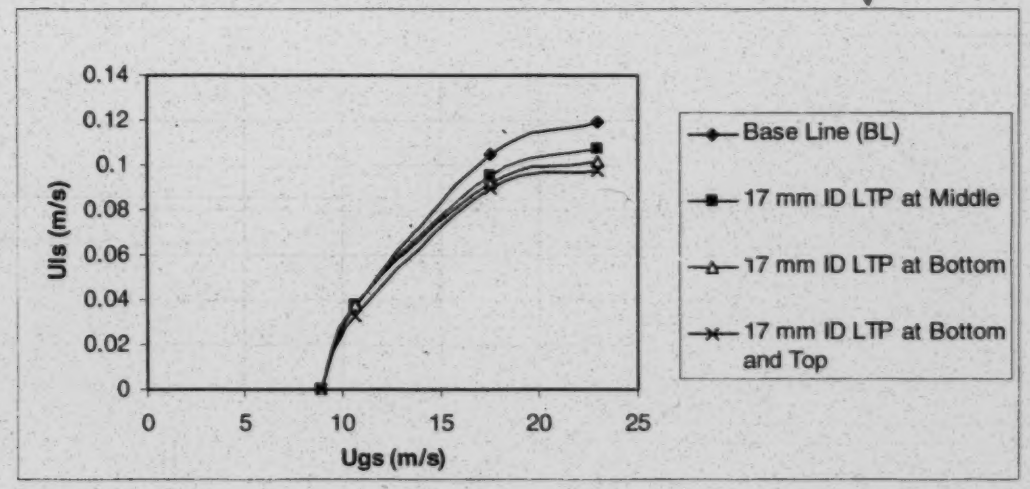

(b)

Figure 4.24. Comparison of superficial liquid velocity as a function of superficial air velocity for the 20 mm ID (the base line and three different LTP placements for S=4.16 %. (a) 19 mm LTP (b) 17 mm LTP

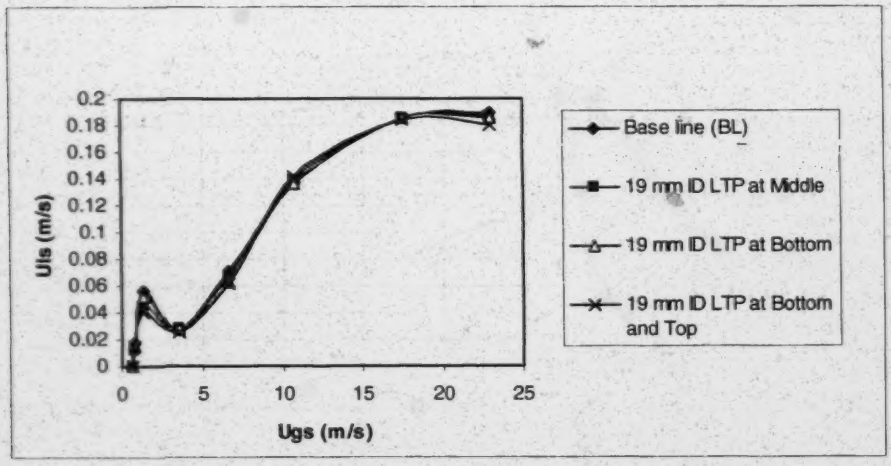

(a)

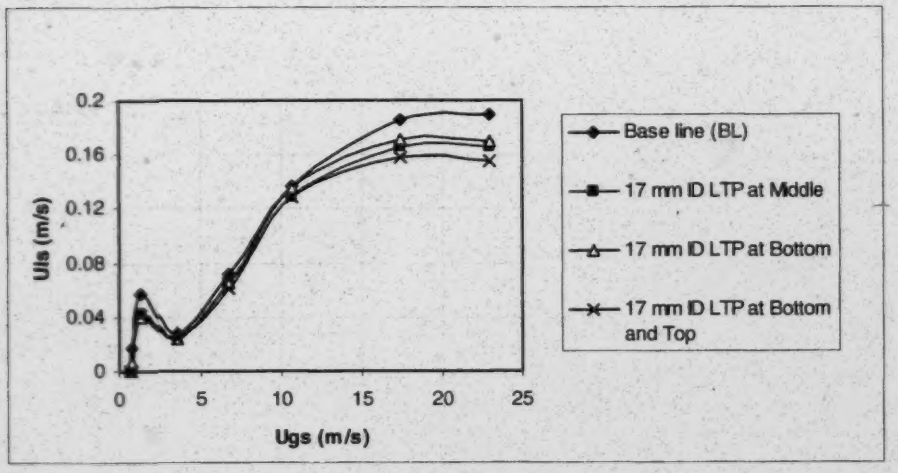

(b)

Figure 4.25. Superficial liquid velocity as a function of superficial air velocity for the 20 mm ID tube using three different placements of LTP's for S=16.66 %. (a) 19 mm LTP (b) 17 mm LTP

4.8.1.1 RMS with LTP

It is observed in figs. 4.26, 4.27, 4.28, 4.29, 4.30 and 4.31 that for low superficial air velocities (0 to 2.3 m/s) there is no difference in the RMS regardless the use of LTP and its location. This occurs for low submergence levels (figs) because there is no water lifted under low air injection and the LTP is not even reached with the water. The peak RMS values in the transition region tend to be lower when using LTP at the middle of the

tube (fig.s 4.26 to 4.335). Though the 17 mm ID LTP imposes a bigger local diameter reduction does not increase the oscillations in the transition region as seen in figures 4.26 to 4.32. For very low submergence level (4.16 %, fig. 4.26) the RMS values in the annular flow region, when employing the 19 mm ID LTP, have the trend to be lower when compared to the base line. That is not the case of the bigger area reduction (17 mm ID LTP), which generally has bigger values in the annular region.

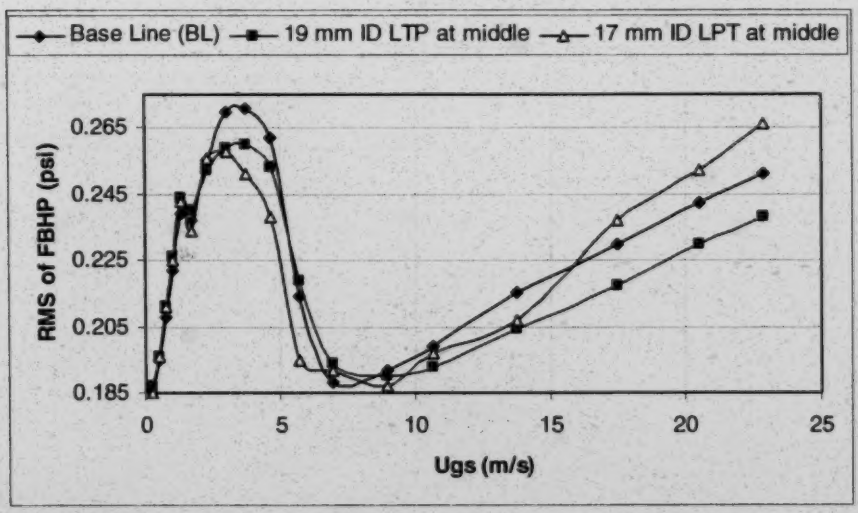

Figure 4.26. RMS versus gas superficial velocity for base-line and for two LTP designs positioned at ½ depth (20 mm tube, S=4.16 %)

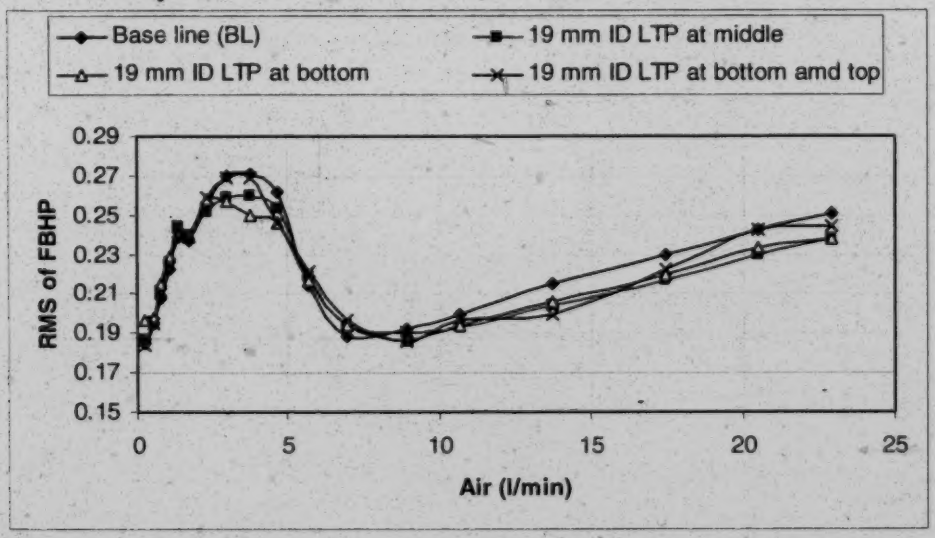

Figure 4.27. RMS versus flowrate of gas for base-line and 19 mm LTP's positioned at ½, top and bottom (20 mm tube, S=4.16 %)

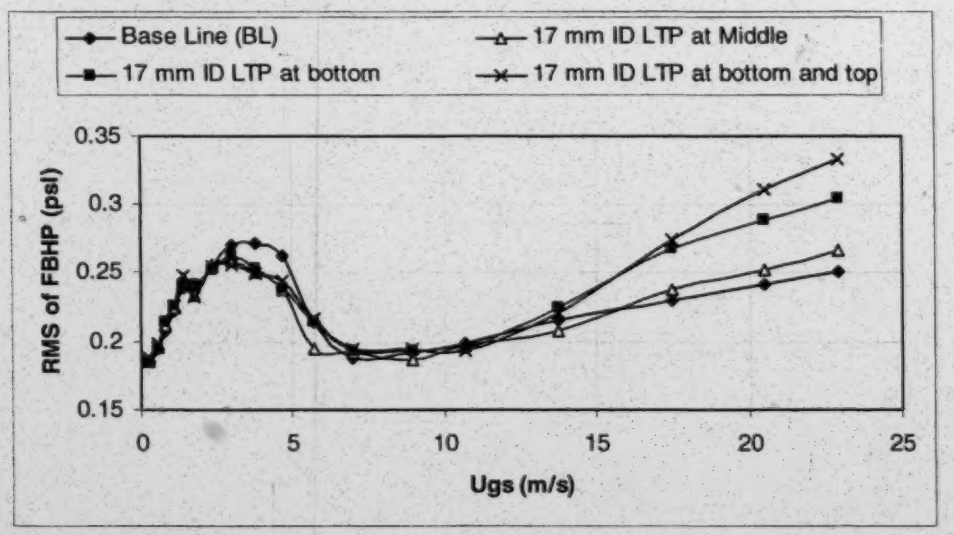

Figure 4.28. RMS versus gas superficial velocity for base-line and three 17 mm LTP's positions (20 mm tube, S=4.16 %)

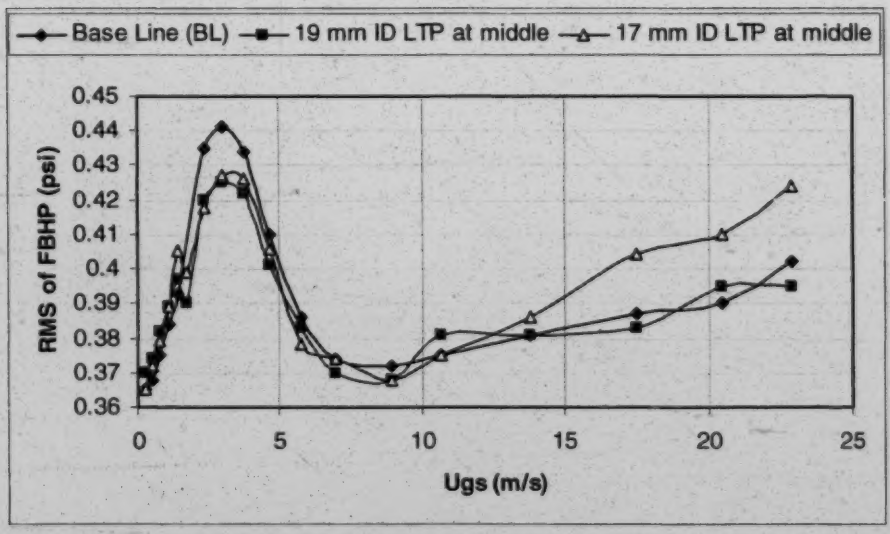

Figure 4.29. RMS versus gas superficial velocity for base-line and for two LTP designs positioned at ½ depth (20 mm tube, S=8.33 %)

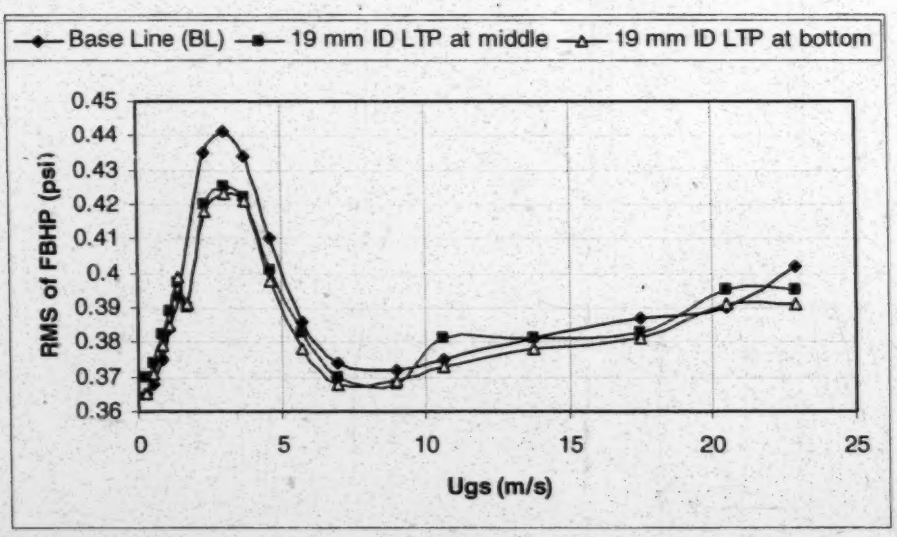

Figure 4.30. RMS versus gas superficial velocity for base-line and two 19mm LTP positions (20 mm tube, S=8.33 %)

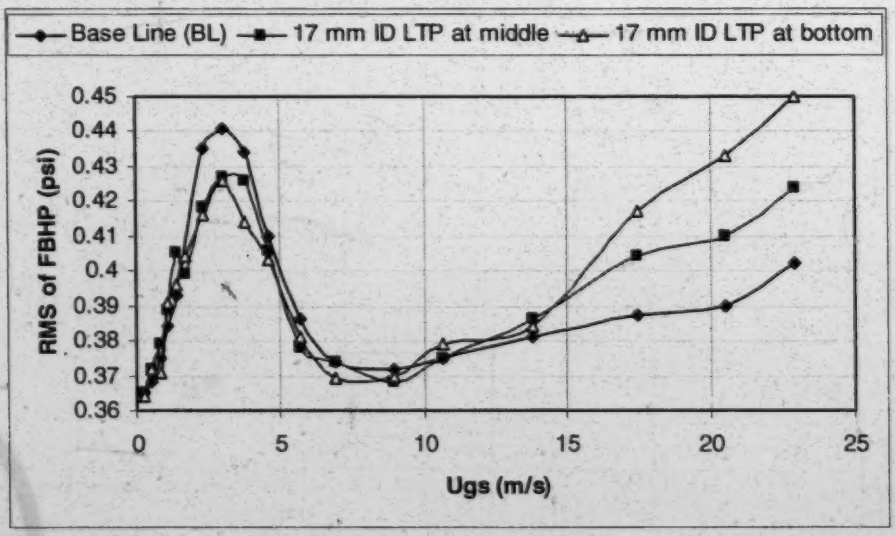

Figure 4.31. RMS versus gas superficial velocity for base-line and two 17 mm LTP positions (20 mm tube, S=8.33 %)

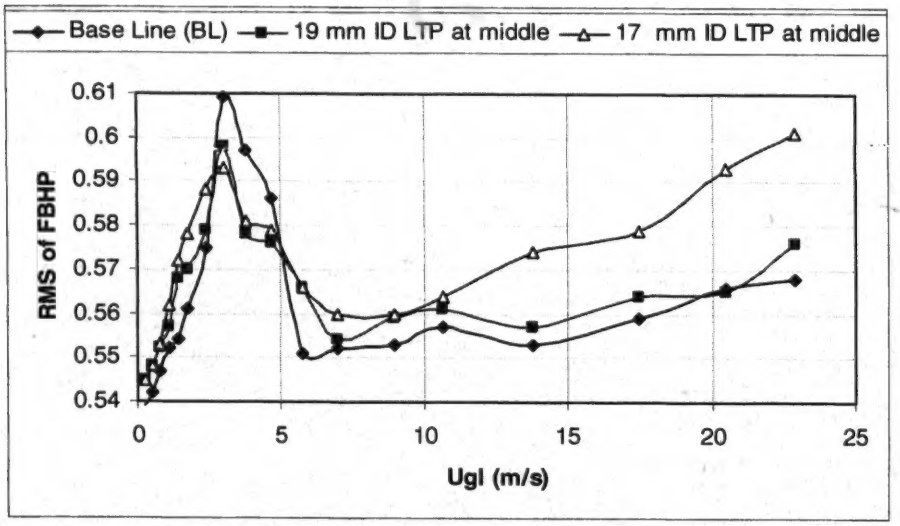

Figure 4.32. RMS versus gas superficial velocity for base-line and two LTP designs positioned at ½ depth (20 mm tube, S=12.5 %).

Figures 4.26, 4.29, 4.32 and 4.35 compare the performance of the two LTP employed in the 20 mm tube located at haft of the tube. Basically, they have similar behavior in the transition region where the RMS values are similar. However for the annular region the 17 mm ID LTP imposes bigger oscillations generating bigger values of RMS except for S= 16.66 % (figure 5.35) where their RMS values are similar.

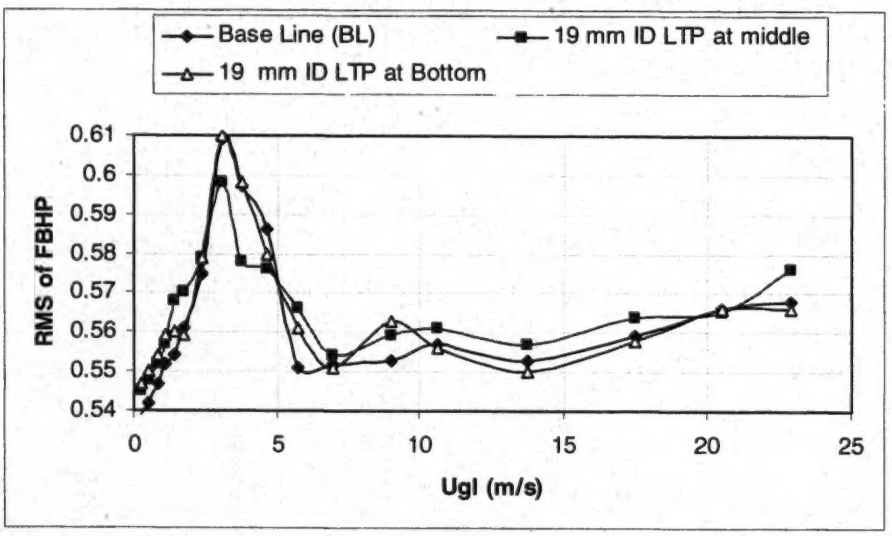

Figure 4.33 RMS versus gas superficial velocity for base-line and two LTP designs positioned at ½ depth (20 mm tube, S=12.5 %)

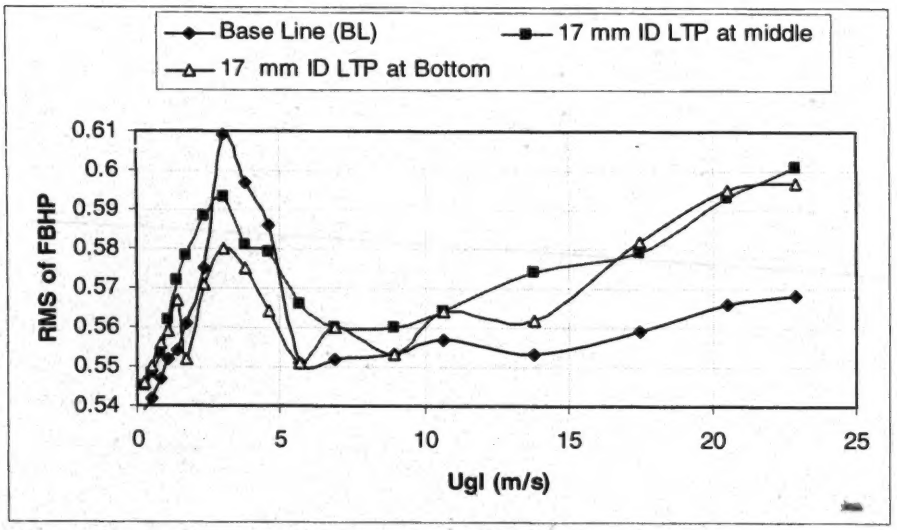

Figure 4.34 RMS versus gas superficial velocity for base-line and 17 mm LTP's positioned at bottom and ½ depth (20 mm tube, S=12.5 %)

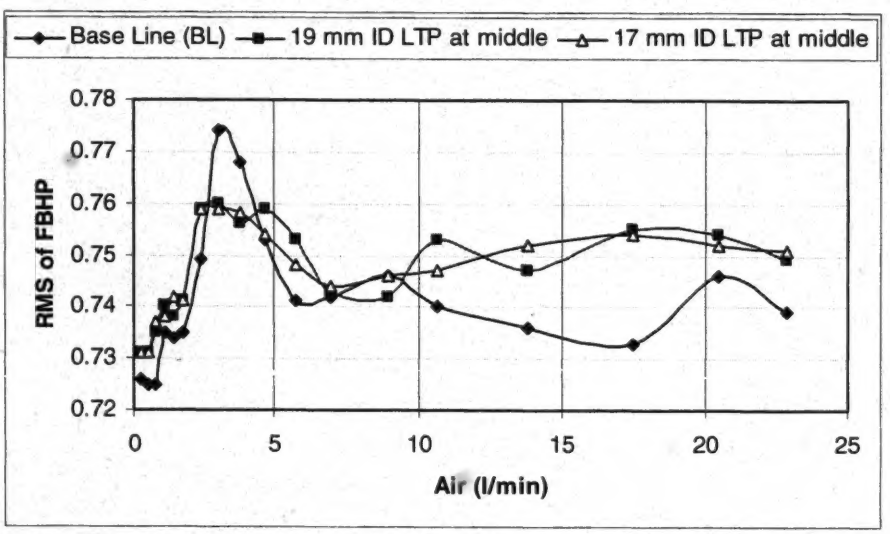

Figure 4.35 RMS versus gas injected for base-line and two LTP designs positioned at ½ depth (20 mm tube, S=16.6 %)

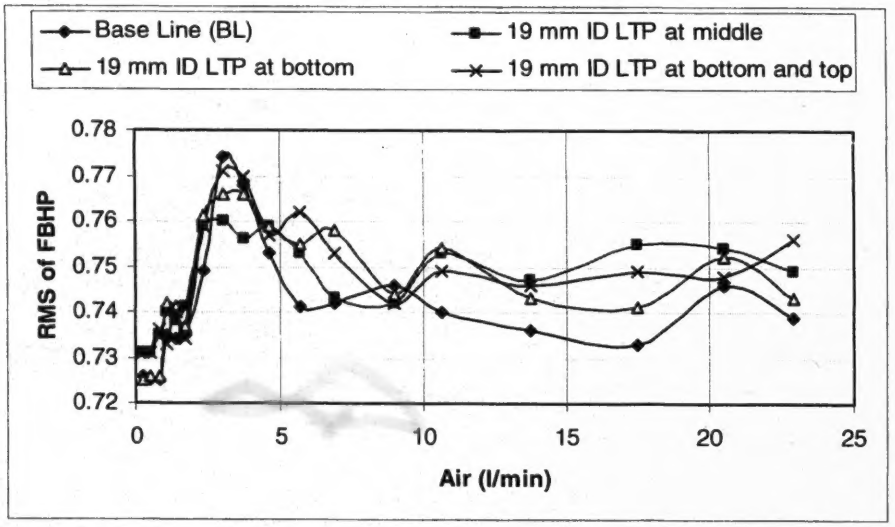

Figure 4.36 RMS versus gas injected for base-line and 19 mm LTP designs positioned at ½ depth, bottom and top (20 mm tube, S=16.6 %)

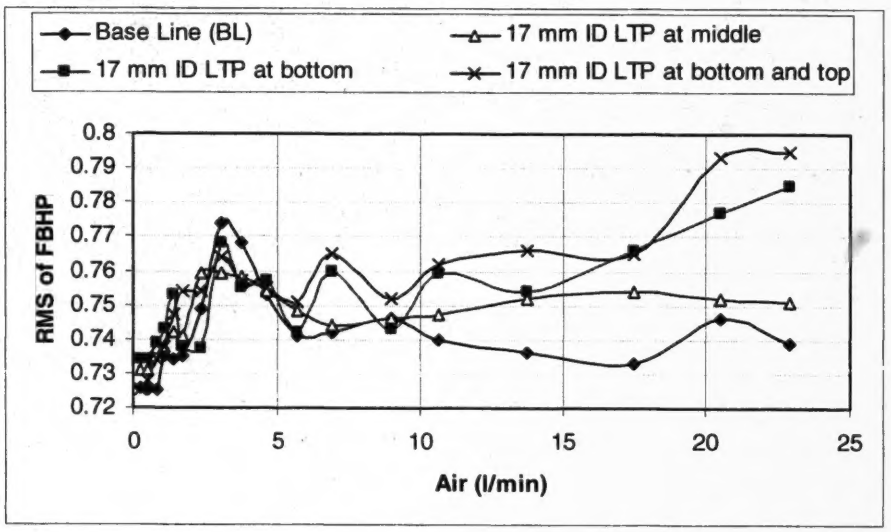

Figure 4.37 RMS versus gas injected for base-line and 17 mm LTP designs positioned at ½ depth, bottom and top (20 mm tube, S=16.6 %)

When comparing how the position of the LTP's affects the degree of oscillation it is observed from graphs 4.28 and 4.37 that the use of two 17 mm ID LTPs at top and bottom contributes to increase the RMS in the annular region. The effect of these two LTPs in the transition region compares with the other designs from the oscillations point

of view. The RMS results for the different positions for the 19 mm ID LTP are not significantly different from each other even if two 19 mm ID LTP (top and bottom) are inserted (figure 4.36).

4.8.2 LTP for SDT

The insertion of LTP at the middle of the 12 mm tube for very low submergence level tends to improve the water produced under annular flow (fig. 4.38). The onset of production is not affected by the 11 mm ID and 9 mm ID LTP. As seen in fig. 4.38, the 11 mm LTP (16 % of reduction of flow area) indicates the best performance when compared to base-line and 9 mm LTP (reducing the flow area by 43.75 %). For higher submergence level the water production improvement observed with LTP (either 9 mm or 11 mm ID LTP) tends to decrease (figs 4.39, 4.40, 4.41). It is likely that despite the LTP promotes the atomization of the film, therefore, the creation of droplets; the transporting of the liquid as film becomes more important if the submergence level is higher. Since the LTP restricts the flow of the film, it ends having a negative effect in the liquid transporting. Within the range of slug flow (figs. 4.39 to 4.41) the use of LTP lower the water produced significantly. In this case the local area reduction imposed by the LTP obstructs the flow of the liquid slug partially destroying it.

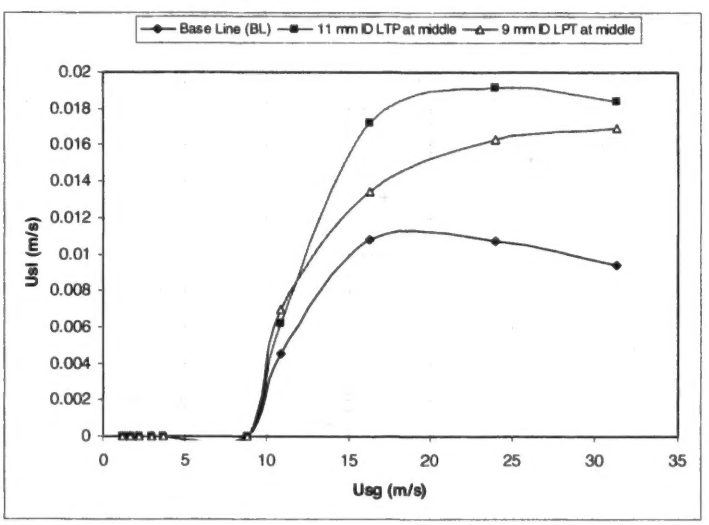

Figure 4.38 Superficial liquid velocity versus superficial air velocity for the 12 mm ID tube for 4.16 % submergence using two different LTP positioned at 1/2 of tube depth

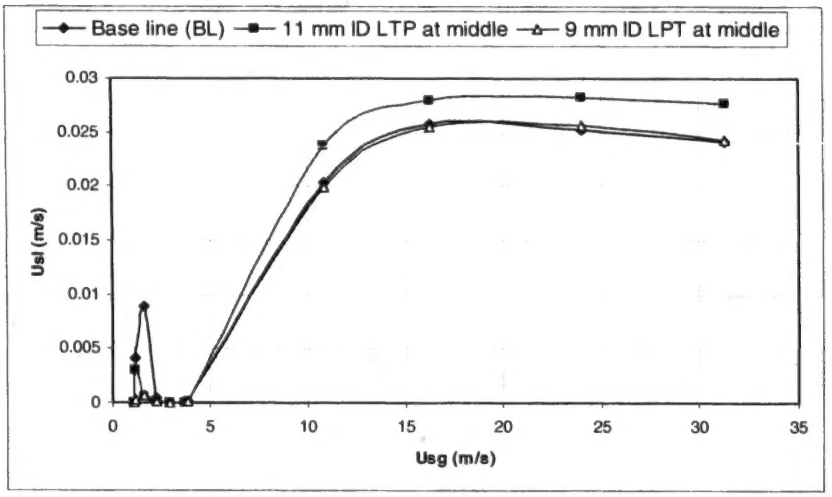

Figure 4.39 Superficial liquid velocity versus superficial air velocity for the 12 mm ID tube for 8.33 % submergence using two different LTP positioned at ½ depths

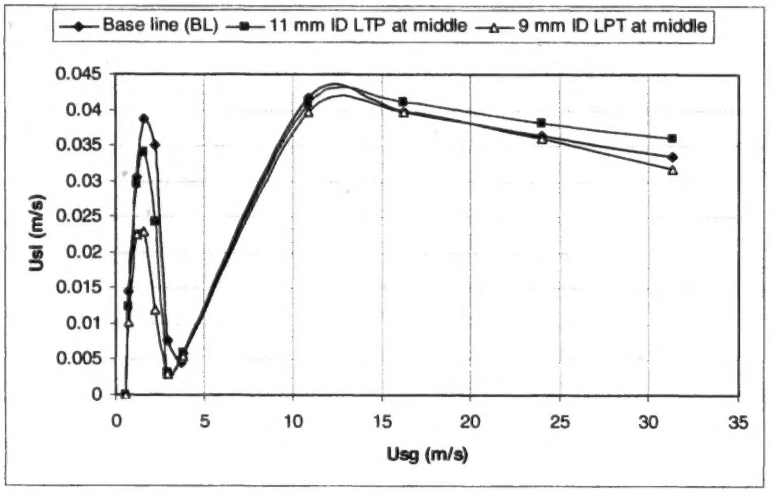

Figure 4.40 Superficial liquid velocity as a function of superficial air velocity for the 12 mm ID tube for 12.5 % submergence using two different LTP at the middle of the tube

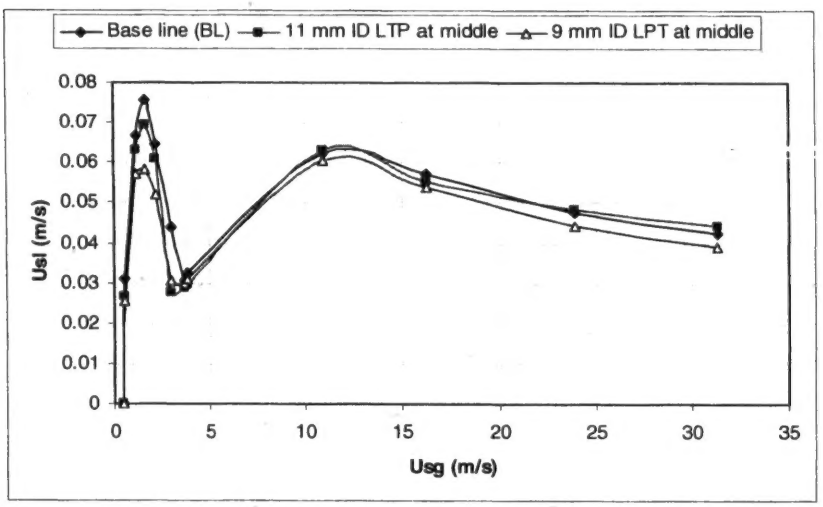

Figure 4.41 Superficial liquid velocity as a function of superficial air velocity for the 12 mm ID tube for 16.66 % submergence using two different LTP at the middle of the tube

4.8.2.1 Photographic evidence ((12 mm tube equipped with 11 mm LTP)

Photographic evidence is shown in figs 4.42 and 4.43. As It is observed in figs 4.42 and 4.43 (base-line and LTP) that LTP promotes the atomization and entrainment of droplets. It seems that when transporting small amount of water (4.16 % submergence) under annular flow regime with this tube the lifting of liquid as droplets can be bigger than as a film. Even if at any time it appears that there is more water contained in the film than in the droplet core, the sizable difference between the upward film and droplet-gas core velocities suggests that water is mainly transported as droplets in the gas core.

Figure 4.42. Snapshots comparing the base-line and LTP gas-liquid upward flow in 12 mm tube and S=4.16 % (a) Ugs = 10.89 m/s with 11 mm LTP. (b) Ugs = 10.9 m/s without LTP. (c) Ugs = 23.9 m/s with 11 mm LTP. (b) Ugs = 23.9 m/s base-line

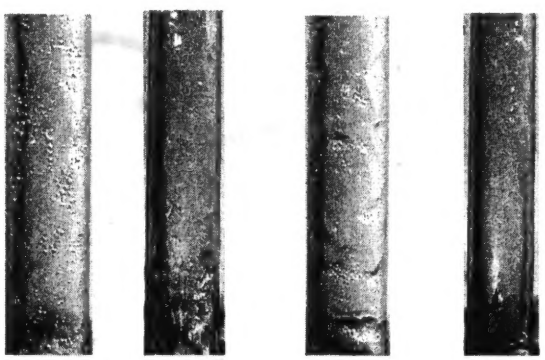

Figure 4.43. Snapshots comparing the base-line and LTP gas-liquid upward flow in 12 mm tube and S=16.16 % (a) Ugs = 10.89 m/s with 11 mm LTP. (b) Ugs = 10.9 m/s without LTP. (c) Ugs = 23.9 m/s with 11 mm LTP. (b) Ugs = 23.9 m/s base-line

4.8.2.2 RMS for 12 mm tube with LTP

The results are summarized in figs 4.44, 4.45, 4.46, 4.47. RMS versus superficial gas velocity illustrated in figs. 4.44-4.47 indicate a comparable or somewhat higher values than for LTP experiments than for base-line. For extreme high superficial air velocities the RMS using the 9 mm LTP indicates a remarkably lower values than with the 11 mm LTP and base-line. This is an indication that for very high superficial air velocities it is

possible to transport more liquid in SDT tube using a larger area reduction (9 mm ID LTP). However, this statement is limited to laboratory conditions; the film-core conditions typical for base-line experiments are re-gained after a certain distance from the LTP or a great number of LTP should be introduced.

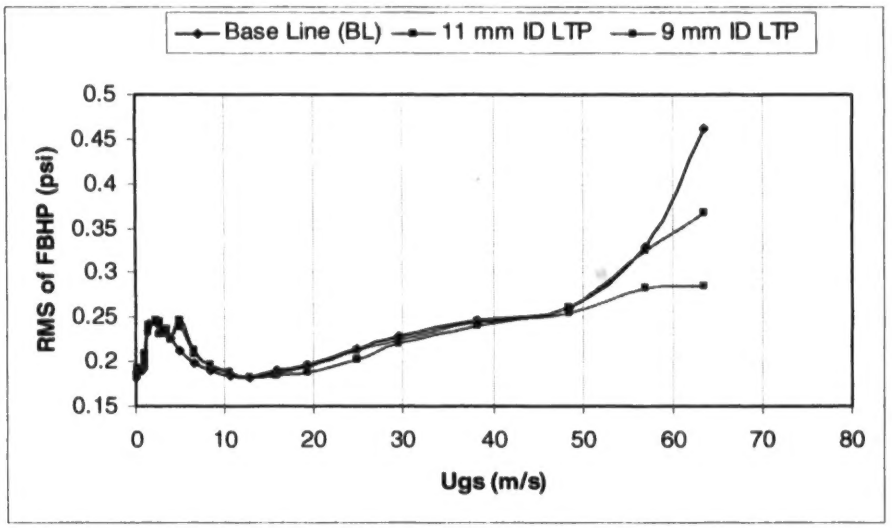

Figure 4.44 RMS versus superficial gas velocity observed for the base-line and two sizes of LTP located at ½ of depth (12 mm tube and S= 4.16 %)

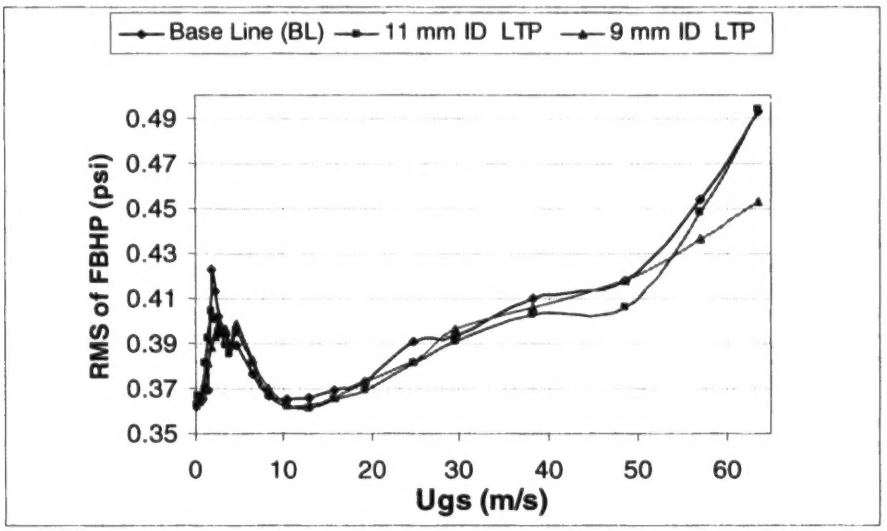

Figure 4.45 RMS versus superficial gas velocity observed for the base-line and two sizes of LTP located at ½ of depth (12 mm tube and S= 8.33 %)

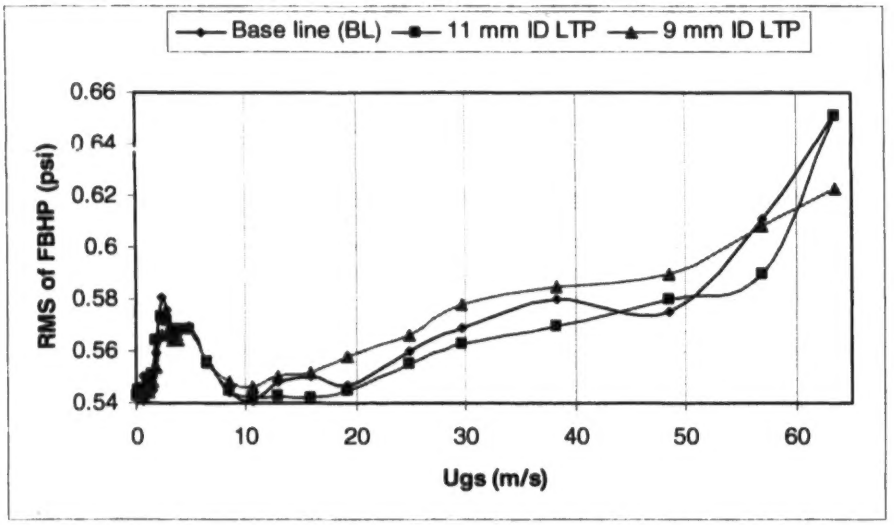

Figure 4.46 RMS versus superficial gas velocity observed for the base-line and two sizes of LTP located at ½ of depth (12 mm tube and S= 12.5 %)

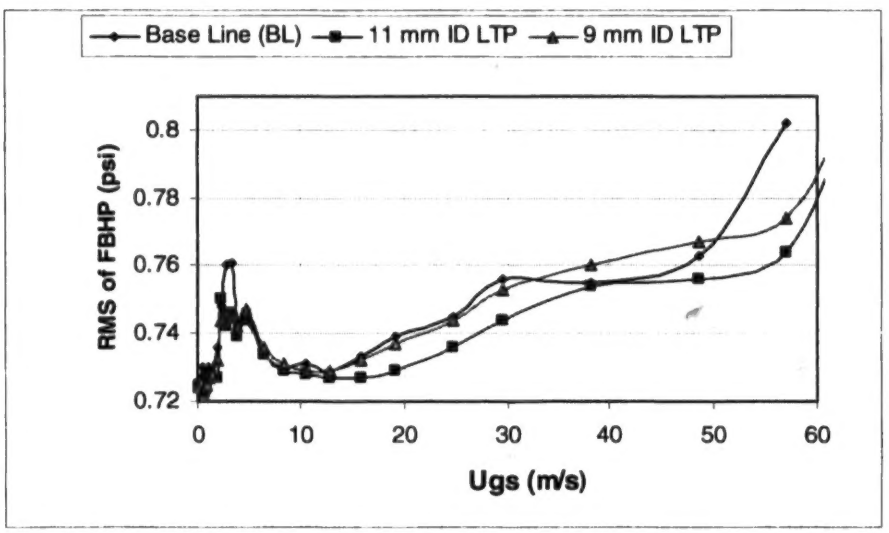

Figure 4.47 RMS versus superficial gas velocity observed for the base-line and two sizes of LTP located at ½ of depth (12 mm tube and S= 16.6 %)

4.8 Experiments with 8 mm tube using LTP

Figs. 4.48 and 4.49 compares the RMS obtained for base-line and for tubes with LTP inserts. The volume of liquid transported with this tube is very limited compared with the

12 mm and 20 mm. The peak value of the RMS tends to be much higher with the 7 mm LTP than for the base line test. (fig. 4.48, 4.49) and this difference grows with submergence level. This is not the case, as previously discussed, for the 12 and 20 mm tubes where this difference at peak RMS value tends to be diminished with increasing of submergence.

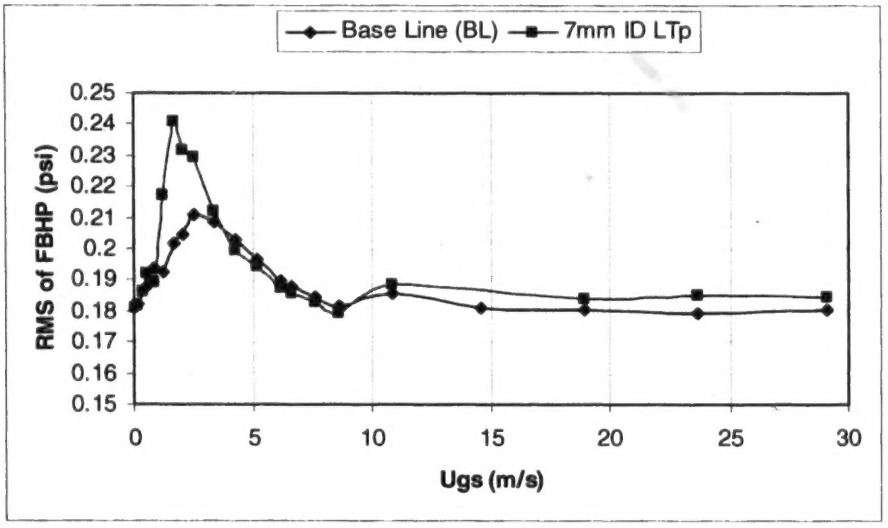

Figure 4.48. RMS of FBHP for 8 mm tube using 7 mm ID LTP for 4.16 % submergence level.

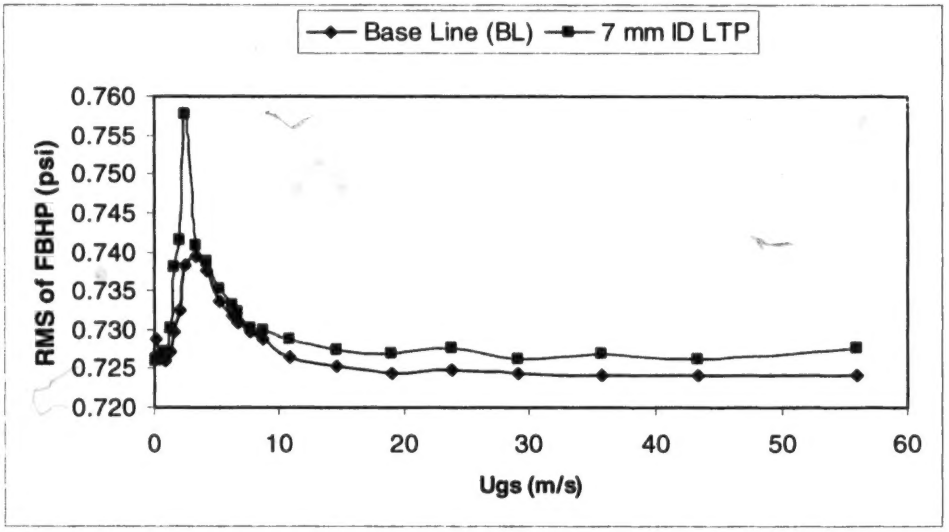

Figure 4.49. RMS of FBHP for 8 mm tube using 7 mm ID LTP for 16.66 % submergence level.

CHAPTER 5
NUMERICAL ANALYSIS

In this chapter the experimental data is compared with theoretical models presented in chapter 2. Chen -Brill model [12] and the Tengesdal empirical formulation [20] for the prediction of slug-churn transition. These results are compared with the experimentally values observed for each tube and submergence level as well. Then Turner and Flow Reversal models describing churn-annular (developed) are utilized to calculate this transition boundary. Further, the experimental data obtained in this study (within the range of slug-to-annular transitions) are compared with Putra [8] and Ansari [7] models. These models have been written using an Excel program with suitable macros used for introducing specific input conditions.

5.1 Slug-churn transition stage

Fig. 5.1 compares the experimentally obtained gas lift characteristic (D=20 mm, S=16.6%) with transition points calculated for water-air using Tengesdal and Pura's models for transition stage slug-churn. As observed in fig. 5.1 the Chen-Brill model predicts very well the boundary for this transition whereas Tengesdal correlation indicates a much higher superficial gas velocity.

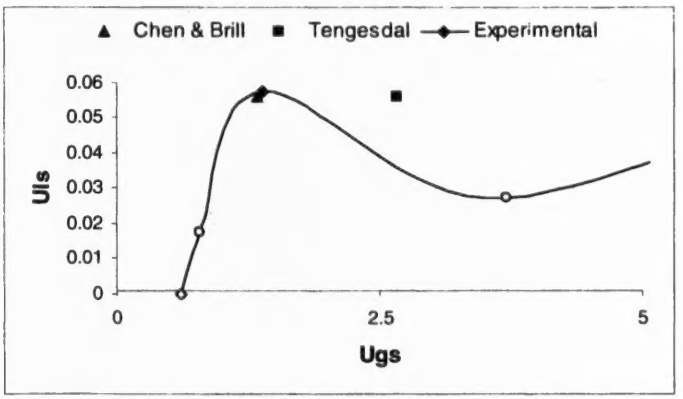

Figure 5.1 Calculated slug-churn transition boundary and the production characteristic determined in this study (D=20 mm S=16.66 %)

Experiments performed in 12 mm tube indicate a net liquid production (pseudo-slug flow pattern) for S> 8.33 %. Fig. 5.2 compares the experimental production characteristic with calculated transition stage (STC) for this tube. For this riser the experimental air superficial velocity at which the transition occurs (first stage of STA) is independent of the submergence level, that is, the amount of water being transported does not affect it but the gas velocity. This is not the case for Chen-Brill model [12] and Tengesdal correlation [20] where the superficial liquid velocity affects the value of the superficial gas velocity corresponding to the transition. Chen-Brill model predicts fairly well the transition for 16.66 % submergence level as observed in fig. 5.2 whilst Tengesdal overestimates this value. For lower submergence levels the Chen-Brill model appears to be less accurate in predicting transition as observed in the laboratory. For these experimental conditions (low submergence) Tengesdal appears to offer better predictions. (fig. 5.2).

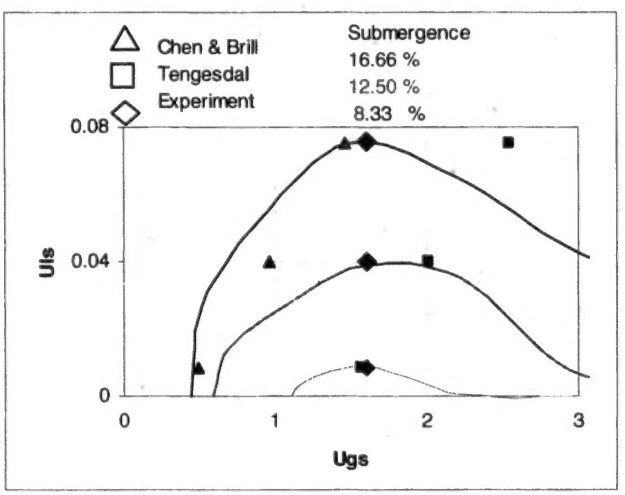

Figure. 5.2 Calculated slug-churn transition boundary and laboratory measured gas lift characteristic (D=12mm, S=16.6%)

The minimum submergence level, in the case of the 8 mm ID tube where the onset of net liquid production is observed (as pseudo slug regime), is as low as 6.25 % submergence level. Fig. 5.3 shows the experimental and calculated slug-churn transition for 16.66 %

level. The calculation of the transition with Chen-Brill model almost match the experimental value as observed in fig. 5.3.

Fig. 5.4 indicates that the Tengendel correlation better predicts the slug-churn transition in all cases for the 4 mm tube. Being closer the prediction for 16.66 % submergence level where there is almost perfect match. The error in the prediction increases for lower submergence levels underestimating the transition. In this case Chen-Brill model fails to offer a good prediction for any of the submergence levels employed in this case.

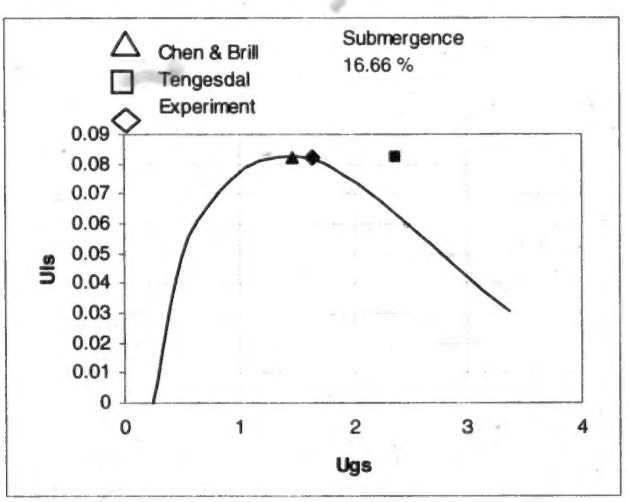

Figure 5.3 Calculated slug-churn transition boundary and measured production characteristic for the 8 mm tube (air-water).

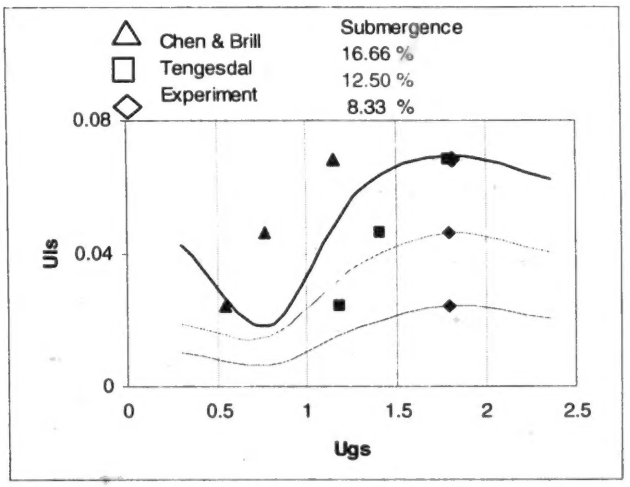

Figure 5.4 Calculated slug-churn transition boundary and measured characteristics for the 4 mm tube (air-water).

5.2 Churn-to-annular transition stage - comparison of experimental results with numerical models

Since the churn-annular (developed) transition stage takes place at higher air superficial velocities compared to the slug-churn stage it is difficult to accurately determine by direct observation when this transition occurs. The RMS does not show precisely when this transition occurs either. Yet, a range of gas velocities can be determined by slowly injecting air and directly observing. Fig. 5.5 show this range observed for the range of diameter tubes employed for this research. For base-line experimental conditions (water-air at20 ° C and 101 kPa) Turner formula predicts the CTA transition velocity of almost 15 m/s regardless of the tube diameter. Whilst the flow reversal criterion [25] predicts lower critical velocities for smaller diameter tubes as shown in fig. 5.5. The observations certainly indicate that the transition CTA is between these two calculations. In the case of the 20 mm ID tube there is not great difference between Turner and flow reversal criteria.

It was clear from the direct observations of the experiments conducted that the amount of liquid being lifted, which depends on the submergence level, does not affect the transition to annular flow.

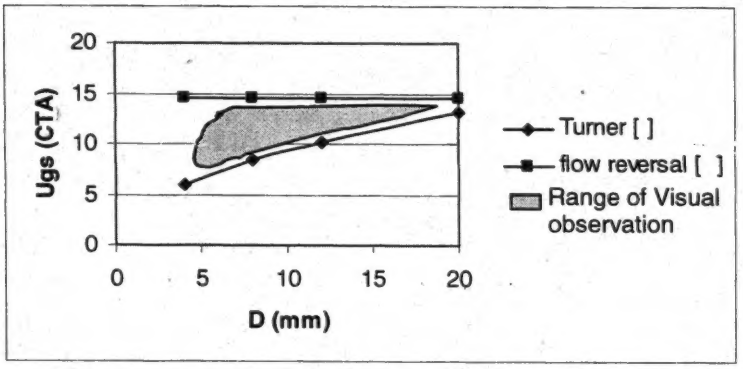

Figure 5.5 Calculated churn-annular transition boundary and visual observations.

5.3 Production characteristic – comparison of experimental and modeled data for 20 mm tubes

Fig. 5.5 compares the production characteristic [U(ls)=F(U(gs)] obtained during present investigations with data modeled using Ansari [10] model for the slug region. The modeled data indicates a higher gas velocity at the onset of liquid production (1.2 versus 0.6 m/s) and a lower maximum superficial liquid velocity compared with the experimental one.

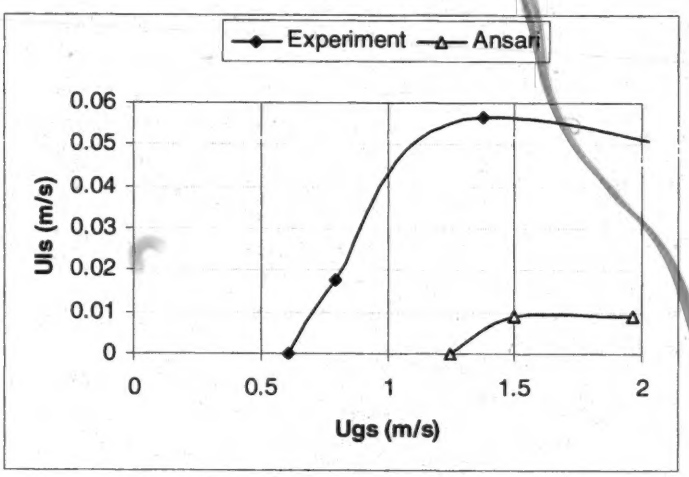

Figure 5.6 Superficial velocity of liquid (water) versus air superficial velocity – laboratory (D=20 mm S=16.6%) versus modeled data (Ansari [10])

Fig. 5.6 shows the critical length that it would be reached by injecting different air flow rates with its corresponding amount of liquid transported by it (16.66 % submergence level). The critical length is calculated using the model proposed by Becaria [2] called Small Diameter Pipe (SDP). The critical length is nothing else but the maximum vertical distance a certain liquid flowrate can be lifted as slug flow pattern under given reservoir pressure (submergence), and gas flowrate. The SDP model was developed and validated for smaller pipe diameters and yet, predict satisfactorily the present laboratory findings for 20 mm tubes.

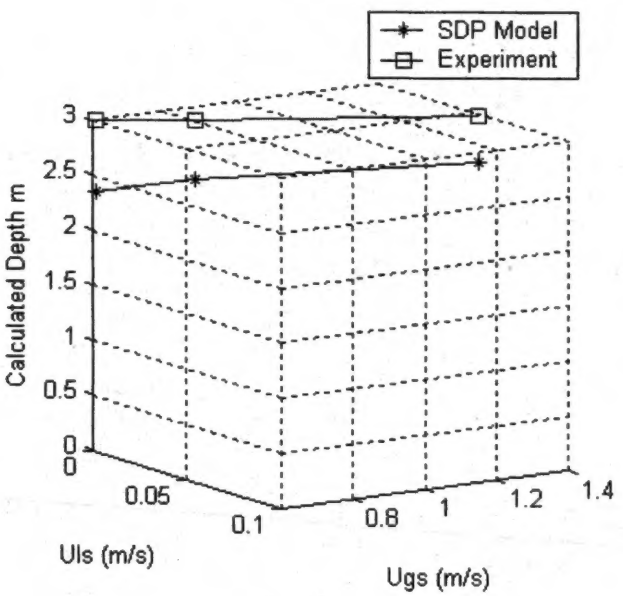

Figure 5.7 The SDP [2,4] model developed for small diameter pipes (under pseudo-slug flow pattern) and present data obtained in laboratory (D=20 mm, S=16.6% or 50.8 cm H_2O)

For S=35 % (fig. 5.8) the SDP model indicates a good match for low gas flowrates and overestimates the critical depth at higher gas flowrates.

Fig. 5.9 comparing the calculated production characteristics using Ansari [10] and Hasan [7] models and present experimental data (D=20 mm, S=35%) indicates that relatively large differences are observed between prediction of well accepted models and

experiments. These differences are partially related to various models assumptions and to the fact that the gas-liquid flow pattern is not perfectly developed in a 3m depth tube.

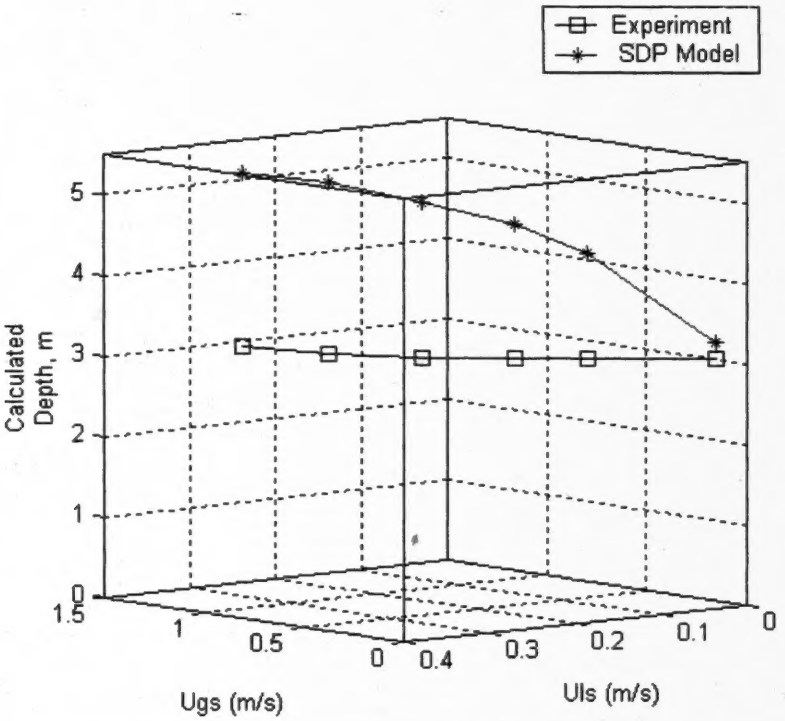

Figure 5.8 Maximum transportation depth versus gas injected calculated with the SDP model [2,4] and present experiments (D=20mm, S=35% or 106.7 cm H_2O)

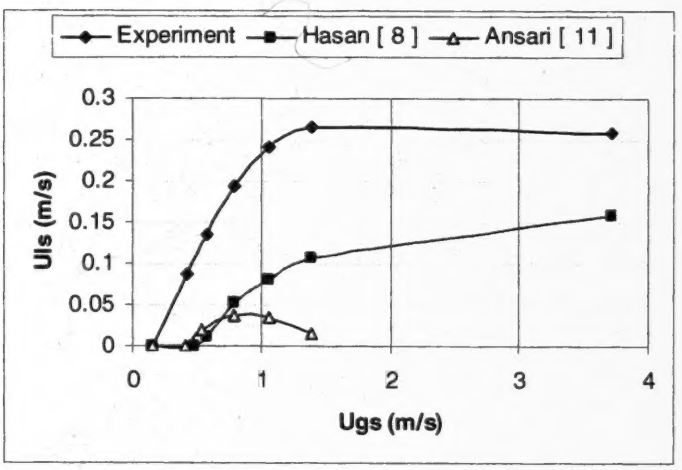

Figure 5.9 Calculated (Ansari [10] and Hasan [7]) and measured production characteristic (D=20 mm, S=35%)

5.4 Putra's laboratory data and model for pressure drop during STC transition

The model proposed by Putra [12] for assessing transition from slug to churn (as an intermediary transition stage in the slug-to-annular transition) is compared with his experiments in order to verify the excel model elaborated for this thesis. Considering the experimental data from table 5.1 the Excel program was run and it was obtained the data that is shown as Putra model in table 5.1. It was also known that the two fluids employed by Putra were air and water, that ID diameter tube was 38 mm and that the maximum operation pressure was 20 psig.

Fig. 5.8 shows graphically the comparison of the curves between the Putra experiments and mathematical model. The shape of the curves is similar and there is good agreement between them. There might be some minor differences between the model actually elaborated by Putra and the model prepared for this research. For instance, the correlation for the friction factor utilized in this research is given by 2.60 for the turbulent (smooth) case while Putra uses Colebroke correlation (roughness is considered).

Table 5.1. Data within churn flow pattern [12]

	pressure drop (psi/20 ft)	
SCFM	**Putra experiments**	**Putra model**
10	1.55	1.5
20	1.15	1
30	0.72	0.63
40	0.4	0.34
50	0.22	0.27
60	0.2	0.25

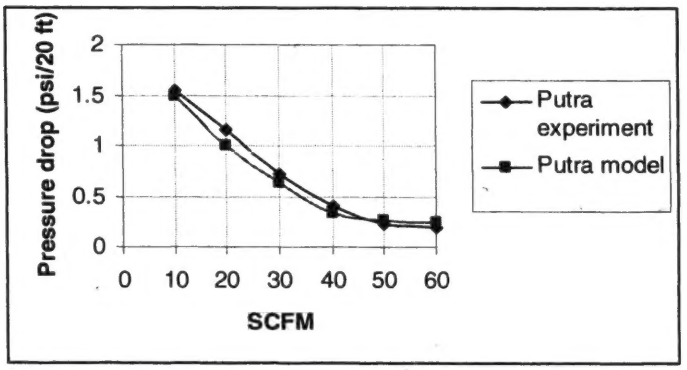

Figure 5.10 Pressure drop versus gas injection experimental results and modeled data (Putra's [12] model) for churn flow pattern

5.5 Comparison of experimental data with Ansari's model [10] for annular flow

In order to verify the model elaborated for this research based on Ansari model for annular flow the experimental data used by Alves [29] have been compared with Ansari's model (model adapted for this work using bexcel) (Table 5.2). This corresponds to field data where the pressure was measured every 100 m. The gas production was 188 SCMD, liquid production 8.5 m^3/day, the specific gravity of gas 0.65, liquid density 880 kg/m^3 and diameter tube 0.062 m. The superficial gas velocity was kept constant since Alves indicated [34 that despite the gas expansion when going up in the tube from bottom to top the condensation of heavy ends occurring as temperature and pressure decreases offsets the volume of the gas expansion leading to an almost linear pressure drop variation with depth.

Table 5.2 as well as fig. 5.11 shows that using the Ansari's model (adapted in this work for Excel) in the annular flow pattern zone produces good results.

Table 5.2 Input data [35] used for validation of Ansari's model in the annular flow pattern zone

Depth (m)	Pressure (10^5 pa)		
	Alves test	Ansari Model	%E
0	110.385	109.00	1.25
100	110.81	110.49	0.29
200	111.9	111.98	-0.07
300	113.245	113.48	-0.21
400	114.56	114.97	-0.36
500	116.11	116.47	-0.31
600	117.89	117.97	-0.07
700	121.085	119.47	1.33
800	122.67	120.98	1.38
900	123.31	122.48	0.67
1000	124.885	123.99	0.72
1100	126.965	125.50	1.16
1200	128.65	127.01	1.28
1300	130.415	128.52	1.45
1500	133.615	131.55	1.54

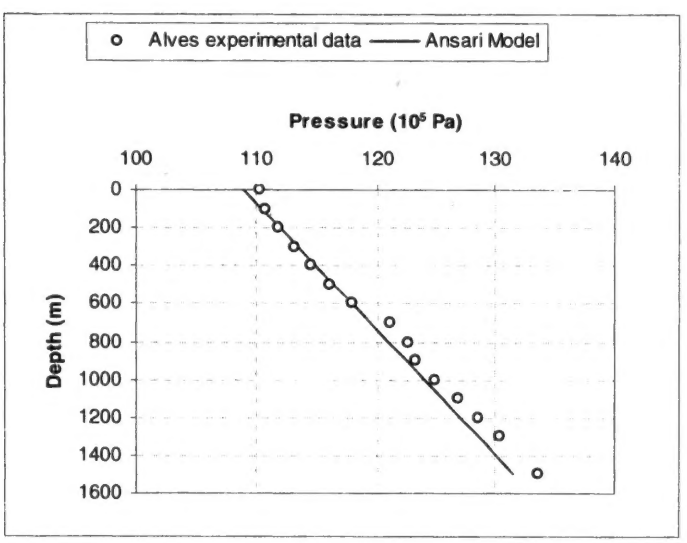

Figure 5.11. Comparison between field data and Ansari model

5.6 Comparison of the experimental results and Putra's model for churn flow

Fig. 5.12 compares experimental production characteristic data (D=20 mm, S=16.6%) with calculated data (Putra's Model [12]). Calculated and experimental data compare satisfactorily as it can be assumed that Putra's model is valid for the churn transition stage only except for the very beginning of the transition.

In the case of 12.5 % submergence level the prediction of the onset of production by Putra's model is quite accurate however for the other two point there is some discrepancies between modeled and experimental data.. For high superficial air velocity Putra model tends to underestimate the water produced. For 8.33 % submergence the onset of production is underestimated. This is worsened for 4.16 % submergence.

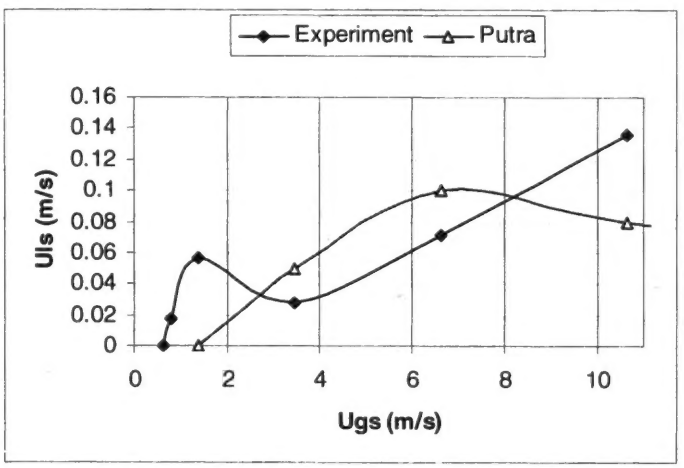

Figure 5.12 Experimental results (D=20 mm, S=16.6%) and calculated data using Putra's model [12]

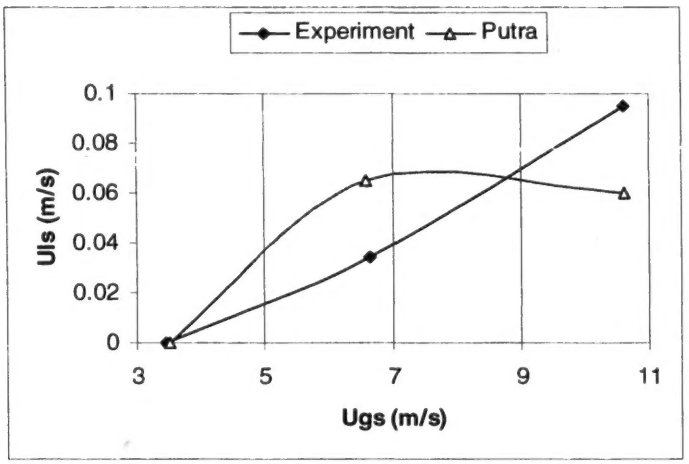

Figure 5.13 Experimental results (D=20 mm, S=12.5%) and calculated data using Putra's model [12]

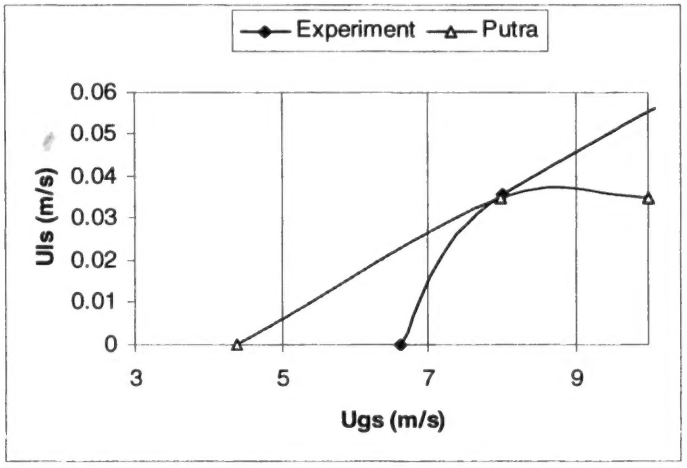

Figure 5.14 Experimental results (D=20 mm, S=8.33%) and calculated data using Putra's model [12]

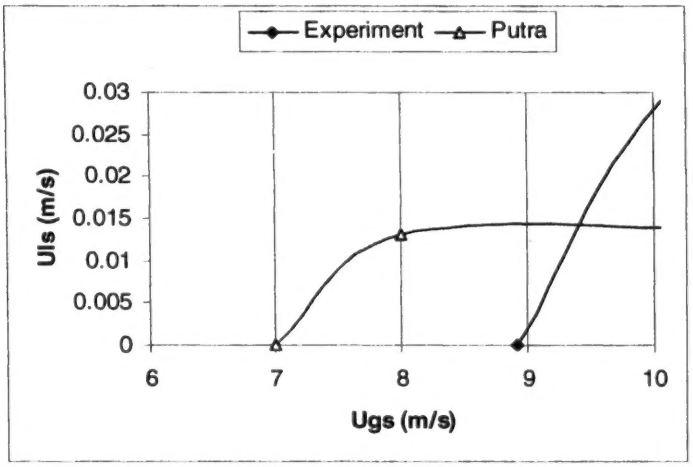

Figure 5.15 Experimental results (D=20 mm, S=4.16%) and calculated data using Putra's model [12]

In the case of the 12 mm tube Putra's model results compare well with the experimental data for high values of gas superficial velocities as can be seen in figs 5.16 through 5.18. However for intermediate gas superficial velocities the model overestimates the liquid production and for the very beginning of the transition there is a significant under - prediction of the lab results.

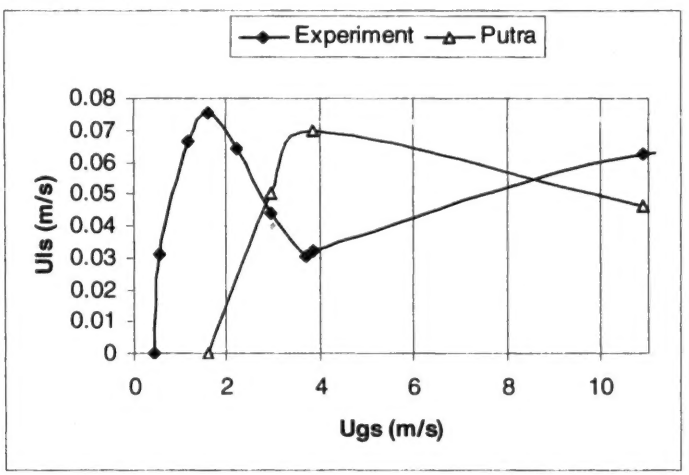

Figure 5.16 Experimental results (D=12 mm, S=16.16%) and calculated data using Putra's model [12]

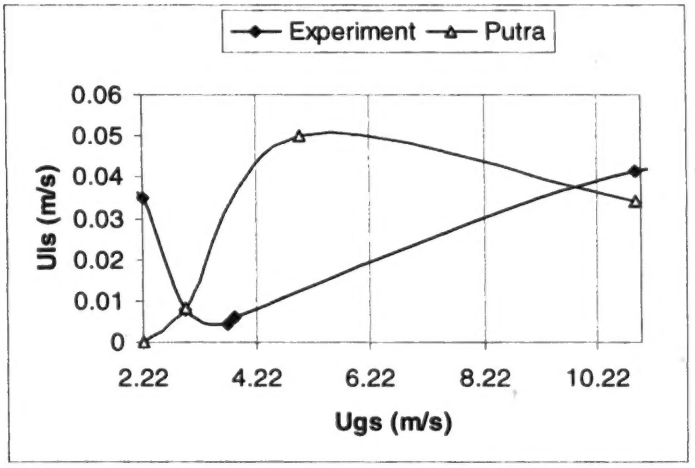

Figure 5.17 Experimental results (D=12 mm, S=8.33%) and calculated data using Putra's model [12]

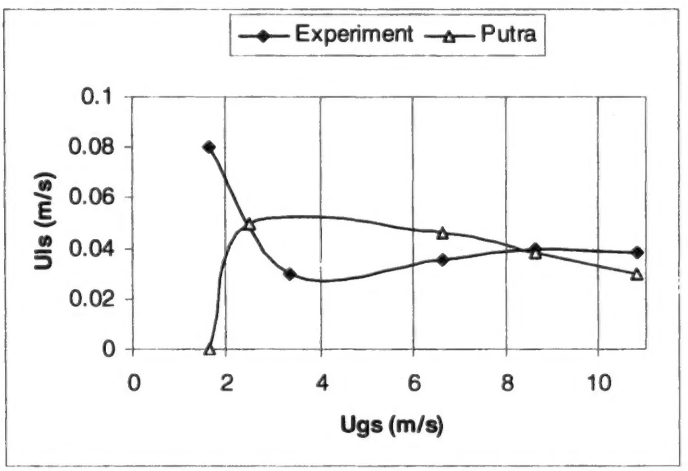

Figure 5.18 Experimental results within churn flow and Putra's model prediction (8 mm tube and S=16.66 %)

5.7 Comparison of calculated (Ansari model [11]) and experimental pressure drop in the annular flow pattern zone

Near atmospheric conditions have been used for all described experiments.. Figs. 5.19 and 5.20 illustrate the calculated (Ansari model [10] for three distinct pressures) and measured BHP pressure versus Ugs (annular flow pattern in a 20 mm ID tube and 3 m length). A minimum value of the BHP is observed for all cases illustrated in fig. 5.19.. The BHP of the experimental data does not coincide in this case with the Ansari prediction.

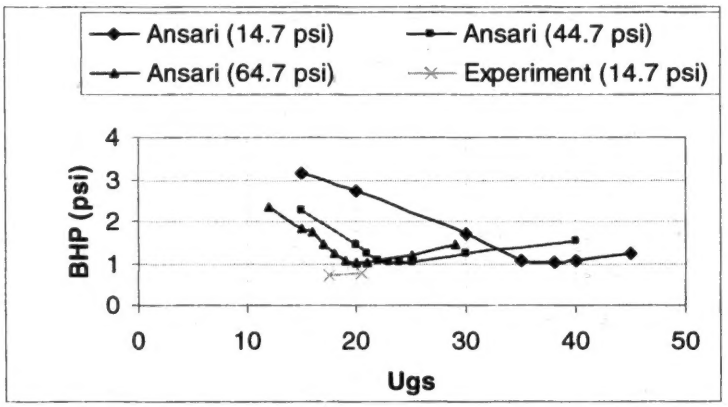

Figure 5.19 Calculated and experimemental BHP versus superficial gas velocity (D=20 mm, S=16.6% , U(ls)= 0.18 m/s)

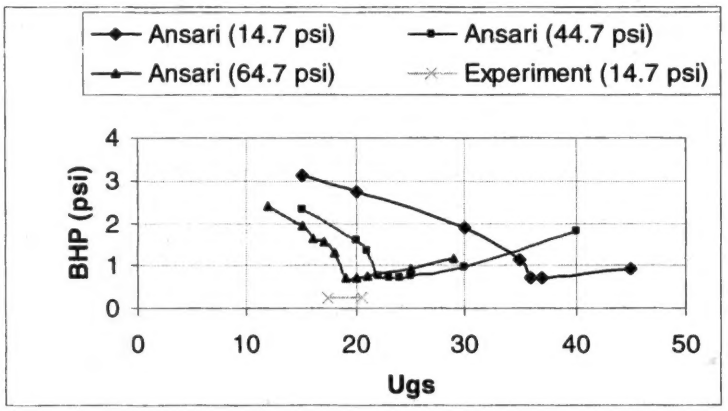

Figure 5.20 Calculated and experimental BHP versus superficial gas velocity data (D=20 mm, S=16.6% , U(ls)= 0.1 m/s)

In the case of the 12 mm ID tube the lowest pressure drop modeled by Ansari at atmospheric conditions coincides with the experiments as seen in fig. 5.22. Though there is an overestimation by Ansari model in this case both results are not too far. Fig. 5.22 compares calculated (Ansari [10] annular flow model) and measured BHP versus U(gs) for different diameters.

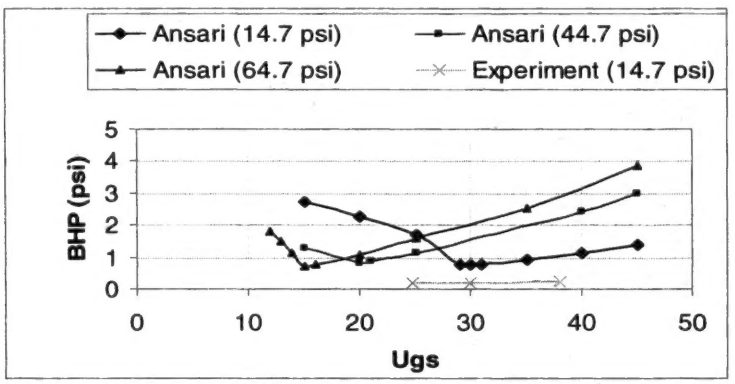

Figure 5.21 Calculated and experimental BHP versus superficial gas velocity data (D=12 mm, S=16.6% , U(ls)= 0.042 m/s)

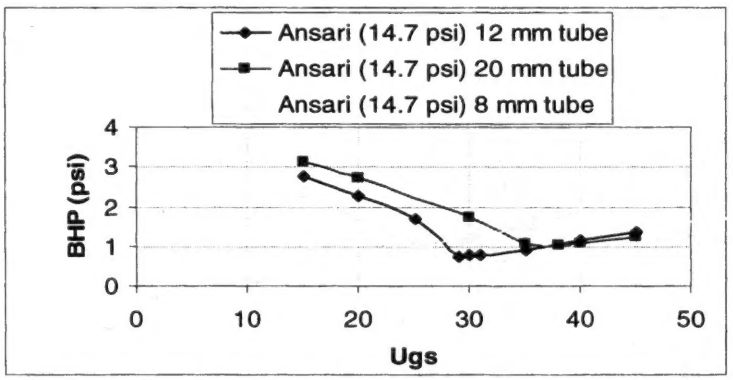

Figure 5.22 Calculated and experimental BHP versus superficial gas velocity data for various tube diameters (D=12 mm, S=16.6% , U(ls)= 0.042 m/s)

5.8 Potential field applications of SDT

If the use of small diameter tubes is intended to maximize the recovery of gas by removing liquids it would be adequate to produce the gas through the annulus space between the casing and the small diameter tube as shown in fig. 5.23. As the reservoir

pressure is considered to be low it might be required the injection of gas to lift the liquid via the small diameter tubing (SDT). The injection of gas could be carried out through a small diameter line and it should be injected at the very bottom of the SDT as show in fig. 5.23.

The pressurized gas to remove the liquids could come from a high pressure gas well or it could be used a compressor for this purpose. If a compressor is used, in order to minimize the pressure in the SDT the suction port of the compressor could be connected to the surface end of the SDT as illustrated in fig. 5.23. Therefore the injection gas would be in a close system whilst the liquid lifted is separated from the gas. Minimizing the pressure in the SDT would allow to go deeper employing SDT to unload liquids.

5.8.1 Hypothetical field Situations

Atmospheric conditions (Table 5.3) are considered first. The amount of liquid to be removed for this example is 0.119 m^3/day (1 bbl/day), which is relatively small. The tube is assumed to be smooth and the pressure is calculated based on Putra's model which is the one that better agrees with the experimental results for moderate superficial velocities.

The second case (Table 5.4) is using a 12 mm tube with similar data as for the first case. It is important to note that the depth of 1000 m seems to be very large for the 12 mm tube; however Putra's model predicts moderate values of pressure drop (for relatively small amount of water), similarly as for the laboratory conditions. In order to actually assess the impact of the depth using the 12 mm tube it is required to conduct tests for large depths and then compare results with laboratory and mathematical models.

Table 5.3. Data for field case (20 mm tube).

Tubing (ID)	20 mm (0.787 in)
Depth	1000 m (3280 ft)
Head Pressure	101.3 kpa (14.7 psi)
Liquid (Water)	0.119 m^3/day (1 bbl/day)
Gas injected (air)	542.87 Sm^3/day (19.17 KSCFD)

Table 5.4. Data for field case (12 mm tube).

SDT (ID)	12 mm (0.472 in)
Depth	1000 m (3280 ft)
Head Pressure	101.3 kpa (14.7 psi)
Liquid (Water)	0.119 m^3/day (1 bbl/day)
Gas injected (air)	195.4 Sm^3/day (6.9 KSCFD)

Fig. 5.25 shows the results predicted by the numerical model for the data in table 5.3 and 5.4. The liquid superficial velocity in the smaller diameter tube must be bigger in order to produce the same liquid. Due to this reason the gradient of pressure is bigger in the 12 mm ID tube. The FBHP predicted for the 20 mm tube is 540 kpa, whereas it is 943 ka for the 12 mm tube. This values corresponds approximately to a column of liquid of 54 m and 94 m respectively. Fig. 5.26 shows the profile for the superficial velocity of the gas for the 20 and 12 mm tube. As observed the gas velocity for the 12 mm tube tends to be smaller basically due to the higher pressure at a given depth.

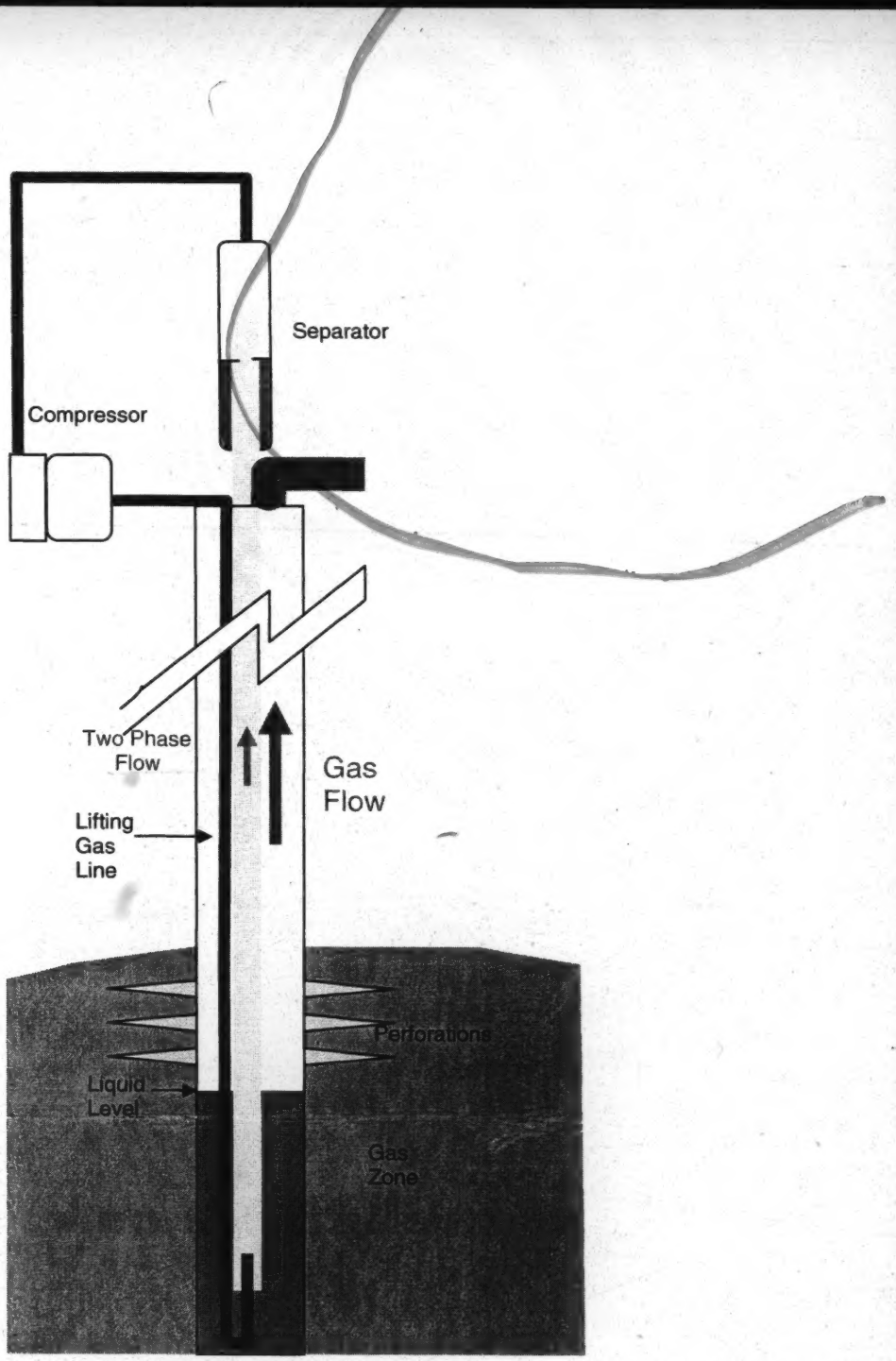

Figure 5.23 Suggested completion schematic for liquid unloading using small diameter tubes

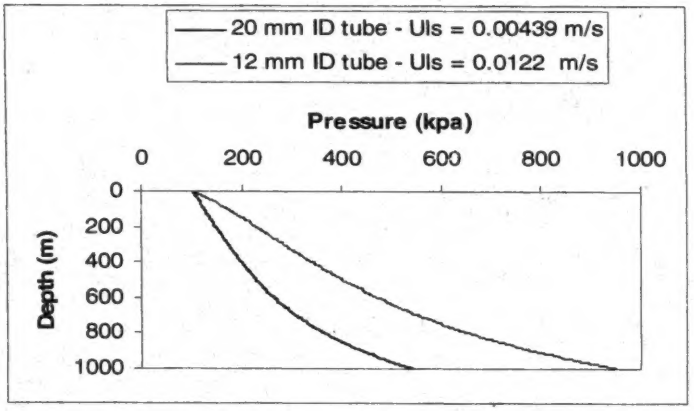

Figure 5.24 Pressure versus depth for 20 mm and 12 mm ID tube removing 0.119 m^3/day of water

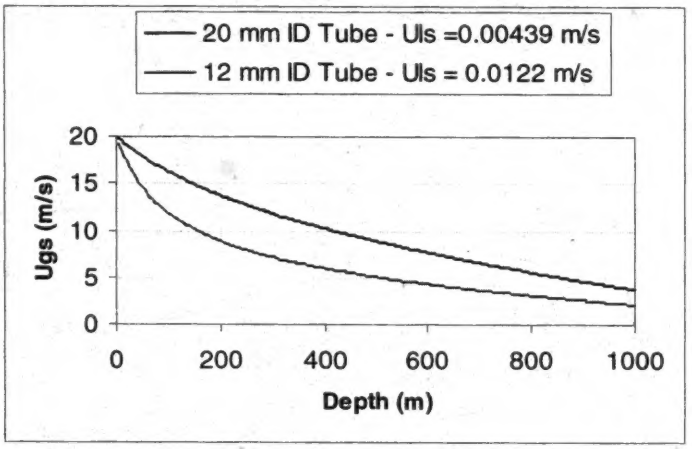

Figure 5.25 Superficial gas velocity versus depth calculations for 20 mm and 12 mm ID tube removing 0.119 m^3/day of water

The gradient of pressure as well as the gas velocity profile is very similar if the liquid superficial velocity is the same in both tubes as observed in figs 5.27 and 5.28 respectively. However, the amount of liquid removed in this case by the 12 mm tube is reduced but at the same time the gas required is also reduced.

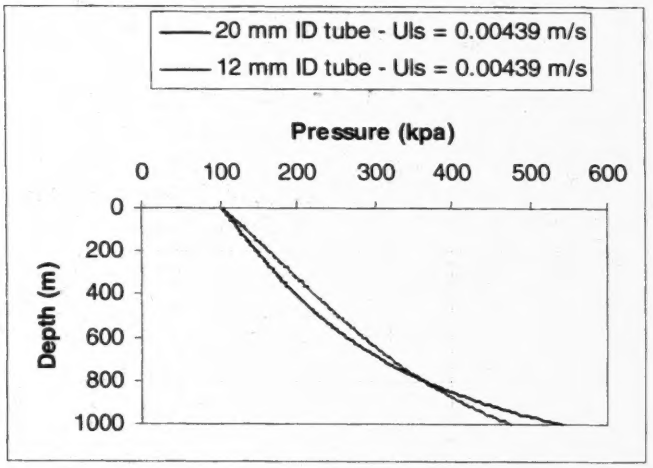

Figure 5.26 Pressure versus depth calculations for 20 mm and 12 mm ID tube for the same liquid superficial velocities [U(ls)=0.0044 m/s]

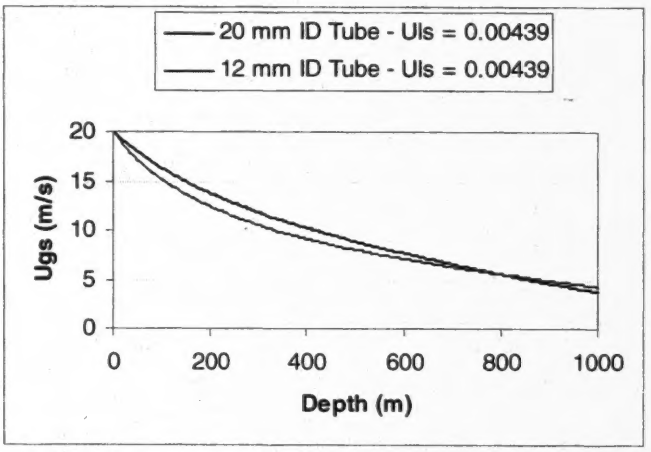

Figure 5.27 Superficial gas velocity versus depth calculated for 20 mm and 12 mm ID tube for the same liquid superficial velocities [U(ls)=0.0044 m/s].

The following examples show the effect of increasing the amount of liquid to be lifted employing SDTs. The liquid flow rate is increased from 0.119 to 2.714 m^3/day.

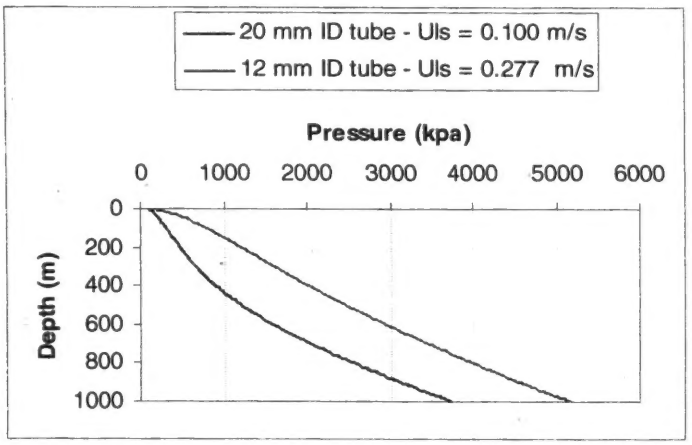

Figure 5.28 Pressure versus depth caloculated for 20 mm and 12 mm ID (2.714 m^3/day of water removed)

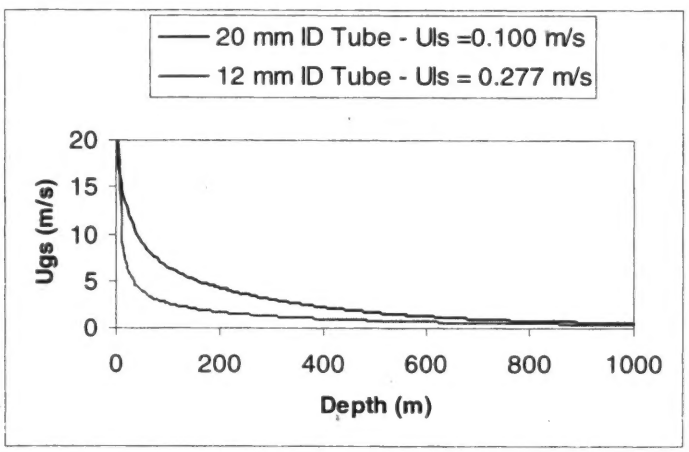

Figure 5.29 Superficial gas velocity calculated for 20 mm and 12 mm ID tube (2.714 m^3/day of water removed)

When increasing the volume of liquid produced by a factor of 22.8 the flowing bottom hole pressure predicted by Putra's model increases significantly. For the 20 mm tube increases from about 540 kpa to 3500 kpa and for the 12 mm tube from about 940 kpa to 500 kpa.

The second case to be considered is when the surface pressure of the SDT is higher than the atmospheric pressure. The surface pressure of the SDTs in the following examples is

500 kpa. In this case the overall pressure drop predicted is smaller for a higher surface pressure as seen in fig. 5.31. However in order to have a higher surface pressure it would be required to have about two times more gas in the system.

The gas superficial velocity profile is similar as observed in fig. 5.32 except near the surface where the velocity of gas is greater when the surface pressure is smaller.

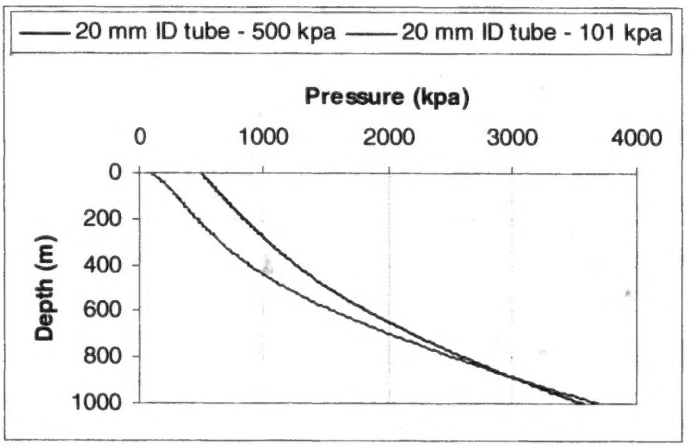

Figure 5.30 Effect of the surface pressure in the prediction of pressure versus depth profile (20 mm tube – 2.714 m^3/day of water)

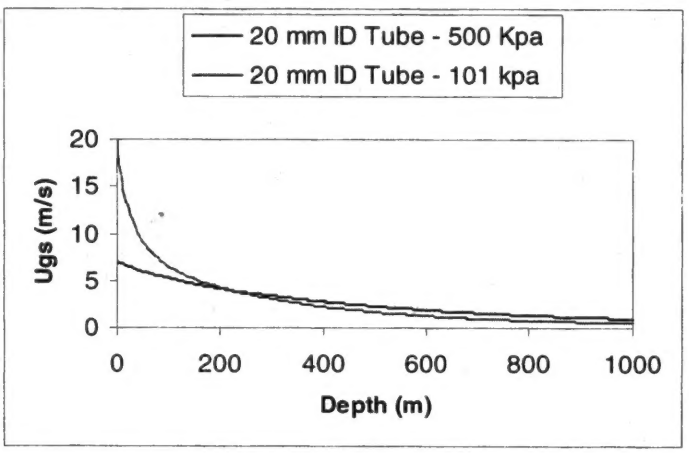

Figure 5.31. Effect of the surface pressure in the prediction of gas superficial velocity versus depth (20 mm tube – 2.714 m^3/day of water)

CHAPTER 6

CONCLUSIONS AND RECOMENDATIONS

6.1 Conclusions

1. The effect of transition from slug to annular (STA) flow patterns on production characteristic was investigated using a laboratory rig.
2. The produced results offer a consistent image of STA transition for: - a broad range of pipe diameters (12 to 20mm) (from SDT to conventional), - low and moderate reservoir pressure (submergence), - interfacial tension from 45 to 70 dyne/cm - position and size of local turbulence promoters.
3. Flow instabilities observed as pressure fluctuations have been quantified using a (new) RMS procedure and results used to assess key slug-to-annular transition steps.
4. Four mechanistic models have been used to describe and compare laboratory results.
5. Brill's [13] model for assessing the boundary transition between slug to churn, satisfactorily compares laboratory data for 16.66 % submergence; for lower submergence, Tengsedal model offers better predictions.
6. The Putra's model prediction of the churn flow pattern shows agreement with the experimental data at intermediate values of superficial gas velocity.
7. Three key features have been identified during STA transition:
   - Maximum (slug) production,
   - Minimum (slug-to-churn) production,
   - Maximum (developed annular) production.
8. A maximum of intensity of pressure oscillations (RMS) was consistently observed to coincide with the minimum production (specific to STC transition).
9. Reducing the superficial tension has a positive effect in reducing the magnitude of pressure oscillations during STC transition, but, at higher gas velocities will act negatively on the amount of liquid transported in the annular flow pattern.

10. At extremely low reservoir pressure the relative amount of liquid (superficial velocity) transported in the slug (or pseudo-slug) flow pattern is higher for small diameter tubes (12 mm) than for conventional tubes (20 mm).
11. For submergence levels in excess of 16.66 % in the 12 mm tube and 35 % in the 20 mm tube more liquid is transported in slug than in annular flow; for smaller level of submergences, more liquid can be lifted in annular than in slug region.
12. Local turbulence promoters (LTP) are slightly modifying the production characteristic observed for the base line (no promoters):
    - For conventional pipe diameters a small negative effect was observed
    - For SDP a small positive effect was recorded.
    - The positive effect of using LTP with SDP is related to the liquid film atomization and the salient role of liquid film in the upward transport of film-droplet core (with SDP).
    - The negative effect of using LTP with conventional pipes suggest that the LTP has no influence in changing the size of the droplet-gas core (controlling the upward liquid flow for conventional diameters) while negatively influence the pressure balance
13. In order to upscale the results from laboratory to field applications additional field tests are required to further validate laboratory (standard pressure) observations

6.2 Recommendations

1. Conduct experiments with higher operational pressure inside the SDT to evaluate experimentally the effect of pressure in the gas lift system. The pressure can be regulated placing a valve where the air exits the flow loop.

2. Modify the flow loop by increasing the length to better understand how this variable can impact the efficiency of the liquid transporting.

3. Investigate the effect of larger tube diameters and tube-casing configurations.

REFERENCES

1. Simpson, D., Lea, J., "COAL BED METHANE PRODUCTION", SPE paper presented at the 2003 SPE Production Operations Symposium, Oklahoma city, OK,22-25 March 2003.

2. Becaria, J. "EXPERIMENTAL OBSERVATIONS AND NUMERICAL MODELING OF GAS LIFTING IN SMALL DIAMETER PIPES IN VIEW OF UNLOADING LIQUIDS FROM WELLS WITH LOW RESERVOIR PRESSURE", University of Alberta, Msc. Thesis, September, 2004

3. Lea, J., Nickens, H., "SOLVING GAS-WELL LIQUID LOADING PROBLEMS". SPE Paper 72092, Distinguished Author Series.

4. Becaria, J., Toma, P. and P, Kuru, E.:"E SMALL-DIAMETER GAS LIFT SYSTEMS - A VIABLE TECHNICAL SOLUTION FOR TRANSPORT OF FLUIDS FROM LOW- PRESSURE RESERVOIRS," CIM Paper 104 (2004) (to be printed in JCPT, May 2006)

5. Stepheson, G., Rouen, R., "GAS-WELL DEWATERING: A COORDINATED APPROACH", SPE paper 58984 presented at the 2000 SPE international petroleum conference held in Mexico, 1-3 February 2000.

6. Van Hout R., Barnea D., Shemer L. "EVOLUTION OF TWO-PHASE SLUG FLOW IN VERTICAL AND INCLINED PIPES". Department of Fluid Mechanics and Heat Transfer, Faculty of Engineering, Tel-Aviv University

7. Hasan A. R.: "VOID FRACTION IN BUBBLY AND SLUG FLOW IN DOWNWARD VERTICAL AND INCLINED SYSTEMS", SPE Production and Facilities, August 1995, SPE 26522.pp. 172-176.

8. Yamasaki, Y. & Yamaguchi, K., " CHARACTERISTICS OF COCURRENT TWO-PHASE DOWNFLOW IN TUBES; VOID FRACTION AND PRESSURE DROP". J. Nuclear Sci. & Tech, April 1979, V. 161, pp. 245

9. Nicklin D. J., Wilkes J. O., and Davidson J. F.: "TWO-PHASE FLOW IN VERICAL TUBES". Trans. Inst. of Chem. Engrs., 1962, V 40. pp. 61

10. Ansari, A.M., Sylvester, N.D., Sarica, C., Shoham, O., Brill, J.P., "\A COMPREHENSIVE MECHANISTIC MODEL FOR UPWARD TWO-PHASE FLOW IN WELLBORES". SPE Production and Facilities, May 1994, pp. 143-150.

11. Brotz, W.:"UBER DIE VORAUSBERECHNUNG DER ABSORPTIONSGESCH-WINDINGKEIT CON GASEN IN STROMENDEN FLUSSIGKEITSSCHICHTEN", Chem. Ing. Tech., 1954, No. 26, pp 470.

12. Putra, S. A., "DEVELOPMENT OF A MECHANISTIC TWO-FLUID CHURN FLOW MODEL AND DESIGN OF TUBING-COLLAR INSERTS FOR ENHANCING LIQUD LIFTING TO PREVENT LIQUID LOAD-UP IN GAS WELLS". Colorado School of Mines. PhD. Thesis, November 3, 2000.

13. X. T. Chen* and J. P. Brill Chen X., Brill J.P. "SLUG TO CHURN TRANSITION IN UPWARD VERTICAL TWO-PHASE FLOW" Department of Petroleum Engineering, The University of Tulsa, Tulsa, OK 74104, U.S.A. Received 18 April 1996; accepted 5 February 1997.

14. Watson M.J., Hewitt G.F. "PRESSURE EFFECTS ON THE SLUG TO CHURN TRANSITION" Department of Chemical Engineering and Chemical Technology, Imperial College of Science, Technology and Medicine, Prince Consort Road, London SW7 2BY, UK Received 25 January 1999; received in revised form 25 May 1999.

15. Costigan G., Whalley P.B. "SLUG FLOW REGIME IDENTIFICATION FROM DYNAMIC VOID FRACTION MEASUREMENTS IN VERTICAL AIR-WATER FLOWS" Department of Engineering Science, University of Oxford, Oxford OX1 3PJ, U.K. (Received 5 January 1996, in revised form 3 Jut)' 1996).

16. Van Hout, R., Shemer, L. and Barnea, D. "SPATIAL DISTRIBUTION OF VOID FRACTION WITHIN A LIQUID SLUG AND SOME OTHER RELATED SLUG PARAMETERS". Int. J. Multiphase Flow 18, 831-845, 1992.

17. Brauner, N. and Barnea, D. SLUG/CHURN TRANSITION IN UPWARD VERTICAL FLOW. Chem. Eng Sci. 41, 159-163.

18. Wallis, G. B. "ONE-DIMENSIONAL TWO-PHASE FLOW". McGraw-Hill, New York. 1969.

19. Fernandes, R. C., Semiat, R. and Dukler, A. E. "HYDRODYNAMIC MODEL FOR GAS-LIQUID SLUG FLOW IN VERTICAL TUBES". *A.1.Ch.E. J. 29, 981-989.* 1983.

20. Tengsedal, J., Sarica, C., Schmidt, Z., Doty., "A MECHANISTIC MODEL FOR PREDICTING PRESSURE DROP IN VAERTICAL UPWARD TWO-PHASE FLOW", Journal of Energy Resources Technology, Vol. 121. 1999.

21. Turner, R.G., Hubbard, M.G., Duckler, A. E., "ANALYSIS AND PREDICTION OF MINIMUM FLOWRATE FOR CONTINUOUS REMOVAL OF LIQUIDS FROM GAS WELLS". SPE 2198, JPT, November 1969, pp. 1475-1482.

22. Toma, P., "MULTIPHASE FLOW IN PIPES", Graduate Course. Handouts from the vertical flow chapter, University of Alberta, Canada. September 2002.

23. Hewitt, G.F. and Taylor, N.S., "ANNULAR TWO-PHASE FLOW", Pergamon. Press, 1970, pp162

24. Turner, R.G., Hubbard, M.G. and Dukler, A.E.: "ANALYSIS AND PREDICTION OF MINIMUM FLOW RATE FOR THE CONTINUOUS REMOVAL OF LIQUIDS FROM GAS WELLS," JPT J. (Nov. 1969). 1475-1482.

25. Barbosa Jr. J.R., Hewitt G.F., Konig G., Richardson S.M. "LIQUID ENTRAINMENT, DROPLET CONCENTRATION AND PRESSURE GRADIENT AT THE ONSET OF ANNULAR FLOW IN A VERTICAL PIPE". Department of Chemical Engineering and Chemical Technology, Imperial College of Science, Technology and Medicine, Prince Consort Road, London SW7 2BY, UK Received 23 March 2001; received in revised form 16 December 2001.

26. Vijayan M., Jayanti S., Balakrishnan A.R., "EFFECT OF TUBE DIAMETER ON FLOODING". Department of chemical engineering, Indian institute of technology, Chennai 600 036 India, International Journal of Multiphase Flow 27 (2001) 797-816.

27. Azzopardi B.J., Wren.E. "WHAT IS ENTRAINMENT IN VERTICAL TWO-PHASE CHURN FLOW?". Multiphase Flow Research Group, Nottingham Fuel and Energy Centre, School of Chemical, Environmental and Mining Engineering, University of Nottingham, University Park, Nottingham NG7 2RD, UK International Journal of Multiphase Flow 30 (2004) 89–103.

28. Azzopardi, B.J., "MECHANISMS OF ENTRAINMENT IN ANNULAR TWO-PHASE FLOW". UKAEA Report AERE-R 11068. 1983.

29. James, P.W., Hewitt, G.F., Whalley, P.B., "DROPLET MOTION IN TWO-PHASE FLOW". UKAEA Report AERE-R 9711. 1980.

30. Ishii, M., Mishima, K., "TWO-FLUID MODEL AND HYDRODYNAMIC CONSTITUTI.

31. Whalley, P.B., "TWO-PHASE FLOW AND HEAT TRANSFER, Oxford University Press, New York, 1996.

32. Kokamustafaogullari, G., Ishii, M. "FOUNDATION OF THE INTERFACIAL AREA TRANSPORT EQUATION AND ITS CLOUSURE RELATIONS", Int. J. Heat Mass Transfer, Vol. 38, No. 3, pp. 481-489, 1995.

33. kurul, Podoski, 1991, ANS proc. "NATIONAL HEAT TRANSFER CONFER"NCE", Minneapolis 1991.

34. Kocamustafaogullari, G., Huang, W.D., Razi, J., "MEASURMENT AND MODELING OF AVERAGE VOID FRATION, BUBBLE SIZE AND INTERFACIAL AREA", Nuclear Engineering and Design, 148, 99, 437-453, 1994.

35. Alves, I.N., Caetano, E.F., Minami, K., Shoham, O. "MODELING ANNULAR FLOW BEHAVIOR FOR GAS WELLS". Paper presented at the 1988 Winter Annual Meeting of ASME, Chicago, Nov 27-Dec 2.

36. Whalley, P.B, Hewitt, G.F. "THE CORRELATION OF LIQUID ENTRAINMENT FRATION AND ENTRAINMENT RATE IN ANNULAR TWO-PHASE FLOW". UKAEA Report AERE-R9187, Harwell. 1978. 14

APPENDIX A

EXPERIMENTAL RESULTS FOR THE WATER/AIR GAS LIFT SYSTEM

A.1 20 mm tube's experimental data

A.1.1 35 % Submergence Level

Table A.1.1. Data for 20 mm Tube. 35 % Submergence level (water-air)

Air Injection l/min	Produced water, l/min			% Variation	% Variation	% Variation
	First Rep.	Second Rep.	Third Rep.	First/Second	Second /Third	First/Third
3	0.00	0.00	0.00	-	-	-
8	1.74	1.56	1.65	11.58	-5.63	5.30
11	2.69	2.43	2.47	10.75	-1.83	8.72
15	3.67	3.72	3.55	-1.37	4.90	3.46
20	4.58	4.62	4.41	-0.89	4.81	3.87
26	4.93	4.98	5.08	-0.90	-1.96	-2.85
70	4.63	4.78	5.25	-3.05	-8.90	-11.68
143	5.65	5.45	5.47	3.61	-0.40	3.20
203	5.79	6.11	5.78	-5.25	5.81	0.26
432	5.38	5.22	5.41	3.00	-3.36	-0.46

A.1.2 16.66 % Submergence Level

Table A.1.2. Data for 20 mm Tube. 16.66 % Submergence level (water-air)

Air Injection l/min	Produced water, l/min			% Variation	% Variation	% Variation
	First Rep.	Second Rep.	Third Rep.	First/Second	Second /Third	First/Third
11.5	0.00	0.00	0.00	-	-	-
15	0.37	0.31	0.32	19.64	-2.35	16.83
26	1.10	1.13	1.07	-2.60	5.71	2.96
70	0.58	0.56	0.54	2.09	3.67	5.83
143	1.36	1.36	1.29	0.53	5.23	5.78
203	2.63	2.62	2.62	0.27	-0.04	0.23
332	3.49	3.50	3.49	-0.04	0.13	0.09
432	3.56	3.59	3.58	-0.74	0.42	-0.33

A.1.3 12.5 % Submergence Level

Table A.1.3. Data for 20 mm Tube. 12.5 % Submergence level (water-air)

Air Injection l/min	Produced water, l/min			% Variation	% Variation	% Variation
	First Rep.	Second Rep.	Third Rep.	First/Second	Second /Third	First/Third
65	0	0.00	0.00	-	-	-
125	0.68	0.60	0.65	14.89	-7.36	6.43
200	1.78	1.76	1.79	1.17	-1.16	0.00
329	2.81	2.80	2.81	0.28	-0.22	0.06
432	2.81	2.83	2.82	-0.43	0.28	-0.16

A.1.4 8.33 % Submergence Level

Table A.1.4. Data for 20 mm Tube. 8.33 % Submergence level (water-air)

Air Injection l/min	Produced water, l/min			% Variation	% Variation	% Variation
	First Rep.	Second Rep.	Third Rep.	First/Second	Second /Third	First/Third
125	0	0	0.00	-	-	-
151	0.70	0.64	0.67	8.20	-4.07	3.80
329	2.27	2.31	2.28	-1.69	1.31	-0.40
432	2.39	2.39	2.39	0.17	-0.18	-0.01

A.1.5 4.16 % Submergence Level

Table A.1.5. Data for 20 mm Tube. 4.16 % Submergence level (water-air)

Air Injection l/min	Produced water, l/min			% Variation	% Variation	% Variation
	First Rep.	Second Rep.	Third Rep.	First/Second	Second /Third	First/Third
168	0	0	0.00	-	-	-
200	0.71	0.69	0.69	3.23	-0.69	2.51
329	1.99	1.98	1.98	0.45	-0.09	0.36
432	2.26	2.26	2.24	-0.02	1.00	0.98

A.1.6 RMS of FBHP for 20 mm tube.

Table A.1.6. RMS of FBHP for 20 mm tube (Water-Air).

Air injection l/m	RMS of FBHP (psi) Submergence level			
	4.16%	8.33%	12.5%	16.66%
5	0.185	0.365	0.539	0.726
10.14	0.195	0.368	0.542	0.725
15	0.208	0.375	0.547	0.725
20	0.222	0.384	0.552	0.735
26	0.239	0.393	0.554	0.734
32.58	0.237	-	0.561	0.735
44.00	0.255	0.435	0.575	0.749
57.02	0.27	0.441	0.609	0.774
71.34	0.271	0.434	0.597	0.768
87.68	0.262	0.41	0.586	0.753
107.81	0.214	0.386	0.551	0.741
130.72	0.188	0.374	0.552	0.742
168.82	0.192	0.372	0.553	0.746
200.64	0.199	0.375	0.557	0.74
259.17	0.215	0.381	0.553	0.736
329.28	0.23	0.387	0.559	0.733
386.42	0.242	0.39	0.566	0.746
431.36	0.251	0.402	0.568	0.739

A.2 12 mm tube's experimental data

A.2.1 16.66 % Submergence Level

Table A.2.1. Data for 12 mm tube. 16.66 % Submergence level (water-Air)

Air Injection l/min	Produced water, l/min First Rep.	Second Rep.	Third Rep.	% Variation First/Second	% Variation Second /Third	% Variation First/Third
3	0.0000	0.0000	0.0000	-	-	-
3.752	0.2057	0.2118	0.2093	-2.86	1.18	-1.71
8.031	0.4638	0.4444	0.4468	4.35	-0.53	3.80
10.94	0.5143	0.5202	0.5028	-1.14	3.47	2.29
15.09	0.4375	0.4330	0.4398	1.04	-1.55	-0.52
20.02	0.2717	0.3013	0.3214	-9.81	-6.28	-15.47
25.12	0.2143	0.2076	0.1993	3.21	4.15	7.50
26.06	0.2174	0.2214	0.2206	-1.81	0.37	-1.45
74	0.4225	0.4245	0.4225	-0.47	0.47	0.00
110	0.3947	0.3879	0.3782	1.75	2.59	4.39
163	0.3273	0.3273	0.3125	0.00	4.73	4.73
212	0.2857	0.2866	0.2885	-0.32	-0.64	-0.95

A.2.2 12.5 % Submergence Level

Table A.2.2. Data for 12 mm tube. 12.5 % Submergence level (water-Air)

Air Injection l/min	Produced water, l/min			% Variation	% Variation	% Variation
	First Rep.	Second Rep.	Third Rep.	First/Second	Second /Third	First/Third
4	0.0000	0.0000	0.0000	-	-	-
4.714	0.0992	0.0976	0.0992	1.65	-1.63	0.00
8.031	0.2293	0.2017	0.1897	13.69	6.30	20.86
10.94	0.2571	0.2571	0.2740	0.00	-6.14	-6.14
15.09	0.2199	0.2551	0.2390	-13.80	6.72	-8.01
20.02	0.0236	0.0783	0.0530	-69.82	47.65	-55.43
25.12	0.0258	0.0351	0.0288	-26.50	21.64	-10.60
26.06	0.0436	0.0386	0.0375	13.01	2.89	16.28
74	0.2824	0.2844	0.2813	-0.71	1.11	0.39
110	0.2703	0.2765	0.2609	-2.25	5.99	3.60
163	0.2553	0.2609	0.2233	-2.13	16.81	14.33
212	0.2381	0.2344	0.2083	1.59	12.50	14.29

A.2.3 8.33 % Submergence Level

Table A.2.3. Data for 12 mm tube. 8.33 % Submergence level (water-Air)

Air Injection l/min	Produced water, l/min			% Variation	% Variation	% Variation
	First Rep.	Second Rep.	Third Rep.	First/Second	Second /Third	First/Third
7.5	0.0000	0.0000	0.0000	-	-	-
8.031	0.0279	0.0288	0.0262	-3.26	10.10	6.51
10.94	0.0499	0.0714	0.0585	-30.19	22.02	-14.82
15.09	0.0008	0.0056	0.0007	-86.44	742.09	14.16
20.02	0.0002	0.0004	0.0002	-59.38	65.70	-32.69
25.12	0.0006	0.0008	0.0004	-22.49	123.49	73.22
26.06	0.0009	0.0009	0.0010	-6.19	-10.87	-16.39
74	0.1212	0.1471	0.1456	-17.58	0.98	-16.77
110	0.1609	0.1818	0.1829	-11.49	-0.61	-12.03
163	0.1585	0.1829	0.1734	-13.36	5.49	-8.60
212	0.1469	0.1786	0.1648	-17.71	8.33	-10.86

A.2.4 4.16 % Submergence Level

Table A.2.4. Data for 12 mm tube. 4.16 % Submergence level (water-Air)

Air Injection l/min	Produced water, l/min			% Variation	% Variation	% Variation
	First Rep.	Second Rep.	Third Rep.	First/Second	Second /Third	First/Third
8.031	0.0000	0.0000	0.0000	-	-	-
10.94	0.0000	0.0000	0.0000	-	-	-
15.09	0.0000	0.0000	0.0000	-	-	-
20.02	0.0000	0.0000	0.0000	-	-	-
25.12	0.0000	0.0000	0.0000	-	-	-
60	0.0000	0.0000	0.0000	-	-	-
73.9612132	0.0300	0.0309	0.0320	-2.92	-3.43	-6.25
110.2734636	0.0740	0.0745	0.0713	-0.68	4.48	3.77
162.5249028	0.0753	0.0674	0.0753	11.64	-10.49	-0.07
212.4536637	0.0636	0.0614	0.0669	3.53	-8.19	-4.95

A.2.5 RMS of FBHP for 12 mm tube.

Table A.2.5. RMS of FBHP for 12 mm tube.

Air injection l/m	RMS of FBHP (psi) Submergence level			
	4.16%	8.33%	12.5%	16.66%
0.532	0.183	0.362	0.542	0.724
1.508	0.192	0.366	0.544	0.726
2.612	-	-	0.546	-
3.752		0.364	0.542	0.73
5	0.193	0.365	0.55	0.726
6.232	-	-	-	-
7.513		0.371	0.544	0.73
10.14	0.242	0.369	0.545	0.727
12.85	-	0.423	0.559	0.736
15.66	0.245	0.413	0.581	0.748
18.55	-	0.402	0.576	0.76
20	0.236	0.396	-	-
23	-	0.394	0.566	0.761
26	0.227	0.39	0.564	0.744
33	0.212	0.389	0.57	0.747
44	0.198	0.376	0.556	0.734
57	0.191	0.367	0.544	0.73
71	0.184	0.365	0.541	0.731
88	0.183	0.366	0.548	-
108	0.191	0.369	0.55	0.729
131	0.197	0.373	0.547	0.733
169	0.214	0.391	0.56	0.739
201	0.228	0.393	0.569	0.745
259	0.247	0.41	0.58	0.756
329	0.261	0.418	0.575	0.755
386	0.33	0.454	0.611	0.763
431	0.462	0.493	0.652	0.802

A.3 8 mm tube's experimental data

A.3.1 16.66 % submergence level

Table A.3.1. Data for 8mm tube. 16.66 % submergence level

Air Injection		Produced water, l/min		% Variation	% Variation	% Variation
l/min	First Rep.	Second Rep.	Third Rep.	First Rep.	Second /Third	First/Third
0.905	0	0	0	-	-	-
1.928	0.1866	0.1857	0.1831	0.48	1.43	1.92
4.96	0.2432	0.2473	0.2463	-1.67	0.40	-1.28
10.14	0.0925	0.0900	0.0919	2.77	-2.00	0.72
20	0.1091	0.1254	0.1208	-13.02	3.76	-9.75
26	0.1235	0.1167	0.1141	5.83	2.33	8.30
32.58	0.1149	0.1012	0.1101	13.56	-8.11	4.35
44.00	0.1152	0.1200	0.0957	-4.02	25.47	20.43
57.02	0.0974	0.0939	0.0902	3.79	4.02	7.96

A.3.2 4.16 % submergence level

Table A.3.2. Data for 8mm tube. 4.16 % submergence level

Air Injection		Produced water, l/min		% Variation	% Variation	% Variation
l/min	First Rep.	Second Rep.	Third Rep.	First/Second	Second /Third	First/Third
24.5	0	0	0	-	-	-
32.58	0.005462	0.00579374	0.005901	-5.73	-1.82	-7.45
44.00	0.006854	0.00615479	0.007572	11.36	-18.72	-9.49
57.02	0.007009	0.00632004	0.006174	10.90	2.36	13.52

A.3.3 RMS of FBHP for 8 mm tube.

Table A.3.3. RMS of FBHP for 8 mm tube.

Air injection l/m	RMS of FBHP (psi) Submergence level			
	4.16%	8.33%	12.5%	16.66%
0.0581	0.181	-	-	0.726
0.532	0.182	-	-	0.729
1.508	0.188	-	-	0.727
2.612	0.194	-	-	0.726
3.752	0.192	-	-	0.726
5	0.202	-	-	0.727
6.232	0.205	-	-	0.730
7.513	0.211	-	-	0.733
10.14	0.209	-	-	0.738
12.85	0.203	-	-	0.739
15.66	0.197	-	-	0.738
18.55	0.190	-	-	0.734
20	0.188	-	-	0.732
23	0.185	-	-	0.731
26	0.181	-	-	0.730
32.58026	0.185	-	-	0.729
44.00305	0.181	-	-	0.727
57.02367	0.180	-	-	0.725
71	0.179			0.724
88	0.180			0.725

APPENDIX B

EXPERIMENTAL RESULTS FOR THE

WATER-METHANOL/AIR GAS LIFT SYSTEM

B.1 20 mm tube's experimental data

B.1.1 16.66 % Submergence level

Table B.1.1. Data for 20 mm ID tube (water-methanol). 16.66 % Submergence

Air Injection l/min	Produced water, l/min			% Variation First/Second	% Variation Second /Third	% Variation First/Third
	First	Second	Third			
0	0.00	0.00	0.00	-	-	-
10	0.00	0.00	0.00	-	-	-
15	0.53	0.48	0.47	9.64	2.34	12.20
26	0.87	0.87	0.88	-0.01	-0.62	-0.64
65	0.44	0.36	0.38	24.25	-5.55	17.35
125	1.47	1.56	1.66	-6.03	-5.84	-11.52
200	2.19	2.31	2.27	-5.14	1.34	-3.87
329	2.84	3.07	2.83	-7.44	8.37	0.30
432	2.93	2.87	2.87	2.16	-0.09	2.07

B.1.2 12.5 % Submergence level

Table B.1.2. Data for 20 mm ID tube (water-methanol). 12.5 % Submergence

Air Injection l/min	Produced water, l/min			% Variation First/Second	% Variation Second /Third	% Variation First/Third
	First	Second	Third			
11.5	0.00	0.00	0.00	-	-	-
15	0.37	0.31	0.32	19.64	-2.35	16.83
26	1.10	1.13	1.07	-2.60	5.71	2.96
70	0.58	0.56	0.54	2.09	3.67	5.83
143	1.36	1.36	1.29	0.53	5.23	5.78
203	2.63	2.62	2.62	0.27	-0.04	0.23
332	3.49	3.50	3.49	-0.04	0.13	0.09
432	3.56	3.59	3.58	-0.74	0.42	-0.33

B.1.3 8.33 % Submergence level

Table B.1.3. Data for 20 mm ID tube (water-methanol). 8.33 % Submergence

Air Injection l/min	Produced water, l/min			% Variation First/Second	% Variation Second /Third	% Variation First/Third
	First	Second	Third			
0	0	0.00	0.00	-	-	-
125	0	0.00	0.00	-	-	-
151	0.72	0.69	0.74	4.01	-6.29	-2.54
329	1.99	1.94	2.02	3.20	-3.85	-0.77
432	2.14	2.13	2.14	0.53	-0.47	0.06

B.1.4 4.16 % Submergence level

Table B.1.4. Data for 20 mm ID tube (water-methanol). 4.16 % Submergence

Air Injection l/min	Produced water, l/min			% Variation First/Second	% Variation Second /Third	% Variation First/Third
	First	Second	Third			
0	0.00	0.00	0.00	-	-	-
125	0.82	0.64	0.64	-	-	-
151	1.47	1.56	1.53	-5.78	2.33	-3.59
329	1.78	1.78	1.58	0.14	13.02	13.18

B.1.5 RMS of FBHP for 20 mm tube.

Table B.1.5. RMS of FBHP for 20 mm ID tube (water-methanol)

Air injection l/m	RMS of FBHP (psi) Submergence level			
	4.16%	8.33%	12.5%	16.66%
5	0.174	0.349	0.52	0.685
10.14	0.184	0.353	0.523	0.681
15	0.196	0.358	0.52	0.674
20	0.209	0.364	0.519	0.678
26	0.223	-	0.525	0.682
32.58	0.214	0.372	0.534	0.702
44.00	0.218	0.376	0.54	0.711
57.02	0.221	0.375	0.542	0.714
71.34	0.203	0.367	0.533	0.714
87.68	0.194	0.359	0.527	0.706
107.81	0.183	0.348	0.52	0.71
130.72	0.174	0.341	0.519	0.709
168.82	0.174	0.342	0.52	0.701
200.64	0.188	0.344	0.525	0.704
259.17	0.194	0.361	0.527	0.709
329.28	0.21	0.376	0.531	0.706
386.42	0.224	0.379	0.538	0.71
431.36	0.232	0.376	0.534	0.712

B.2 12 mm tube's experimental data

B.2.1 16.66 % Submergence level

Table B.2.1. Data for 12 mm ID tube (water-methanol). 16.66 % Submergence

Air Injection l/min	Produced water, l/min			% Variation First/Second	% Variation Second /Third	% Variation First/Third
	First	Second	Third			
2.15	0.0000	0.0000	0.0000	-	-	-
3.75	0.1356	0.1270	0.1263	6.78	0.57	7.39
11	0.3293	0.3225	0.3160	2.11	2.05	4.21
26	0.1369	0.1311	0.1251	4.45	4.81	9.48
65	0.3309	0.3248	0.3395	1.90	-4.33	-2.51
98	0.2983	0.3001	0.2972	-0.60	0.97	0.37
125	0.2688	0.2859	0.2801	-5.98	2.10	-4.01
201	0.2347	0.2236	0.2304	4.95	-2.96	1.85

B.3 8 mm tube's experimental data

B.3.1 16.66 % Submergence level

Table B.3.1. Data for 8 mm ID tube (water-methanol). 16.66 % Submergence

Air Injection		Produced water, l/min		% Variation	% Variation	% Variation
l/min	First	Second	Third	First/Second	Second /Third	First/Third
0.905	0	0	0	-	-	-
1.928	0.1550	0.1441	0.1331	7.53	8.28	16.44
4.96	0.1389	0.1408	0.1439	-1.31	-2.18	-3.46
10.14	0.0506	0.0463	0.0453	9.36	2.23	11.80
20	0.0877	0.0822	0.0799	6.73	2.96	9.88
26	0.0942	0.0910	0.0936	3.45	-2.69	0.67
32.58	0.0866	0.0877	0.0915	-1.21	-4.18	-5.34
44.00	0.0831	0.0875	0.0861	-5.01	1.62	-3.48
57.02	0.0590	0.0527	0.0614	12.00	-14.29	-4.00

APPENDIX C

EXPERIMENTAL RESULTS FOR THE WATER/AIR GAS LIFT SYSTEM ULIZING LTPs IN THE 20 mm TUBE.

C.1 Data for one 19 mm ID LTP located at the middle of the tube

C.1.1 16.66 % submergence level

Table C.1.1. Data for 20 mm ID tube (water) using one 19 mm ID LTP (middle). 16.66 % Submergence level

Air Injection l/min	Produced water, l/min			% Variation First/Second	% Variation Second /Third	% Variation First/Third
	First	Second	Third			
11.5	0.00	0.00	0.00	-	-	-
15	0.37	0.31	0.32	19.64	-2.35	16.83
26	1.10	1.13	1.07	-2.60	5.71	2.96
70	0.58	0.56	0.54	2.09	3.67	5.83
143	1.36	1.36	1.29	0.53	5.23	5.78
203	2.63	2.62	2.62	0.27	-0.04	0.23
332	3.49	3.50	3.49	-0.04	0.13	0.09
432	3.56	3.59	3.58	-0.74	0.42	-0.33

C.1.2 4.16 % submergence level

Table C.1.2. Data for 20 mm ID tube (water) using one 19 mm ID LTP (middle). 4.16 % Submergence level

Air Injection l/min	Produced water, l/min			% Variation First/Second	% Variation Second /Third	% Variation First/Third
	First	Second	Third			
168	0	0	0.00	-	-	-
200	0.71	0.69	0.69	3.23	-0.69	2.51
329	1.99	1.98	1.98	0.45	-0.09	0.36
432	2.26	2.26	2.24	-0.02	1.00	0.98

C.1.3 RMS of FBHP data.

Table C.1.3. RMS of FBHP for 20 mm ID tube (water) using one 19 mm ID LTP (middle)

Air injection l/m	RMS of FBHP (psi) Submergence level			
	4.16%	8.33%	12.5%	16.66%
5	0.187	0.37	0.545	0.731
10.14	0.196	0.374	0.548	0.731
15	0.211	0.382	0.552	0.735
20	0.226	0.389	0.557	0.74
26	0.244	0.397	0.568	0.738
33	0.24	0.39	0.57	0.741
44	0.252	0.42	0.579	0.759
57	0.259	0.425	0.598	0.76
71	0.26	0.422	0.578	0.756
88	0.253	0.401	0.576	0.759
108	0.219	0.383	0.566	0.753
131	0.194	0.37	0.554	0.743
169	0.19	0.368	0.559	0.742
201	0.193	0.381	0.561	0.753
259	0.204	0.381	0.557	0.747
329	0.217	0.383	0.564	0.755
386	0.23	0.395	0.565	0.754
431	0.238	0.395	0.576	0.749

C.2 Data for one 19 mm ID LTP located at the bottom of the tube

C.2.1 16.66 % submergence level

Table C.2.1. Data for 20 mm ID tube (water) using one 19 mm ID LTP (bottom). 16.66 % Submergence level

Air Injection l/min	Produced water, l/min			% Variation First/Second	% Variation Second /Third	% Variation First/Third
	First	Second	Third			
12	0.0000	0.0000	0.0000	-	-	-
15	0.2987	0.3056	0.2174	-2.25	40.60	37.44
26	0.9638	1.0202	0.8555	-5.53	19.25	12.65
70	0.5296	0.5283	0.5005	0.25	5.55	5.81
143	1.1486	1.1474	1.1914	0.11	-3.69	-3.59
203	2.5554	2.5622	2.6162	-0.27	-2.06	-2.32
332	3.4277	3.5355	3.4789	-3.05	1.63	-1.47
432	3.5559	3.5551	3.5052	0.02	1.42	1.45

C.2.2 4.16 % submergence level

Table C.2.2. Data for 20 mm ID tube (water) using one 19 mm ID LTP (bottom). 4.16 % Submergence level

Air Injection l/min	Produced water, l/min			% Variation First/Second	% Variation Second /Third	% Variation First/Third
	First	Second	Third			
165	0.0000	0.0000	0.0000	-	-	-
200	0.7591	0.7790	0.7751	-2.56	0.51	-2.06
329	1.9892	1.9291	2.0107	3.11	-4.06	-1.07
432	2.2329	2.2330	2.2512	0.00	-0.81	-0.81

C.2.3 RMS of FBHP data

Table C.2.3. RMS of FBHP for for 20 mm ID tube (water) using one 19 mm ID LTP (bottom).

Air injection l/m	RMS of FBHP (psi) Submergence level			
	4.16%	8.33%	12.5%	16.66%
5	0.197	0.365	0.547	0.725
10.14	0.198	0.371	0.55	0.726
15	0.215	0.379	0.554	0.726
20	0.229	0.385	0.559	0.742
26	0.24	0.399	0.56	0.741
33	0.24	0.391	0.559	0.737
44	0.258	0.418	0.579	0.761
57	0.257	0.423	0.61	0.766
71	0.25	0.421	0.598	0.766
88	0.246	0.398	0.58	0.759
108	0.217	0.378	0.561	0.755
131	0.194	0.368	0.551	0.758
169	0.187	0.369	0.563	0.744
201	0.194	0.373	0.556	0.754
259	0.206	0.378	0.55	0.743
329	0.22	0.381	0.558	0.741
386	0.233	0.391	0.566	0.752
431	0.238	0.391	0.566	0.743

C.3 Data for two 19 mm ID LTPs located at the bottom and top of the tube

C.3.1 16.66 % submergence level

Table C.3.1. Data for 20 mm ID tube (water) using two 19 mm ID LTPs (bottom & top). 16.66 % Submergence level

Air Injection l/min	Produced water, l/min			% Variation First/Second	% Variation Second /Third	% Variation First/Third
	First	Second	Third			
11.5	0.0000	0.0000	0.0000	-	-	-
15.0	0.2970	0.2770	0.2656	7.21	4.28	11.80
26.0	0.6958	0.7237	0.7561	-3.86	-4.28	-7.98
70	0.5015	0.4801	0.4770	4.44	0.65	5.12
143	1.1415	1.1578	1.1966	-1.41	-3.24	-4.61
203	2.5875	2.6870	2.6631	-3.70	0.90	-2.84
332	3.4591	3.4601	3.4854	-0.03	-0.73	-0.75
432	3.4897	3.5253	3.5216	-1.01	0.11	-0.90

C.3.2 4.16 % Submergence level

Table C.3.2. Data for 20 mm ID tube (water) using two 19 mm ID LTPs (bottom & top). 4.16 % Submergence level

Air Injection l/min	Produced water, l/min			% Variation First/Second	% Variation Second /Third	% Variation First/Third
	First	Second	Third			
165	0.0000	0.0000	0.0000	-	-	-
200	0.7208	0.7028	0.7966	2.56	-11.77	-9.52
329	1.9618	1.9634	1.9699	-0.08	-0.33	-0.41
432	2.2341	2.2328	2.2498	0.06	-0.76	-0.70

C.3.3 RMS of FBHP data

Table C.3.3. RMS of FBHP for 20 mm ID tube (water) using one 19 mm ID LTP (bottom & top).

Air injection l/m	RMS of FBHP (psi) Submergence level			
	4.16%	8.33%	12.5%	16.66%
5	0.184	-	-	0.731
10.14	0.195	-	-	0.7308
15	0.211	-	-	0.736
20	0.225	-	-	0.733
26	0.239	-	-	0.74
33	0.239	-	-	0.734
44	0.259	-	-	0.759
57	0.269	-	-	0.771
71	0.269	-	-	0.77
88	0.246	-	-	0.757
108	0.221	-	-	0.762
131	0.197	-	-	0.753
169	0.186	-	-	0.742
201	0.197	-	-	0.749
259	0.199	-	-	0.746
329	0.222	-	-	0.749
386	0.242	-	-	0.748
431	0.244	-	-	0.756

C.4 Data for one 17 mm ID LTP located at the middle of the tube

C.4.1 16.66 % submergence level

Table C.4.1. Data for 20 mm ID tube (water) using one 17 mm ID LTP (middle). 16.66 % Submergence level

Air Injection	Produced water, l/min			% Variation	% Variation	% Variation
l/min	First	Second	Third	First/Second	Second /Third	First/Third
12	0.0000	0.0000	0.0000	-	-	-
15	0.0000	0.0000	0.0000	-	-	-
26	0.7430	0.7335	0.7757	1.30	-5.45	-4.21
70	0.4947	0.4824	0.4584	2.54	5.24	7.92
143	1.1352	1.2284	1.2787	-7.59	-3.94	-11.23
203	2.4042	2.4253	2.4081	-0.87	0.71	-0.16
332	3.1126	3.1353	3.1494	-0.72	-0.45	-1.17
432	3.0940	3.1161	3.1304	-0.71	-0.46	-1.16

C.4.2 4.16 % Submergence level

Table C.4.2. Data for 20 mm ID tube (water) using one 17 mm ID LTP (middle). 4.166 % Submergence level

Air Injection	Produced water, l/min			% Variation	% Variation	% Variation
l/min	First	Second	Third	First/Second	Second /Third	First/Third
165	0.0000	0.0000	0.0000	-	-	-
200	0.6739	0.7154	0.7168	-5.79	-0.20	-5.98
329	1.7483	1.6978	1.7446	2.98	-2.69	0.21
432	1.9343	1.9199	1.9055	0.75	0.75	1.51

C.4.3 RMS of FBHP data

Table C.4.3. RMS of FBHP for 20 mm ID tube (water) using one 17 mm ID LTP (middle).

Air injection l/m	RMS of FBHP (psi) Submergence level			
	4.16%	8.33%	12.5%	16.66%
5	0.185	0.365	0.545	0.731
10.14	0.196	0.372	0.548	0.731
15	0.211	0.379	0.553	0.737
20	0.225	0.389	0.562	0.738
26	0.243	0.405	0.572	0.742
33	0.234	0.399	0.578	0.741
44	0.256	0.418	0.588	0.759
57	0.258	0.427	0.593	0.759
71	0.251	0.426	0.581	0.758
88	0.238	0.406	0.579	0.754
108	0.195	0.378	0.566	0.748
131	0.192	0.374	0.56	0.744
169	0.187	0.368	0.56	0.746
201	0.197	0.375	0.564	0.747
259	0.207	0.386	0.574	0.752
329	0.237	0.404	0.579	0.754
386	0.252	0.41	0.593	0.752
431	0.266	0.424	0.601	0.751

C.5 Data for one 17 mm ID LTP located at the bottom of the tube

C.5.1 16.66 % submergence level

Table C.5.1. Data for 20 mm ID tube (water) using one 17 mm ID LTP (bottom). 16.66 % Submergence level.

Air Injection l/min	Produced water, l/min			% Variation First/Second	% Variation Second /Third	% Variation First/Third
	First	Second	Third			
12	0.0000	0.0000	0.0000	-	-	-
15	0.1019	0.1434	0.1609	-28.96	-10.86	-36.68
26	0.8183	0.7604	0.8001	7.63	-4.96	2.29
70	0.4339	0.4856	0.4609	-10.66	5.38	-5.85
143	1.2255	1.2154	1.2315	0.83	-1.31	-0.49
203	2.5605	2.5361	2.5487	0.96	-0.49	0.46
332	3.2233	3.2159	3.2224	0.23	-0.20	0.03
432	3.1989	3.2151	3.2048	-0.50	0.32	-0.18

C.5.2 4.16 % submergence level

Table C.5.2. Data for 20 mm ID tube (water) using one 17 mm ID LTP (bottom). 4.166 % Submergence level

Air Injection l/min	Produced water, l/min			% Variation First/Second	% Variation Second /Third	% Variation First/Third
	First	Second	Third			
165	0.0000	0.0000	0.0000	-	-	-
200	0.6760	0.6286	0.6233	7.55	0.85	8.46
329	1.6903	1.6770	1.6821	0.79	-0.30	0.49
432	1.8591	1.8398	1.8419	1.05	-0.12	0.93

C.5.3 RMS of FBHP data

Table C.5.3. RMS of FBHP for 20 mm ID tube (water) using one 17 mm ID LTP (bottom).

Air injection l/m	RMS of FBHP (psi) Submergence level			
	4.16%	8.33%	12.5%	16.66%
5	0.185	-	0.546	0.734
10.14	0.196	-	0.55	0.734
15	0.214	-	0.556	0.739
20	0.226	-	0.559	0.743
26	0.242	-	0.567	0.753
33	0.241	-	0.552	0.738
44	0.252	-	0.571	0.737
57	0.262	-	0.58	0.768
71	0.253	-	0.575	0.755
88	0.239	-	0.564	0.757
108	0.214	-	0.551	0.742
131	0.193	-	0.56	0.76
169	0.193	-	0.553	0.743
201	0.195	-	0.564	0.759
259	0.224	-	0.562	0.754
329	0.267	-	0.582	0.766
386	0.289	-	0.595	0.777
431	0.304	-	0.597	0.785

C.6 Data for two 17 mm-ID LTPs located at bottom and top of the tube

C.6.1 16.66 % submergence level

Table C.6.1. Data for 20 mm ID tube (water) using one 17 mm ID LTP (bottom & top). 16.66 % Submergence level

l/min	First	Second	Third	First/Second	Second /Third	First/Third
11.5	0.0000	0.0000	0.0000	-	-	-
15.0	0.0000	0.0000	0.0000	-	-	-
26.0	0.7276	0.7579	0.7972	-4.00	-4.93	-8.74
70	0.4838	0.4413	0.4693	9.64	-5.98	3.08
143	1.1491	1.1272	1.1700	1.95	-3.66	-1.78
203	2.4093	2.4376	2.4279	-1.16	0.40	-0.77
332	2.9573	2.9634	2.9748	-0.20	-0.38	-0.59
432	2.9194	2.9259	2.9148	-0.22	0.38	0.16

C.6.2 4.16 % Submergence level

Table C.6.2. Data for 20 mm ID tube (water) using one 17 mm ID LTP (bottom & top). 4.16 % Submergence level

Air Injection l/min	Produced water, l/min			% Variation First/Second	% Variation Second /Third	% Variation First/Third
	First	Second	Third			
165	0.0000	0.0000	0.0000	-	-	-
200	0.7037	0.7366	0.7075	-4.46	4.12	-0.53
329	1.8069	1.7771	1.8133	1.68	-2.00	-0.35
432	2.0177	2.0247	2.0346	-0.34	-0.49	-0.83

C.6.3 RMS of FBHP

Table C.6.3. RMS of FBHP for 20 mm ID tube (water) using one 17 mm ID LTP (bottom & top).

Air injection l/m	RMS of FBHP (psi) Submergence level			
	4.16%	8.33%	12.5%	16.66%
5	0.188	-	-	0.725
10.14	0.198	-	-	0.728
15	0.213	-	-	0.734
20	0.226	-	-	0.738
26	0.248	-	-	0.747
33	0.233	-	-	0.754
44	0.254	-	-	0.754
57	0.256	-	-	0.764
71	0.249	-	-	0.757
88	0.244	-	-	0.755
108	0.217	-	-	0.751
131	0.194	-	-	0.765
169	0.195	-	-	0.752
201	0.193	-	-	0.762
259	0.22	-	-	0.766
329	0.274	-	-	0.765
386	0.311	-	-	0.793
431	0.333	-	-	0.795

APPENDIX D

EXPERIMENTAL RESULTS FOR THE WATER/AIR GAS LIFT SYSTEM UTILIZING LTPs IN THE 12 mm ID TUBE.

D.1 Data for the 11 mm ID LTP located at the middle of the tube.

D.1.1 16.66 % submergence level

Table D.1.1. Data for 12 mm ID tube (water) using one 11 mm ID LTP (middle). 16.66 % Submergence level

Air Injection l/min	Produced water, l/min			% Variation	% Variation	% Variation
	First	Second	Third	First/Second	Second /Third	First/Third
3	0.000	0.000	0.000	-	-	-
3.752	0.186	0.181	0.175	2.58	3.52	6.19
8.031	0.434	0.426	0.421	1.81	1.18	3.01
10.94	0.486	0.450	0.474	8.11	-5.00	2.70
15.09	0.411	0.434	0.396	-5.14	9.64	4.00
20.02	0.200	0.172	0.188	16.11	-8.61	6.11
25.12	0.186	0.195	0.201	-4.35	-3.25	-7.45
26.06	0.192	0.195	0.216	-1.44	-9.74	-11.04
74	0.426	0.426	0.429	0.00	-0.71	-0.71
110	0.397	0.368	0.364	7.95	1.23	9.27
163	0.324	0.329	0.329	-1.35	0.00	-1.35
212	0.308	0.300	0.291	2.56	3.13	5.77

D.1.2 12.5 % submergence level

Table D.1.2. Data for 12 mm ID tube (water) using one 11 mm ID LTP (middle). 12.5 % Submergence level

Air Injection l/min	Produced water, l/min			% Variation First/Second	% Variation Second /Third	% Variation First/Third
	First	Second	Third			
4	0.000	0.000	0.000	-	-	-
4.714	0.086	0.084	0.081	2.143	4.196	6.429
8.031	0.182	0.216	0.203	-15.909	6.306	-10.606
10.94	0.222	0.229	0.242	-2.963	-5.344	-8.148
15.09	0.159	0.188	0.149	-15.232	25.781	6.623
20.02	0.018	0.022	0.025	-18.284	-13.699	-29.478
25.12	0.035	0.031	0.032	14.599	-3.185	10.949
26.06	0.041	0.037	0.041	9.322	-10.078	-1.695
74	0.289	0.271	0.273	6.627	-0.565	6.024
110	0.282	0.271	0.284	4.118	-4.520	-0.588
163	0.257	0.259	0.259	-0.714	0.000	-0.714
212	0.250	0.243	0.240	2.778	1.351	4.167

D.1.3 8.33 % submergence level

Table D.1.3. Data for 12 mm ID tube (water) using one 11 mm ID LTP (middle). 8.33 % Submergence level

Air Injection l/min	Produced water, l/min			% Variation First/Second	% Variation Second /Third	% Variation First/Third
	First	Second	Third			
7.5	0.0000	0.0000	0.0000	-	-	-
8.031	0.0196	0.0194	0.0233	0.95	-16.60	-15.80
10.94	0.0038	0.0046	0.0032	-17.46	44.23	19.05
15.09	0.0003	0.0014	0.0012	-80.24	18.07	-76.67
20.02	0.0000	0.0000	0.0000	-	-	-
25.12	0.0000	0.0000	0.0000	-	-	-
26.06	0.0000	0.0000	0.0000	-	-	-
74	0.1633	0.1667	0.1538	-2.04	8.33	6.12
110	0.1890	0.1920	0.1890	-1.57	1.60	0.00
163	0.1920	0.1920	0.1920	0.00	0.00	0.00
212	0.1875	0.1860	0.1890	0.78	-1.55	-0.78

D.1.4 4.16 % submergence level

Table D.1.4. Data for 12 mm ID tube (water) using one 11 mm ID LTP (middle). 4.16 % Submergence level

Air Injection l/min	Produced water, l/min			% Variation First/Second	% Variation Second /Third	% Variation First/Third
	First	Second	Third			
8.031	0.0000	0.0000	0.0000	-	-	-
10.94	0.0000	0.0000	0.0000	-	-	-
15.09	0.0000	0.0000	0.0000	-	-	-
20.02	0.0000	0.0000	0.0000	-	-	-
25.12	0.0000	0.0000	0.0000	-	-	-
60	0.0000	0.0000	0.0000	-	-	-
74	0.0377	0.0458	0.0423	-17.61	8.40	-10.69
110	0.1154	0.1165	0.1188	-0.96	-1.94	-2.88
163	0.1290	0.1319	0.1290	-2.15	2.20	0.00
212	0.1143	0.1319	0.1290	-13.33	2.20	-11.43

D.1.5 RMS of FBHP data

Table D.1.5. RMS of FBHP for 12 mm ID tube (water) using one 11 mm ID LTP (middle).

Air injection	RMS of FBHP (psi)			
l/m	Submergence level			
	4.16%	8.33%	12.5%	16.66%
0.532	0.183	0.363	0.543	0.724
1.508	0.193	0.367	0.545	0.725
2.612	0.188	0.365	0.544	0.724
3.752			0.544	0.725
4.216			0.539	
5	0.191	0.366		0.722
6.232				0.726
7.513	0.209	0.381	0.547	0.729
10.14	0.24	0.392	0.551	0.727
12.85		0.404	0.564	0.727
15.66	0.247	0.4	0.573	0.75
18.55	0.245	0.394	0.572	0.742
20	0.237	0.396		0.745
23	0.236	0.389	0.568	0.746
26	0.225	0.385	0.568	0.739
33	0.247	0.395	0.568	0.744
44	0.213	0.381	0.556	0.734
57	0.195	0.367	0.545	0.729
71	0.188	0.362	0.542	0.728
88	0.183	0.361	0.543	0.727
108	0.185	0.365	0.542	0.727
131	0.189	0.369	0.545	0.729
169	0.203	0.381	0.555	0.736
201	0.221	0.391	0.563	0.744
259	0.24	0.403	0.57	0.754
329	0.261	0.406	0.58	0.756
386	0.325	0.448	0.59	0.764
431	0.368	0.494	0.651	0.806

D.2 Data for the 9 mm ID LTP located at the middle of the tube.

D.2.1 16.66 % Submergence level

Table D.2.1. Data for 12 mm ID tube (water) using one 9 mm ID LTP (middle). 16.66 % Submergence level

Air Injection	Produced water, l/min			% Variation	% Variation	% Variation
l/min	First	Second	Third	First/Second	Second /Third	First/Third
3	0.000	0.000	0.000	-	-	-
3.752	0.179	0.173	0.168	3.73	2.88	6.72
8.031	0.389	0.387	0.389	0.54	-0.54	0.00
10.94	0.393	0.398	0.391	-1.09	1.66	0.55
15.09	0.346	0.367	0.346	-5.77	6.12	0.00
20.02	0.216	0.209	0.198	3.60	5.65	9.46
25.12	0.203	0.209	0.198	-2.54	5.22	2.54
26.06	0.208	0.210	0.212	-0.87	-1.31	-2.16
74	0.416	0.407	0.409	2.31	-0.56	1.73
110	0.379	0.358	0.362	5.79	-1.00	4.74
162	0.293	0.299	0.308	-2.03	-2.90	-4.88
212	0.270	0.264	0.265	2.25	-0.37	1.87

D.2.2 12.5 % Submergence level

Table D.2.2. Data for 12 mm ID tube (water) using one 9 mm ID LTP (middle). 12.5 % Submergence level

Air Injection	Produced water, l/min			% Variation	% Variation	% Variation
l/min	First	Second	Third	First/Second	Second /Third	First/Third
4	0.000	0.000	0.000	-	-	-
4.714	0.070	0.069	0.067	0.581	2.890	3.488
8.031	0.160	0.153	0.144	4.255	6.633	11.170
10.94	0.154	0.153	0.158	0.513	-3.061	-2.564
15.09	0.072	0.090	0.081	-19.931	11.588	-10.653
20.02	0.023	0.018	0.018	27.536	0.000	27.536
25.12	0.039	0.032	0.033	19.355	-2.703	16.129
26.06	0.043	0.035	0.035	25.225	-2.158	22.523
74	0.267	0.262	0.281	1.667	-6.740	-5.185
110	0.270	0.276	0.261	-2.252	5.991	3.604
163	0.245	0.244	0.244	0.510	0.000	0.510
212	0.220	0.211	0.214	4.587	-1.754	2.752

D.2.3 8.33 % Submergence level

Table D.2.3. Data for 12 mm ID tube (water) using one 9 mm ID LTP (middle). 8.33 % Submergence level

Air Injection	Produced water, l/min			% Variation	% Variation	% Variation
l/min	First	Second	Third	First/Second	Second /Third	First/Third
7.5	0.0000	0.0000	0.0000	-	-	-
8.031	0.0011	0.0020	0.0022	-44.40	-7.24	-48.43
10.94	0.0029	0.0064	0.0053	-54.69	20.45	-45.43
15.09	0.0005	0.0014	0.0012	-63.44	13.95	-58.34
20.02	0.0002	0.0004	0.0002	-59.38	65.70	-100.00
25.12	0.0006	0.0008	0.0004	-22.49	123.49	-100.00
26.06	0.0009	0.0009	0.0010	-6.19	-10.87	-100.02
74	0.1387	0.1356	0.1297	2.31	4.52	6.94
110	0.1739	0.1727	0.1727	0.72	0.00	0.72
163	0.1739	0.1739	0.1739	0.00	0.00	0.00
212	0.1633	0.1667	0.1644	-2.04	1.39	-0.68

D.2.4 4.16 % Submergence level

Table D.2.4. Data for 12 mm ID tube (water) using one 9 mm ID LTP (middle). 4.16 % Submergence level

Air Injection	Produced water, l/min			% Variation	% Variation	% Variation
l/min	First	Second	Third	First/Second	Second /Third	First/Third
8.031	0.0000	0.0000	0.0000	-	-	-
10.94	0.0000	0.0000	0.0000	-	-	-
15.09	0.0000	0.0000	0.0000	-	-	-
20.02	0.0000	0.0000	0.0000	-	-	-
25.12	0.0000	0.0000	0.0000	-	-	-
60	0.0000	0.0000	0.0000	-	-	-
74	0.0502	0.0462	0.0449	8.79	2.69	11.72
110	0.0851	0.0923	0.0968	-7.80	-4.62	-12.06
163	0.1132	0.1091	0.1091	3.77	0.00	3.77
212	0.1143	0.1154	0.1154	-0.95	0.00	-0.95

D.2.5 RMS of FBHP data

Table D.2.5. RMS of FBHP for 12 mm ID tube (water) using one 9 mm ID LTP (middle).

Air injection	RMS of FBHP (psi)			
l/m	Submergence level			
	4.16%	8.33%	12.5%	16.66%
0.532	0.184	0.363	0.532	0.724
1.508	0.192	0.366	0.544	0.726
2.612	0.192	-	0.544	0.726
3.752	0.19	0.366	0.543	
5	0.191	0.367	0.543	0.724
6.232	0.194	0.369	0.544	0.725
7.513	0.203	0.369	0.544	0.727
10.14	0.233	0.381	0.548	0.728
12.85	-	0.388	0.554	0.732
15.66	0.246	0.393	0.566	0.744
18.55	0.231	0.398	0.567	0.746
20	0.236	0.399	0.566	0.746
23	0.231	0.396	0.564	0.745
26	0.224	0.389	0.564	0.742
33	0.239	0.399	0.569	0.747
44	0.209	0.383	0.556	0.736
57	0.196	0.37	0.548	0.731
71	0.189	0.363	0.546	0.729
88	0.183	0.363	0.55	0.729
108	0.186	0.366	0.552	0.732
131	0.195	0.373	0.558	0.737
169	0.213	0.382	0.566	0.744
201	0.225	0.396	0.578	0.753
259	0.244	0.406	0.585	0.76
329	0.254	0.418	0.59	0.767
386	0.2826	0.436	0.608	0.774
431	0.285	0.453	0.623	0.808

APPENDIX E

EXPERIMENTAL RESULTS FOR THE WATER/AIR GAS LIFT SYSTEM UTILIZING A 7 mm ID LTP IN 8 mm ID TUBE.

E.1 RMS of FBHP

Table E.1. RMS of FBHP for 8 mm ID tube (water) using one 8 mm ID LTP (middle).

Air injection	RMS of FBHP (psi)	
l/m	Submergence level	
	4.16%	8.33%
0.0581	0.18112	0.726034713
0.532	0.181476	0.726351543
1.108	0.186362	0.726409317
1.508	0.192076	0.72635728
2.612	0.189025	0.727074758
3.752	0.217408	0.730186234
5	0.240627	0.738034171
6.232	0.231753	0.741389121
7.513	0.229581	0.757662661
10.14	0.211837	0.740916257
12.85	0.199573	0.73868736
15.66	0.194132	0.735301878
18.55	0.187155	0.733182449
20	0.185621	0.732153513
23	0.182783	0.730219317
26	0.179471	0.729973583
30	0.18869	0.728886758
40	-	0.727310827
50	0.183854	0.726850581
60	0.185002	0.72753956
70	0.184525	0.726344575
80	-	0.726966234
90	-	0.726205152
100	-	0.727686002